**Charles University**
**Faculty of Science**

Study programme: Chemistry


**Jakub Obuch**

# Lanthanide complexes of DOTA-"*trans*"-diamide
# Lanthanoidové komplexy "*trans*"-diamidu DOTA

**BACHELOR'S THESIS**

Supervisor: Prof. RNDr. Petr Hermann, Dr.

Prague, 2019

Hereby I declare that this Thesis is my original work and that I have properly cited all the information resources. This work has not been submitted either for any other or for the same academic degree.

Prohlašuji, že jsem závěrečnou práci zpracoval samostatně a že jsem uvedl všechny použité informační zdroje a literaturu. Tato práce ani její podstatná část nebyla předložena k získání jiného nebo stejného akademického titulu.

In Prague, September 1, 2019 Jakub Obuch

# Abstract

Macrocyclic complexes are of great interest due to their utilization in many medicinal applications, such as MRI contrast agents and radiopharmaceuticals. These complexes overcome the toxicity of free heavy metal ions and, thus, enable their use *in vivo*. In this Thesis, diamide derivative of DOTA (*t*DODAM) and its lanthanide(III) complexes were prepared and characterised in solution and in the solid state. For cerium(III) complex, formation and dissociation kinetics were studied. Structure and dynamics of europium(III) complex were investigated by multinuclear NMR spectroscopy and various 2D NMR techniques. Similarly to Ln(III)-DOTA complexes, the complexes form square-antiprismatic (SA) and twisted-square-antiprismatic (TSA) isomers and their ratio in solution was determined across the lanthanide series. Structures of 7 lanthanide(III) complexes in the solid state were determined. Thermodynamic data were obtained for Cu(II), Zn(II), Pb(II), Ce(III), Eu(III) and Lu(III) complexes by potentiometric titration.


Keywords: macrocyclic ligands, complexes, lanthanides



# Abstrakt

Makrocyklické ligandy se už dlouho těší značného zájmu, protože jsou používány v mnoha medicinálních aplikacích. Jejich komplexy jsou využívány jako kontrastní látky pro MRI a další zobrazovací metody, a také jako radiofarmaceutické preparáty. Tyto komplexy, často odvozené od těžkých kovů, jsou výrazně méně toxické než „volné“ aqua-ionty těchto kovů, a umožňují tedy jejich použití *in vivo*. V této práci byl připraven diamidový derivát ligandu DOTA (*t*DODAM) a jeho komplexy s trojmocnými lanthanoidy. Připravené látky byly charakterizovány v roztoku a v pevné fázi. V případě ceritého komplexu byla studována kinetika jak jeho vzniku, tak i rozkladu. Dále byla pomocí multinukleární spektroskopie NMR a různých metod 2D-NMR studována struktura a dynamika europitého komplexu v roztoku. Podobně jako komplexy DOTA s trojmocnými lanthanoidy, i komplexy ligandu tDODAM tvoří dva izomery se čtvercově-antiprizmatickou (SA) a s deformovanou čtvercově- antiprizmatickou (TSA) geometrii. Vzájemný poměr těchto izomerů v roztoku byl stanoven napříč lanthanoidovou řadou. Struktury 7 komplexů s ionty Ln(III) byly stanoveny pomocí rentgenové difrakce. Potenciometrickými titracemi byla získána termodynamická data pro ligand samotný a pro jeho komplexy s ionty $Cu^{2+}$, $Zn^{2+}$, $Pb^{2+}$, $Ce^{3+}$, $Eu^{3+}$ a $Lu^{3+}$.


Klíčové slova: makrocyklické ligandy, komplexy, lanthanoidy

# Contents

# Chapter 1

# Theoretical Background

Health is arguably one of the most important aspects of life. Therefore, many human activities are strongly connected with healthy life. Medicine is one of the most studied fields of science and many other natural sciences help medicine to be more efficient. Chemistry provides medicine with synthetic drugs but also, together with physics, provides means of imaging the human body without causing unnecessary harm.

## 1.1 Macrocyclic complexes in medicine

Many medical applications rely on certain properties of metal ions, like paramagnetic relaxation enhancement for MRI (magnetic resonance imaging), $\beta^+$ radioactive decay for PET (positron emission tomography) or other decay modes for therapeutic radiopharmaceuticals. Unfortunately, many metal ions suitable for these applications are highly toxic (e.g. $LD_{50}$ of $GdCl_3 \cdot 6\,H_2O$ is 200 $mg \cdot kg^{-1}$ [1]) which means that they cannot be used in their free ionic form. Solution of this problem is to incorporate the metal ion into a stable complex which will not dissociate in the body and will be excreted unchanged with no adverse effects. There are two matters to consider: thermodynamic stability and kinetic inertness. Thermodynamic stability of complex [M(L)] is given by its stability constant $\beta$ that is given by Equation (1.1). Measure of kinetic inertness is the observed rate constant ${}^{\mathrm{d}}k_{\mathrm{obs}}$ of decomplexation reaction (Equation (1.2)).

$$\beta = \frac{[\mathrm{ML}]}{[\mathrm{M}][\mathrm{L}]} \tag{1.1}$$

$$\mathrm{ML} \xrightarrow{{}^{\mathrm{d}}k_{\mathrm{obs}}} \mathrm{M} + \mathrm{L} \tag{1.2}$$

### 1.1.1 Contrast agents for MRI

One of the most used diagnostic tools of modern medicine is magnetic resonance imaging (MRI). The MRI is a diagnostic method based on nuclear magnetic resonance effect. In $^{1}$H MRI, water protons in the body are observed, since water is the most abundant hydrogen-containing molecule in the human body. Primarily, the water content in different tissues is observed. If the $T_1$-weighting image is measured, the signal is proportional to the hydrogen longitudinal relaxation rate $R_1$. Relaxation rate of water protons depends on the chemical composition of the tissue but the contrast between different tissues is often too low to provide useful information. Therefore, a number of MRI contrast agents have been designed in order to enhance the differences in the relaxation rates. Typically, contrast agents are based on complexes of paramagnetic metal ions such as gadolinium(III) or high-spin manganese(II). The first gadolinium(III)-based contrast agent approved for clinical usage was Gd(III)-DTPA complex (Magnevist®) (Fig. 1.1). [2] Such contrast agents are based on the paramagnetic relaxation enhancement effect. The Gd(III)-DTPA complex is an example of a contrast agent based on an open-chain ligand. This type of contrast agents suffers from low kinetic inertness. As an example, half-time of dissociation of the Gd(III)-DTPA complex in 0.1M aq. HCl at room temperature is 10 min, whereas half-times of dissociation of the Gd(III)-DO3AP$^{H}$ and Gd(III)-DOTA complexes are 3 h and more than 1 month under the same conditions, respectively. [3] The other contrast agents are based on macrocyclic ligands. Complexes of such ligands are inherently more kinetically inert and are among the most thermodynamically stable complexes. An example of a macrocyclic contrast agent is gadolinium(III) complex of DOTA (Dotarem®) (Fig. 1.1). DOTA is octadentate ligand which features macrocyclic cavity, size thereof is suitable for lanthanide(III) ions. DOTA is prototypical structural motif for lanthanide(III) complexing ligands. The ninth coordination site in the structure of larger lanthanide(III) complexes is, in aqueous solutions, occupied by water molecule. This water molecule is not bound too strongly. Therefore, it exchanges with water molecules in bulk solution. This provides a mechanism for transfer of magnetic properties of Gd(III) ions to the bulk water molecules, thus increasing their relaxation rate. Manganese(II)-based MRI contrast agents are safer due to the lower toxicity of manganese and an example of a manganese(II)-based contrast agent is Mn(II)-dipyridoxaldiphosphate (ligand DPDP is shown in Fig. 1.1) (Teslascan®) which is used for liver imaging. [4] In the case of these so called $T_1$ contrast agents, the contrast is "bright", meaning that the area containing the contrast agent enhances the signal whereas in the case of $T_2$ contrast agents the contrast is "dark". $T_2$ contrast agents are predominantly based on superparamagnetic iron oxide nanoparticles (SPIONs). [5]

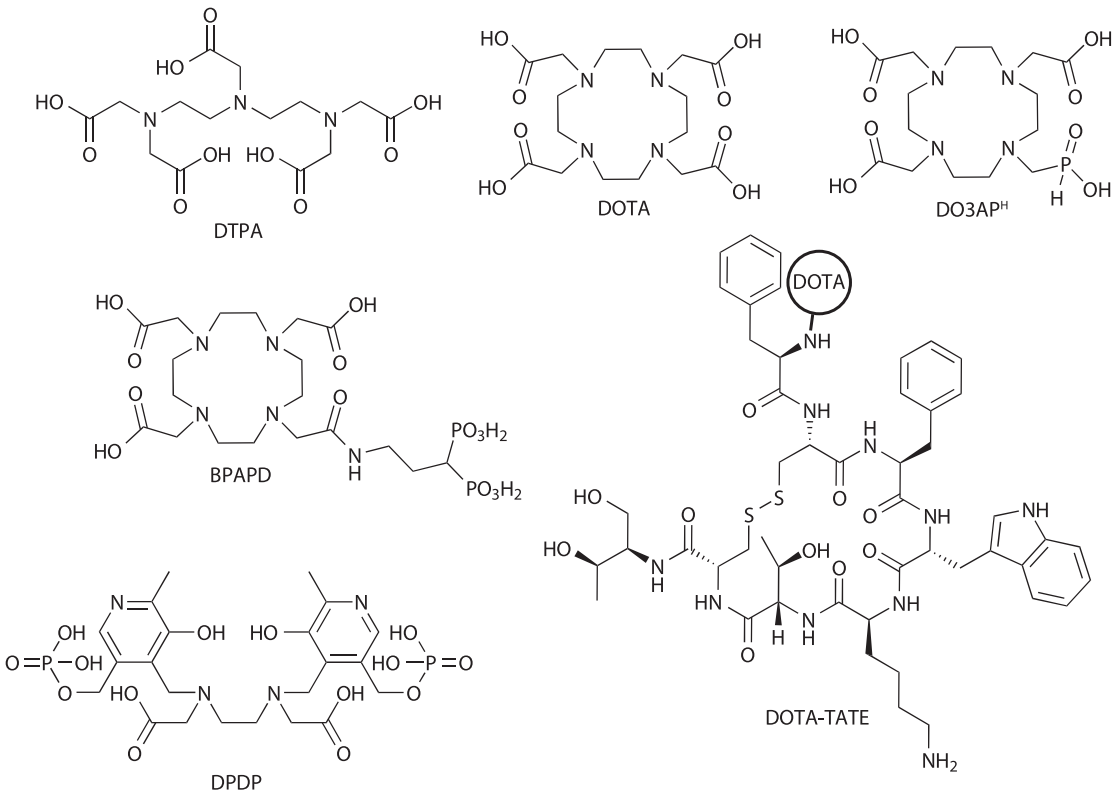


Figure 1.1: Ligands mentioned in text.

### 1.1.2 Radiopharmaceuticals

Radiopharmaceuticals rely on using radioactive elements to image or treat diseased tissue, mainly tumors. Radioactive elements are usually incorporated in some type of organic carrier molecule which enables selective targeting of cancer cells. In the case of radioactive metals, complexes with macrocyclic ligands can be used with benefits, since these complexes are stable and, thus, the radiotoxicity of the radiometal is greatly reduced. If the metal has several radioisotopes that can be used in different medicinal methods, such as copper-64 ($\beta^+$ radionuclide suitable for PET) and copper-67 ($\beta^-$ radionuclide suitable for therapy), both radioisotopes can be used with the same carrier, thus allowing **thera**py and diag**nostics** at the same time. Such applications are called *theranostics* and are promising approach of oncological medicine.

Macrocyclic ligands also may have a functional group to conjugate biomolecules. The biomolecule allows to selectively observe (in case of molecular imaging) or treat (in case of radiotherapy) a part of the body which has a high affinity towards the biomolecule. A prominent examples of such complexes are complexes of DOTA-TATE (Fig. 1.1) and related conjugates. In this molecule, octapeptide is bound to a molecule of

DOTA via an amidic bond. DOTA-TATE is a somatostatin receptor antagonist, *i.e.* this molecule will accumulate on somatostatin receptors (which occur in higher concentration at some abnormally growing sites). Thus, provided that suitable metal is coordinated in the macrocyclic cavity, it can be used as a diagnostic tool or even for targeted therapy. In practice, its gallium-68 complex is used for PET imaging and lutetium-177 complex is used for tumor therapy (sold under commercial name Lutathera®).

Another example of targeted radiotherapy is the use of complexes with bis(phosphonate) pendant arms, e.g. ligand BPAPD (Fig. 1.1). Such complexes show significant uptake by bone metastases and can be used to diagnose and cure bone tumors. [6] However, using larger biomolecules such as proteins or antibodies can be difficult, since the usual conditions for coordinating metal ions into macrocyclic ligands are rather drastic: e.g. 20 min at 80 °C and pH = 4.5 for Lu(III) [7], although continuous microflow systems are more efficient (44 s at 80 °C). [8] Such high temperature would cause the protein to denaturate, thus becoming biologically inactive. The temperature of complexation reaction could be reduced provided that this reaction is fast enough at lower temperatures. It must be noted that with some radionuclides, the time needed to form the complex has to be as short as possible due to fast radioactive decay (e.g. for $^{213}$Bi $\tau_{1/2}$ = 45.6 min or $^{68}$Ga $\tau_{1/2}$ = 68 min). [9] Therefore, there is significant interest to find macrocyclic ligands with faster complexation kinetics but, still, their complexes must be kinetically inert.

## 1.2 Techniques of study of macrocyclic ligands and their complexes

### 1.2.1 NMR

Nuclei with non-zero nuclear spin ($^{1}$H, $^{13}$C, $^{19}$F, $^{31}$P and many more) placed in external magnetic field occur in multiple energy levels based on the orientation of the magnetic moment with respect to the external magnetic field. The orientation of the magnetic moment of spin-1/2 nuclei in equilibrium can be either parallel or anti-parallel, parallel orientation being lower in energy.[1] Energy difference $\Delta E$ between these two states is given by Equation (1.3) where $\gamma$ is gyromagnetic ratio of the nuclei under investigation, $\hbar$ is reduced Planck constant and $B$ is magnetic field intensity given by sum of external magnetic field intensity $B_0$ and local magnetic field $B_1$ (Equation (1.4)). Local magnetic field is defined by Equation (1.5) where $\sigma$ is shielding constant (or more

[1] valid only for nuclei with positive gyromagnetic ratio, an example of a nucleus with negative gyromagnetic ratio is $^{15}$N

precisely shielding tensor) determined by chemical environment of a given nucleus.

$$\Delta E = -\gamma\hbar B = h\nu \tag{1.3}$$

$$B = B_0 + B_1 \tag{1.4}$$

$$B_1 = B_0 \cdot \sigma \tag{1.5}$$

Differences of the shielding constants of non-equivalent nuclei are manifested in different chemical shifts $\delta$ in NMR spectrum. Chemical shift is defined by Equation (1.6) where $\nu$ is Larmor frequency of observed nucleus and $\nu_0$ is Larmor frequency of reference signal (such as hydrogen nuclei of tetramethylsilane) and is measured in ppm (parts per million).

$$\delta = \frac{\nu - \nu_0}{\nu_0} \cdot 10^6 \text{ ppm} \tag{1.6}$$

A sum of all magnetic moments is called *magnetisation* and its magnitude and orientation can be measured. In the presence of a magnetic field, magnetisation is oriented parallel to the external magnetic field and precedes around the vector of the magnetic field induction $\vec{B_0}$ (its direction is in the $z$-axis). By applying an electromagnetic pulse with certain frequency, the orientation of a nuclear spin can be changed. After application of this pulse, the *Larmor precession* of the magnetisation occurs in the *xy* plane and is macroscopically observable. Its frequency $\nu$ is given by energy difference $\Delta E$ of the two spin states. When the electromagnetic pulse is turned off, the magnetisation vector returns to the equilibrium position through exchanging energy with its surrounding in a process known as *longitudinal relaxation* (also *spin-lattice relaxation*). This process is characterised by relaxation time $T_1$ or relaxation rate $R_1 = T_1^{-1}$. There is also another type of relaxation: *transversal relaxation* (also *spin-spin relaxation*). This process is coherence loss of the magnetic moment vectors in the *xy* plane. This type of relaxation is characterised by relaxation time $T_2$. Fast transversal relaxation leads to broader peaks; full width of the peak at half maximum (FWHM) is related to $T_2$ relaxation time by Equation (1.7).

$$\text{FWHM} = \frac{1}{\pi T_2} \tag{1.7}$$

NMR is generally one of the most important methods to characterise any organic molecule. Simple 1D experiments combined with 2D experiments are mostly sufficient to confirm the structure of a prepared compound. In addition to structural information, NMR can be used to obtain several physical and chemical characteristics of the studied compound. Various thermodynamical and kinetical parameters can be obtained by using suitable NMR experiments. In particular, several parameters directly related to MRI (relaxivities[2] and relaxation times) are obtained through NMR experiments.

[2] Relaxivity is defined as the relaxation rate enhancement effect induced by the paramagnetic compound normalized to its concentration.

### 1D NMR of paramagnetic molecules

Presence of paramagnetic metal ion in macrocyclic complexes has substantial effect on 1D NMR spectra and their measurement. The $T_1$ relaxation time is shortened due to paramagnetic relaxation enhancement which allows for shorter relaxation delays to be used and thus faster data acquisition. On the other hand, $T_2$ relaxation time is also shortened compared to diamagnetic compounds and thus the peaks in the spectrum are broader, sometimes even immeasurable. Due to the broadening of peaks, spin-spin coupling is usually not observed. Effect of the paramagnetic center on the chemical shift of the nuclei in the complex is also important. Lanthanide induced shift (LIS) has two contributions: contact shift and pseudo-contact shift. Contact shift is proportional to unpaired electron density at the position of the nucleus of the observed atom and is not easily calculated. Pseudo-contact shift depends on the position of the observed nucleus in respect to the paramagnetic ion, which means that a lot of structural information can be obtained by measuring NMR spectra of paramagnetic complexes. Since the signals are often highly shifted, it is important to record the NMR spectrum over a larger spectral window, sometimes several hundreds ppm wide for $^1$H NMR. This causes technical difficulties, since the excitation profile of the electromagnetic pulse is not homogeneous over such large frequency range and, therefore, spectra might need to be recorded in several parts.

### Concentration determination of paramagnetic complex in solution

$^1$H NMR spectrum can also provide us with information about the concentration of a paramagnetic compound in solution. Disregarding contact and pseudocontact shift, the presence of a paramagnetic compound affects the chemical shifts of all proton nuclei in the solution equally. If the measurement is done using NMR tube and coaxial insert tube, both containing the same standard compound (usually *t*BuOH or TMS), and only one of them contains the paramagnetic species, the concentration of the paramagnetic compound can be determined from the difference of the chemical shifts of the standard compound. The chemical shift difference due to the bulk magnetic susceptibility $\Delta$ is given by Equation (1.8) [10] where $c$ is the molar concentration of the paramagnetic species, $s$ is a constant depending on shape of the sample and its position in respect to the magnetic field (for cylindrical sample parallel to the magnetic field $s = \frac{1}{3}$), $T$ is temperature and $\mu_{\text{eff}}$ is effective magnetic moment of the paramagnetic ion (*e.g.* for $Gd^{3+}$ $\mu_{\text{eff}}$ = 8.10 [11]).

$$\Delta = \frac{4\pi cs}{T}\left(\frac{\mu_{\text{eff}}}{2.84}\right)^2 \cdot 10^3 \tag{1.8}$$

**2D NMR**

Multidimensional experiments provide us with more information about molecular structure than 1D spectra. The type of obtained information can be related to physical characteristics of the molecules as whole (e.g. Diffusion Ordered SpectroscopY (DOSY)) or mutual interactions of nuclei in the molecule. These interactions can be either through space (e.g. Nuclear Overhauser Effect SpectroscopY (NOESY)) or through bonds (e.g. COrelation SpectroscopY (COSY), Heteronuclear Single Quantum Coherence (HSQC) and many more). These experiments use more complicated pulse sequences and their principle is outside the scope of this Thesis. Another type of experiments observe chemical exchange between non-equivalent nuclei. The simplest example of such experiments are variable-temperature (VT) studies of primary amides. At a low temperature, two peaks belonging to amidic protons are found in the spectrum, which coalesce at a higher temperature and, finally at high temperature, the exchange between the two nuclei is so fast that this process is not observable by NMR and only one (average) peak is observed. Variable-temperature experiment gives activation energy of the exchange of two protons and, thus, their exchange rates. In more complex molecules, this simple approach is usually not feasible. Instead, 1D or 2D EXSY (EXchange SpectroscopY) is used. 2D EXSY experiment uses the same pulse sequence as NOESY (Fig. 1.2), yet the origin of crosspeaks is different. [12]

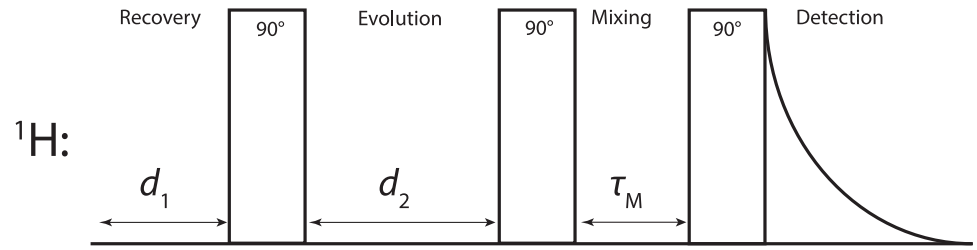


Figure 1.2: Pulse sequence of 2D-EXSY or 2D-NOESY experiment. $d_1$ is relaxation delay during which the magnetisation returns to equilibrium, $d_2$ is interpulse delay and its value is changed during the experiment between acquisitions in order to get the spectrum in the indirect dimension and $\tau_M$ is EXSY (or NOESY) mixing time.

### $^{1}$H NMRD profiles and $^{17}$O VT NMR

Several experiments have to be done in order to examine relaxivity enhancement properties of a paramagnetic compound (which could be considered as a potential MRI contrast agent). Since MRI contrast agents are to be used *in vivo*, these experiments are carried out in aqueous solutions and relaxation rate of water protons is being observed. In order to fully describe the properties of a potential contrast agent, relaxation rate of water is measured at different field strengths, temperatures and pH conditions. From technical point of view, this is not so simple. Most NMR spectrometers operate at one fixed Larmor frequency. Therefore, it would be necessary to use many spectrometers with different magnetic field strengths. This problem is solved by using field-cycling relaxometers. These machines allow us to obtain relaxation rates at different magnetic field strengths. $^{1}$H NMRD profile is a dependence of water proton relaxivity $r_1$ (defined by Equation (1.9) where $\left[\mathrm{Gd}^{3+}\right]$ is molar concentration of gadolinium(III) in the solution in mmol dm$^{-3}$) on proton Larmor frequency.

$$r_1 = \frac{1}{T_1 \cdot \left[\mathrm{Gd}^{3+}\right]} \tag{1.9}$$

The $T_1$ relaxation time is measured using *inversion recovery* experiment. This experiment utilizes a pulse sequence consisting of two pulses. First, 180° pulse inverts the spin into $-z$ axis. During delay with variable length $\delta$, the spin relaxes and after the second, 90° pulse the FID is recorded. The pulse sequence diagram is shown in Fig. 1.3. Dependence of integral intensity of the peak on the length of the delay $\delta$ is fitted by simple exponential Equation (1.10) where $I(\delta)$ is intensity of peak obtained using interpulse delay $\delta$ and $I_0$ is maximum integral intensity, that is integral intensity of peak obtained using such long interpulse delay that all spins have already returned to equilibrium position before the 90° reading pulse.

$$I(\delta) = I_0(1 - e^{\frac{\delta}{T_1}}) \tag{1.10}$$

The $^{17}$O VT NMR is an experiment consisting of measuring a series of 1D $^{17}$O NMR spectra of $^{17}$O-enriched water at temperatures ranging usually from 5 to 80 °C. The main information obtained is the linewidth of the water peak and its chemical shift. This peak is broadened by exchange of the bulk water with the directly coordinated water molecule, *i.e.* inner-sphere water molecule. Linewidth is directly related to the spin-lattice relaxation time of the nucleus under observation. This in turn is related to the water exchange rate constant.

Fitting of $^{17}$O VT NMR and $^{1}$H NMRD profiles gives several parameters of the molecule in solution, among others residence time of coordinated water molecule $\tau_{\mathrm{M}}$ and its rotational correlation time $\tau_{\mathrm{R}}$. $\tau_{\mathrm{M}}$ is inverse of exchange rate constant $k_{\mathrm{ex}}$ and

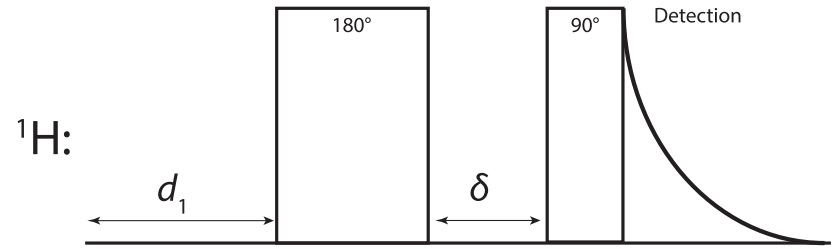


Figure 1.3: Pulse sequence of inversion recovery experiment. $d_1$ is relaxation delay which is chosen as at least 5 times the maximum expected value of $T_1$ in order to let the magnetisation return to equilibrium and $\delta$ is interpulse delay and its value is changed.

describes the kinetics of coordinated water molecule exchange. Rotational correlation time is the average time it takes for a molecule to rotate one radian and is a measure of the particle size.

### 1.2.2 Luminescence spectrophotometry

Luminescence spectrophotometry allows us to determine a number of directly coordinated water molecules $q$ on the central lanthanide(III) ion. Luminescent life-time of the central ion depends on its environment. Some closely located groups may effectively quench the luminescence. For example, water molecule is an efficient quencher since the OH bond vibrations have energy close to the energy of the excited state of the lanthanide(III) ion. Therefore, water molecule can absorb energy of excited electronic state of the lanthanide(III) ion. On the other hand, deuterated water has different vibration energies and is not a good quencher. Therefore, lanthanide(III) ion will have longer life-time if it is surrounded by heavy water molecules than in the case of being surrounded by ordinary water molecules. Thus, determination of the number of coordinated water molecules, $q$, is based on the difference of luminescent life-times of the complex in aqueous solution and in solution in $D_2O$. Empirical equation that is suitable for this purpose was derived by Horrocks *et al* (Equation (1.11)). [13]

$$q = 1.11(\tau^{-1}_{H_2O} - \tau^{-1}_{D_2O} - 0.31 + 0.45 \cdot n_{OH} + 0.99 \cdot n_{NH} + 0.075 \cdot n_{O=CNH}) \qquad (1.11)$$

where $\tau_i$ is luminescence life-time in environment $i$, $n_{OH}$, $n_{NH}$ and $n_{O=CNH}$ are numbers of alcoholic OH, aminic NH and amidic NH oscillators in the first coordination sphere of the metal ion. This equation holds correct only for europium(III) complexes.

### 1.2.3 UV-VIS spectrophotometry

UV-VIS spectrophotometry is based on absorption of light by solutions. Most common causes for the light absorption in this wavelength range is excitation of (non)bonding electrons into higher energy levels. Experimentally measured quantity is absorbance

$A$ which is defined as negative decadic logarithm of transmittance $T$ (Equation (1.12)).

$$A = -\log T = -\log \frac{I}{I_0} \tag{1.12}$$

where $I$ is the intensity of transmitted light and $I_0$ is the intensity of the received light. Also, according to the Lambert-Beer law (Equation (1.13)), absorbance is directly proportional to concentration of the compound $c_i$ absorbing at the specific wavelength $\lambda$ where $\varepsilon_{\lambda,i}$ is molar extinction coefficient of compound $i$ at the wavelength $\lambda$ and $l$ is length of optical path.

$$A_{\lambda,i} = \varepsilon_{\lambda,i} c_i l \tag{1.13}$$

UV-VIS spectrophotometry can be used to observe kinetics of reactions provided that the absorption profiles of reactant and product are different. In the case of complexation reactions of lanthanide(III) ions by macrocyclic ligands, this condition is fulfilled, since the coordination sphere of the metal ion is changed dramatically during the coordination (Equations. (1.14), (1.15), see below). Free lanthanide(III) ions exist in aqueous solution as nonaaqua ions $[Ln(H_2O)_9]^{3+}$ (Ln = La–Eu) or octaaqua ions $[Ln(H_2O)_8]^{3+}$ (Ln = Sm–Lu) while after reaction with typical macrocyclic ligand $H_nL$, complexes of $[Ln(L)(H_2O)]^{3-n}$ structure for larger lanthanide(III) ions or $[Ln(L)]^{3-n}$ structure for smaller lanthanide(III) ions form, respectively, where $n$ is the charge of the fully deprotonated ligand. The position of *hydration break*, *i.e.* the place in the lanthanide series behind which the dehydrated structure is preferred, depends on the ligand structure. Thus, at least four water molecules are changed for nitrogen ligands from macrocyclic amines and four other water molecules are changed for other functional groups, such as acetates, phosphonates etc in the pendant arms. This change of the coordination environment is manifested in UV-VIS spectra as change of the wavelength of the absorption bands. In this work, UV-VIS spectrophotometry was used to observe kinetics of complex formation and dissociation. Cerium(III) ion has strong absorption bands in UV region. Due to its only one unpaired f-electron, ligand-to-metal charge transfer (LMCT) absorption bands are very prominent.

### 1.2.4 Complexation kinetics

Complexation reactions of f-group cations with macrocyclic ligands occur mostly by two-step mechanism (one notable exception are complexes of DOTAM where complexes form directly by reaction of the fully deprotonated ligand with the metal ion and no intermediate was detected by UV-VIS spectroscopy [14], although such diprotonated *out-of-cage* complex with gadolinium(III) was isolated in the solid state and characterised by X-ray diffraction. [15]) In the first step, weak *out-of-cage* complex forms quickly. In this complex, only the heteroatoms of the pendant arms are coordinated to the metal ion. Since the macrocyclic amino groups in this intermediate are

protonated, the rate-determining step of the full complexation is the deprotonation of the macrocyclic amines and the simultaneous transfer of the metal ion into the macrocyclic cavity. Thus, more stable (and kinetically inert) *in-cage* complex forms and this transfer is catalysed by a base. The process of complexation of $Ce^{3+}$ ion with ligand can be described using chemical Equations (1.14) and (1.15) (charges are omitted for sake of clarity, superscripts OC and IC designate *out-of-cage* and *in-cage* complexes, respectively).

$$Ce^{3+} + H_2L \overset{{}^{f}K}{\rightleftharpoons} [Ce(H_2L)]^{OC} \tag{1.14}$$

$$[Ce(H_2L)]^{OC} \xrightarrow{{}^{f}k} [Ce(L)]^{IC} + 2\,H^{+} \tag{1.15}$$

Therefore, the process of the lanthanide(III) ion complex formation is characterised by two constants: stability constant of the *out-of-cage* complex ${}^{f}K$ (defined by Equation (1.16)) and the rate constant of the lanthanide(III) ion transfer into the macrocyclic cavity ${}^{f}k$.

$${}^{f}K = \frac{[Ce(H_2L)]^{OC}}{[Ce^{3+}][H_2L]} \tag{1.16}$$

The overall rate of the complexation is defined by Equation (1.17) where, in the notation of the relative concentrations of the complex species, one pair of square brackets is omitted for the sake of clarity.

$${}^{f}v = \frac{\mathrm{d}[CeL]^{IC}}{\mathrm{d}t} = {}^{f}k[Ce(H_2L)]^{OC} \tag{1.17}$$

Further, we can substitute for the concentration of the *out-of-cage* complex from Equation (1.16) to get Equation (1.18).

$${}^{f}v = {}^{f}k{}^{f}K[Ce^{3+}][H_2L] \tag{1.18}$$

Under ligand excess conditions, we need to consider that the free metal ion concentration $[Ce^{3+}]$ in the solution is lowered by formation of the *out-of-cage* complex (whereas $[H_2L]$ is considered to be approximately equal to the total analytical concentration of the ligand in all its forms in the pH range 3–7, see distribution diagram Fig. 4.9a, p. 41). Therefore, the total analytical concentration of the metal ion $c_{Ce^{3+}}$ is given by Equations (1.19) and (1.20).

$$c_{Ce^{3+}} = [Ce^{3+}] + [Ce(H_2L)]^{OC} \tag{1.19}$$

$$c_{Ce^{3+}} = [Ce^{3+}]\left(1 + {}^{f}K[H_2L]\right) \tag{1.20}$$

Finally, we can substitute $[Ce^{3+}]$ from Equation (1.20) to Equation (1.18) to obtain the rate of the complex formation under ligand excess conditions Equation (1.21).

$$ {}^{\mathrm{f}}v = \frac{{}^{\mathrm{f}}k\,{}^{\mathrm{f}}K[H_2L]c_{Ce^{3+}}}{1 + {}^{\mathrm{f}}K[H_2L]} \tag{1.21} $$

Since large excess of the ligand is used, Equation (1.21) can be simplified to Equation (1.22) where observed rate constant ${}^{\mathrm{f}}k_{\mathrm{obs}}$ is defined by Equation (1.23).

$$ {}^{\mathrm{f}}v = {}^{\mathrm{f}}k_{\mathrm{obs}} \cdot c_{Ce^{3+}} \tag{1.22} $$

$$ {}^{\mathrm{f}}k_{\mathrm{obs}} = \frac{{}^{\mathrm{f}}k\,{}^{\mathrm{f}}K\,[H_2L]}{1 + {}^{\mathrm{f}}K\,[H_2L]} \tag{1.23} $$

Analogical derivation was used to obtain the definition of the observed formation rate constant under metal ion excess (Equation (1.24)).

$$ {}^{\mathrm{f}}k'_{\mathrm{obs}} = \frac{{}^{\mathrm{f}}k'\,{}^{\mathrm{f}}K'\left[Ce^{3+}\right]}{1 + {}^{\mathrm{f}}K'\left[Ce^{3+}\right]} \tag{1.24} $$

From Equations (1.23) and (1.24), it follows that the parameters ${}^{\mathrm{f}}k$, ${}^{\mathrm{f}}K$ and ${}^{\mathrm{f}}k'$, ${}^{\mathrm{f}}K'$, respectively, can be determined by measuring complexation kinetics under different ligand or metal ion excess at different pH values.

### 1.2.5 Dissociation kinetics

Dissociation of lanthanide(III) complexes of macrocyclic ligands occurs in strongly acidic solutions. This reaction can occur both as acid-catalysed and spontaneous, and can be generally expressed by Equations (1.25) and (1.26), respectively.

$$ [Ce(L)] \xrightarrow{{}^{\mathrm{d}}k_{00}} Ce^{3+} + L \tag{1.25} $$

$$ [Ce(L)] + H^{+} \xrightarrow{{}^{\mathrm{d}}k_{01}} Ce^{3+} + HL \tag{1.26} $$

If this would be the valid mechanism of the acid-catalysed dissociation, the observed dissociation rate constant could be expressed as Equation (1.27) where ${}^{\mathrm{d}}k_{00}$ is spontaneous dissociation rate of the complex [Ce(L)] and ${}^{\mathrm{d}}k_{01}$ is first-order acid-catalysed dissociation rate constant.

$$ {}^{\mathrm{d}}k_{\mathrm{obs}} = {}^{\mathrm{d}}k_{00} + {}^{\mathrm{d}}k_{01} \cdot [H^{+}] \tag{1.27} $$

In some cases, the major complex species in the solution (here [Ce(L)]) does not dissociate at all (*i.e.* ${}^{\mathrm{d}}k_{00} = {}^{\mathrm{d}}k_{01} = 0$) but it undergoes protonation (Equation (1.28)) yielding

protonated intermediate that dissociates either spontaneously (Equation (1.29)) or by acid-catalysed reaction (Equation (1.30)).

$$[\mathrm{Ce(L)}] + \mathrm{H^+} \overset{^{\mathrm{d}}K_{\mathrm{A}}}{\rightleftharpoons} [\mathrm{Ce(HL)}] \tag{1.28}$$

$$[\mathrm{Ce(HL)}] \xrightarrow{^{\mathrm{d}}k_{10}} \mathrm{Ce^{3+}} + \mathrm{HL} \tag{1.29}$$

$$[\mathrm{Ce(HL)}] + \mathrm{H^+} \xrightarrow{^{\mathrm{d}}k_{11}} \mathrm{Ce^{3+}} + \mathrm{H_2L} \tag{1.30}$$

Then the dissociation rate is defined by Equation (1.31) where [complex] is the total analytical concentration of the complex species in the solution.

$$^{\mathrm{d}}v = {}^{\mathrm{d}}k_{\mathrm{obs}}[\mathrm{complex}] \tag{1.31}$$

Two reactions contribute to the dissociation rate and Equation (1.31) can thus be divided into two terms as shown in Equation (1.32) where $^{\mathrm{d}}k_{10}$ is acid-uncatalysed dissociation rate constant of the protonated complex and $^{\mathrm{d}}k_{11}$ is first-order acid-catalysed dissociation rate constant of the protonated complex.

$$^{\mathrm{d}}v = {}^{\mathrm{d}}k_{10}[\mathrm{Ce(HL)}] + {}^{\mathrm{d}}k_{11}[\mathrm{Ce(HL)}][\mathrm{H^+}] \tag{1.32}$$

The concentration of the protonated complex [Ce(HL)] can be substituted from the definition of the dissociation constant of the protonated form (Equation (1.33)) into Equation (1.32) to obtain Equation (1.34).

$$K_{\mathrm{a}} = \frac{[\mathrm{Ce(L)}][\mathrm{H^+}]}{[\mathrm{Ce(HL)}]} \tag{1.33}$$

$$^{\mathrm{d}}v = \left({}^{\mathrm{d}}k_{10} + {}^{\mathrm{d}}k_{11}[\mathrm{H^+}]\right)\left(\frac{[\mathrm{Ce(L)}][\mathrm{H^+}]}{K_{\mathrm{A}}}\right) \tag{1.34}$$

Equations (1.31) and (1.34) can be combined to obtain Equation (1.35).

$$^{\mathrm{d}}k_{\mathrm{obs}}[\mathrm{complex}] = \left({}^{\mathrm{d}}k_{10} + {}^{\mathrm{d}}k_{11}[\mathrm{H^+}]\right)\left(\frac{[\mathrm{Ce(L)}][\mathrm{H^+}]}{K_{\mathrm{A}}}\right) \tag{1.35}$$

Total complex concentration $[\mathrm{complex}] = [\mathrm{Ce(L)}] + \dfrac{[\mathrm{Ce(L)}][\mathrm{H^+}]}{[\mathrm{Ce(HL)}]}$ can be substituted into Equation (1.35) and after re-arranging, the observed dissociation rate constant Equation (1.36) is obtained.

$$^{\mathrm{d}}k_{\mathrm{obs}} = \frac{{}^{\mathrm{d}}k_{10} \cdot \dfrac{[\mathrm{H^+}]}{K_{\mathrm{A}}} + {}^{\mathrm{d}}k_{11} \cdot \dfrac{[\mathrm{H^+}]^2}{K_{\mathrm{A}}}}{1 + \dfrac{[\mathrm{H^+}]}{K_{\mathrm{A}}}} \tag{1.36}$$

### 1.2.6 Potentiometry

Potentiometric titrations allow us to experimentally determine the protonation constants of the prepared ligand and stability constants of its complexes. Glass electrode is an ion-selective electrode that is selective for $H^+$ ions, although, in strongly basic solutions, $OH^-$ ions and cations of the base can also contribute to its potential (alkaline electrode error). On the other hand, in strongly acidic solutions, surface of the glass membrane is over-saturated with $H^+$ ions and the observed potential is biased. Therefore, the useful pH range in potentiometric titrations is limited to roughly 1.5–12. Potential of the electrode is given by Equation (1.37) where the term $E_0$ contains the standard potentials of the electrodes used and contributions of inert ions to the liquid-junction potential, $S$ is Nernstian slope, ideally equal to 59.1 mV and $j_1$ and $j_2$ compensate for acidic and alkaline errors, respectively, and $K_w$ is ionic product of water under the conditions of the titration.

$$E = E_0 + S \cdot \log [H^+] + j_1 \cdot [H^+] + j_2 \cdot \frac{K_w}{[H^+]} \tag{1.37}$$

This equation is used for calibration of the glass electrode by strong acid-strong base titration.

## 1.3 Structure of complexes of macrocyclic ligands

Structure of complexes of macrocyclic ligands in solution will be explained here using a lanthanide(III) complex of DOTA as an example. Eight coordination sites are occupied with donor atoms of the ligand. Four nitrogen atoms of the macrocycle form $N_4$ plane and four oxygen donor atoms of the pendant arms form $O_4$ plane and the planes are mutually parallel. There are two possible geometries of the complex according to the torsion angle between these two planes. The structure can be square antiprismatic (SA) with torsion angle ideally equal 45° or twisted-square antiprismatic (TSA) with torsion angle ideally equal −22.5°. While SA isomer is preferred for smaller lanthanide(III) ions, TSA isomer is preferred for larger ones as it has larger macrocyclic cavity. Ninth ($O_4$ plane capping) coordination site is usually occupied by a water molecule. In the end of the lanthanide series, coordinated water molecule may be lost and so-called TSA' isomer becomes more stable. These isomers are in dynamic equilibrium in solution and interconvert by processes of arm rotation and ring inversion. These movements are shown in Fig. 1.4. The dynamics of these isomers in solution for europium(III) complex of DOTA has been recently studied by EXSY. [16]

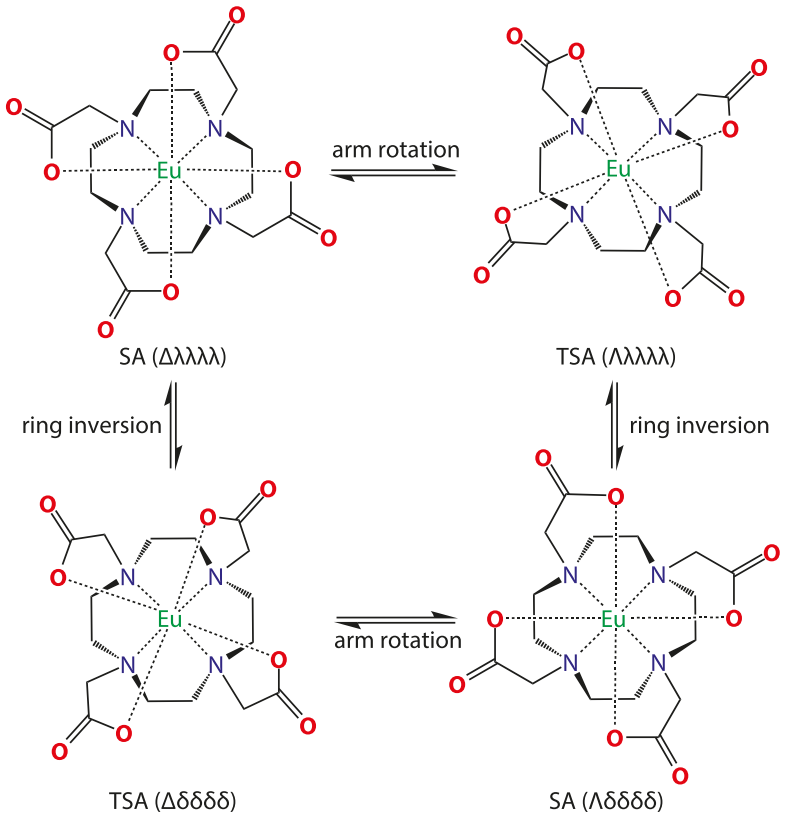


Figure 1.4: Four stereoisomers of complex $[Eu(dota)(H_2O)]^-$ present in solution. Water molecule is omitted for clarity.

## 1.4 Ligand design

One of the most studied macrocyclic ligands is DOTA (2605 references in SciFinder database as of 26/04/2019). Formation and dissociation kinetics of its cerium(III) complex have been investigated [17] as well as stability constants of its complexes with various metal ions [18, 19] and also solution dynamics of its europium(III) complex. [16] Analysis of relaxometric measurements of its gadolinium(III) complex has also been done. [20]

The most common way how to attach biological vectors to DOTA skeleton is through formation of an amide. Therefore, amide derivatives of DOTA are of interest as well. Both DOTA and DOTA-tetraamide (DOTAM: 68 references in SciFinder database as of 07/05/2019 and DOTA-$(MeAM)_4$: 30 references) have been studied. Similarly to DOTA, formation kinetics of its lanthanide(III) complexes have been studied [14], stability constants of its complexes [21] and also relaxometric measurements of its gadolinium(III) complex have been done. [22]

Other simple amide derivatives of DOTA have not been studied. We decided to prepare the simplest *trans*-diamide derivative of DOTA and study its properties to fill in the gap in the DOTA—DOTAM series. Several *trans*-diamide derivatives of DOTA have been synthesised and studied. The simplest derivative studied so far was bis-(dimethyl amide) derivative of DOTA (DO2A-2DMA), the lanthanide(III) complexes thereof have been studied only from NMR and relaxometric point of view. [23] Europium(II/III) complexes of *trans*-bis-(glycinamide) (DO2A2Am$^{Gly}$) derivative were studied as $T_1$ MRI contrast agents in the case of Eu(II) complex and CEST [3] contrast agent in the case of Eu(III) complex allowing for bimodal imaging sensitive to oxygen concentration. Redox properties of Eu(III)/Eu(II) system were investigated as well as its NMR properties in solution. [24, 25] Recently, bis(*N*-4'-trifluoromethylphenyl) derivative of DOTA-diamide (DO2A2Am$^{TFMP}$) has been synthesised and studied as a dual $^{1}H/^{19}F$ MRI probe. [26] In summary, several DOTA-diamide derivatives have been studied but only a little chemical information (such as kinetics of complex formation and dissociation or thermodynamic stability constants) has been published.

In the effort to find a ligand with faster complexation kinetics, it was tried to increase the stability of the *out-of-cage* complex by attaching a strongly coordinating pendant arm (bisphosphonate in DO3A-AM$^{BP}$ or phosphinate-iminodiacetate in DO3AP$^{IDA}$). [27, 28] However, this was unsuccessful as although the stability constant of the *out-of-cage* complex increased, the rate constant of the metal ion transfer into the macrocyclic cavity decreased due to too high stability of the *out-of-cage* complex and, thus, making the overall complexation reaction slower. Therefore, we decided to study kinetics of a ligand, that has two weaker coordinating acetamide pendant arms and also to fill in the gap in the DOTA—DOTAM series in this aspect. The ligands mentioned in this section are shown in Fig. 1.5.

[3] CEST = chemical exchange saturation transfer

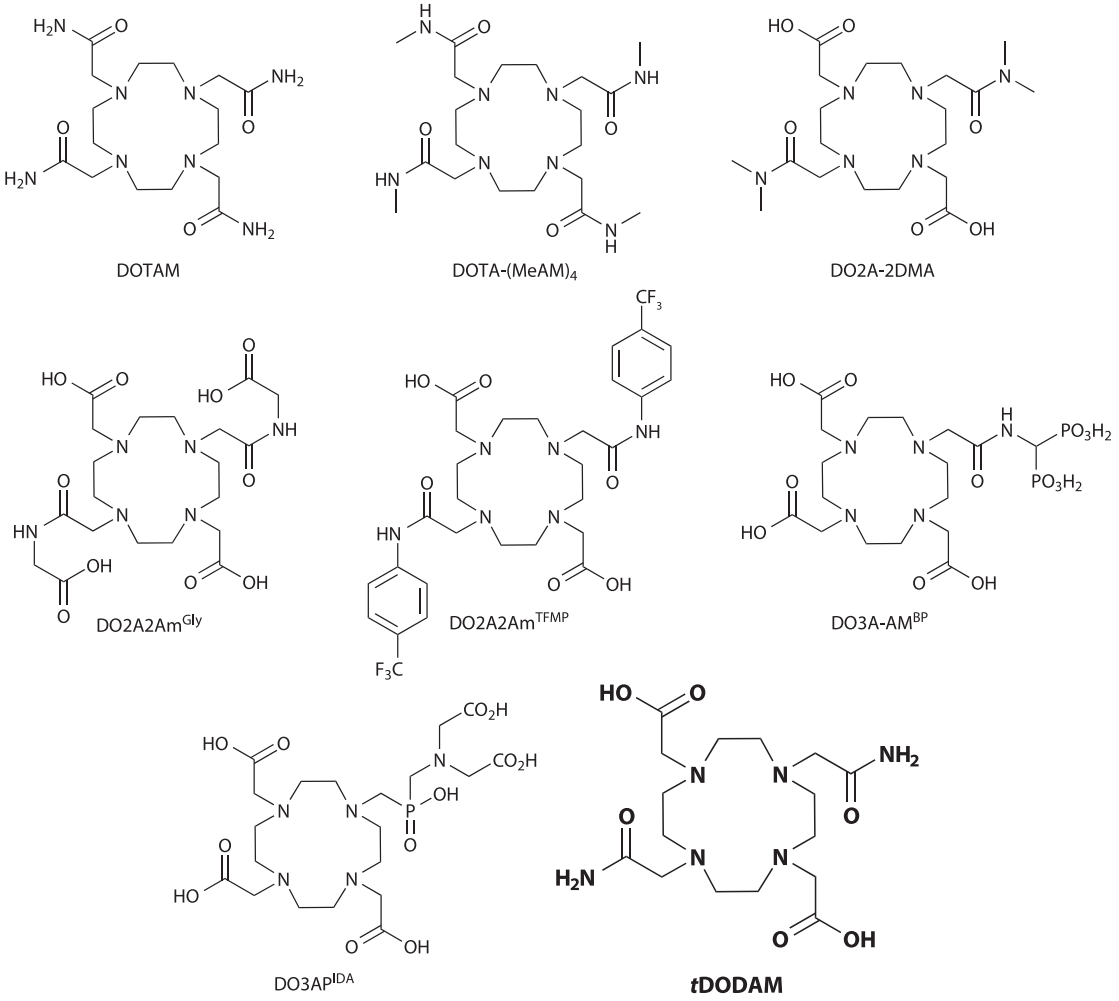


Figure 1.5: Diamide ligands known from literature and other relevant ligands mentioned in section 1.4.

# Chapter 2

# Aim of the Thesis

The aim of this Thesis is to prepare *trans*-DOTA-diamide ligand (*t*DODAM, Fig. 2.1) and to study its properties. In particular to:

- Study the formation and the dissociation kinetics of its cerium(III) complex by UV-VIS spectrophotometry
- Determine the protonation constants of the ligand and stability constants of its complexes by potentiometry
- Study the structure of its lanthanide(III) complexes in solution by NMR and luminescence spectrophotometry and in the solid state by X-ray diffraction
- Study the dynamics of its europium(III) complex in solution by $^{1}$H – $^{1}$H-2D EXSY.

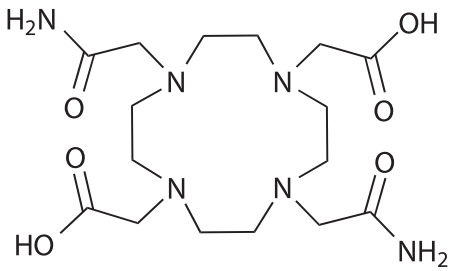


Figure 2.1: Structure of the prepared ligand *t*DODAM.

# Chapter 3

# Experimental Section

## 3.1 General remarks

All chemicals and solvents were obtained from commercial sources (Lachema, Sigma Aldrich, Acros, Fluka) and used without further purification.

NMR spectra of synthetic intermediates and the title ligand were obtained using Bruker Ascend 400 NMR spectrometer equipped with broadband probe or Varian VNMRS 300 equipped with four-nuclei autoswitchable probe. NMR titration was done using Varian VNMRS 300 and NMR spectra of lanthanide(III) complexes were obtained using Varian VNMRS 400 equipped with four-nuclei autoswitchable probe and Bruker Avance III 600 equipped with triple resonance cryoprobe, respectively. The spectra were referenced on TMS ($\delta_H$ = 0.00 ppm, $\delta_C$ = 0.00 ppm in $CDCl_3$) or *t*BuOH ($\delta_H$ = 1.24 ppm, $\delta_C$ = 30.3 ppm in $D_2O$) and analysed in program MestReNova. Unless otherwise stated, all measurements were done at 25 °C.

MS spectra were obtained using mass spectrometer Bruker Esquire 3000 using electrospray ionisation and ion-trap detection in both positive and negative mode.

UV-VIS spectra were obtained using spectrophotometer Specord 50 Plus (Analytic Jena AG) in the range of wavelengths from 190 to 400 nm (in the range 190–320 nm and 320–400 nm deuterium and halogen lamps were used, respectively). The temperature was maintained by the Peltier Block at 25.0 ± 0.1 °C.

Silica gel 60 $F_{254}$ (Merck) plates were used for thin-layer chromatography (TLC). Spots were visualised by UV detection for compounds containing aromatic ring (Compounds **2, 3**) and Dragendorff reagent (solution of $Bi(NO_3)_3$ and KI in aqueous acetic acid) was used for other compounds.

The purity of the prepared compounds was also checked using HPLC machine equipped with UV detector (at 254 nm and 210 nm). Reverse-phase Reprosil-C8 Gold and Reprosil-C18 Gold columns were used. For elution, mixture of deionised water (Millipore) (A), acetonitrile (Rotisolv, HPLC grade) (C) and 0.1% aqueous solution of tri-

fluoroacetic acid (B) was used. The composition of the mixture was gradually changed as shown in Table 3.1.

Table 3.1: HPLC conditions used to check the purity of the prepared compounds

| **P34** | | | | **P59** | | | |
|---|---|---|---|---|---|---|---|
| time (min) | A | B | C | time (min) | A | B | C |
| 0 | 85 | 10 | 5 | 0 | 95 | 5 | 0 |
| 5 | 0 | 10 | 90 | 10 | 85 | 5 | 10 |
| 10 | 0 | 10 | 90 | 20 | 70 | 5 | 25 |
| 11 | 85 | 10 | 5 | 30 | 0 | 5 | 95 |
| 21 | 85 | 10 | 5 | 35 | 0 | 1 | 99 |

The stock aqueous solution of HCl (≈ 0.03 M) for potentiometry was prepared from 35 % aqueous HCl (analytical grade). Commercial $(NMe_4)Cl$ was recrystallised from boiling *i*PrOH and the solid salt was dried over $P_2O_5$ in vacuum to constant weight. Carbonate-free $(NMe_4)OH$ solution (≈ 0.2 M) was prepared from the recrystallised $(NMe_4)Cl$ using ion exchanger Dowex 1 in the $OH^-$-form (elution with carbonate-free water, under argon). The hydroxide solution was standardized against potassium hydrogen phthalate and the stock HCl solution against the ≈ 0.2 M $(NMe_4)OH$ solution. Stock solutions of the individual metal cations were prepared by dissolving hydrates of metal chlorides in deionised water and the metal ions contents were determined by titration with a standard $Na_2(H_2edta)$ solution. For potentiometric titrations, pH-meter PHM 240 equipped with combined glass electrode GK 2401C was used. The determined equilibrium constants are concentration constants. Throughout the Thesis, pH means $-\log[H^+]$. The potentiometric measurements were conducted by Mgr. Zuzana Böhmová.

For general pH measurements, pH-meter Jenway 3505 equipped with freshly calibrated (buffers with pH = 7.00 and 4.00) H-pH-1 electrode was used. To calculate pD of NMR samples in $D_2O$, the pH reading was corrected by factor of +0.41.

Diffraction data were collected at 120 K (Cryostream Cooler, Oxford Cryosystem) by Bruker D8 VENTURE Kappa Duo PHOTON100 diffractometer with IμS micro-focus sealed tube using Mo-$K\alpha$ radiation ($\lambda$ = 0.71073 Å). The frames were integrated with the Bruker SAINT software package using a narrow-frame algorithm. Data were corrected for absorption effects using the multi-scan method (SADABS). All structures were solved by direct methods (SHELXT2014 ) [29] and refined using full-matrix least-squares techniques (SHELXL2018, shelXle). [30, 31] All non-hydrogen atoms were refined anisotropically. All hydrogen atoms were found in the difference density map. However, the appropriate numbers of hydrogen atoms bound to carbon atoms were fixed in theoretical positions using $U_{eq}(H) = 1.2U_{eq}(C)$ to keep a number of parame-

ters low, and only hydrogen atoms bound to heteroatoms (N, O) were tried to be fully refined. However, in some cases, positions of hydrogen atoms bound to heteroatom had to be fixed to original coordinates as group geometry during refinement became unrealistic (too long or short bonds). The X-ray data were acquired by RNDr. Ivana Císařová, CSc. and the structures were refined by Doc. RNDr. Jan Kotek, PhD.

Relaxometric measurements were done with assistance from Dr. Fabio Carniatto during my stay in Alessandria (1 week) and the experimental results were fitted by Prof. Mauro Botta (both Department of Science and Technology, University of Eastern Piedmont, Alessandria, Italy). Low-field part of the $^1$H NMRD profiles (proton Larmor frequency range 0.01–10 MHz) was obtained using fast field-cycling Stelar Smart Tracer relaxometer. High-field part of the $^1$H NMRD profiles (proton Larmor frequency range 20–120 MHz) was obtained using Stelar Spinmaster high-field relaxometer. BMS measurements were obtained using Bruker Avance III 500.

## 3.2 Synthesis of *t*DODAM

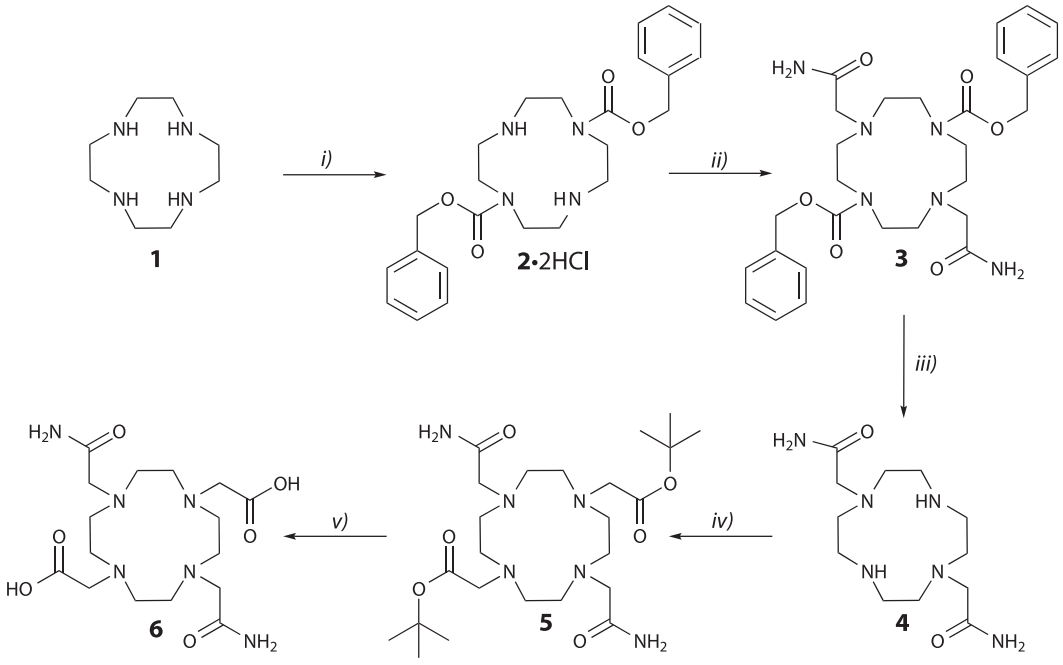


Scheme 3.1: *i)* $PhCH_2OCOCl/CHCl_3$, 0 °C → RT[1], overnight (87 %) *ii)* $ClCH_2CONH_2/K_2CO_3$/MeCN, 65 °C, 3 d (74 %) *iii)* $H_2$/10% Pd(C) / EtOH, RT, overnight (95 %) *iv)* $BrCH_2CO_2{}^tBu/K_2CO_3$/MeCN, RT, 2 d (96 %) *v)* $CF_3CO_2H/CH_2Cl_2$, 35 °C, overnight (86 %).

[1] RT = room temperature

### 3.2.1 Synthesis of compound 2 · 2 HCl

Cyclen (compound **1**) (8.14 g; 47.2 mmol) was dissolved in chloroform (300 ml) in 500-ml round-bottom flask and the solution was placed into an ice bath. Using linear pump, benzyl chloroformate (22 g; 129 mmol; 2.7 equiv; 90% purity as determined using $^1$H NMR) was added during 1 h. The reaction mixture was stirred overnight giving a suspension of a white compound. The solvent was removed by rotary evaporation and the residue was triturated by $Et_2O$ (≈ 100 ml) using ultrasonic agitation. The suspension was transferred onto a fritted glass filter, the white solid was washed with $Et_2O$ and dried on air yielding **2** · 2 HCl (21.0 g; 87 %). **$^1$H NMR ($D_2O$, 300 MHz):** 7.50–7.42 (10H, bs, Ph), 5.20 (4H, s, OC$H_2$Ph), 3.65 (8H, s, OC(O)NC$H_2$), 3.25 (8H, bs, OC(O)NCH$_2$C$H_2$); **$^{13}$C{$^1$H} NMR ($D_2O$, 101 MHz):** 158.5 (*C*=O), 135.6 (Ph), 128.9 (Ph), 128.8 (Ph), 128.4 (Ph), 68.6 (O*C*H$_2$Ph), 46.9 (OC(O)N*C*H$_2$), 43.3 (OC(O)NCH$_2$*C*H$_2$). **MS (ESI):** found (calcd) (+) 441.2 (441.2) [M + H]$^+$. **TLC:** ($SiO_2$/25% aq. $NH_3$—EtOH = 1:5): $R_f$(**1**) = 0, $R_f$(**2**) = 0.3. **HPLC (UV):** (Reprosil-C8 Gold/P34): $t$ = 7.06 min.

### 3.2.2 Synthesis of compound 3

Diprotected cyclen dihydrochloride salt (compound **2** · 2 HCl) (1.00 g; 1.95 mmol) and 2-chloroacetamide (1.29 g; 13.8 mmol; 7.1 equiv) were dissolved in acetonitrile (150 ml) in 250-ml round-bottom flask. Dried $K_2CO_3$ (2.25 g; 16.3 mmol; 8.3 equiv) was added and the reaction mixture was stirred at 65 °C for 3 days. The reaction mixture was filtered and the solvent was removed to dryness by rotary evaporation. The solid residue was dissolved in chloroform (30 ml), transferred into 100-ml separatory funnel and the solution was washed with water (3 × 30 ml). The organic layer was dried with $K_2CO_3$ which was subsequently removed by filtration through a cotton plug. Chloroform was removed by rotary evaporation to dryness. The crude product was re-dissolved in a minimal amount of boiling acetonitrile and left to cool down and crystallise in freezer overnight. The solid white product was filtered, washed with $Et_2O$ and dried on air yielding **3** (0.798 g; 74 %). **$^1$H NMR ($CDCl_3$, 300 MHz):** 7.35 (10H, s, Ph), 7.14 (2H, bs, CON$H_2$), 5.20 (2H, bs, CON$H_2$),5.10 (4H, s, PhC$H_2$), 3.42 (8H, s, C$H_2$NCO$_2$Bn), 3.11 (4H, s,C$H_2$CO), 2.78 (8H, s, C$H_2$NCH$_2$CO); **$^{13}$C{$^1$H} NMR ($CDCl_3$, 101 MHz):** 171.8 (*C*ONH$_2$), 155.1 N(*C*O), 134.4 (Ph), 126.8 (Ph), 126.6 (Ph), 126.5 (Ph), 65.7 (Ph*C*H$_2$), 56.0 (N*C*H$_2$CO), 53.1 (*C*H$_2$NCO$_2$), 46.6 (N*C*H$_2$). **MS (ESI):** found (calcd) (+) 593.1 (593.2) [M + K]$^+$. **TLC:** ($SiO_2$/(25% aq. $NH_3$—EtOH = 1:5)—EtOAc = 7:3): $R_f$(**2**) = 0.3, $R_f$(**3**) = 0.9. **HPLC (UV):** (Reprosil-C8 Gold/P34): $t$ = 6.85 min.

### 3.2.3 Synthesis of compound 4

Diprotected cyclen-diacetamide (compound **3**) (3.07 g; 5.54 mmol) was dissolved in absolute ethanol (225 ml) in 500-ml round-bottom flask on heating and 10% Pd/C

(0.307 g; 10 %) was added. The flask was flushed with argon in order to remove air and a balloon with hydrogen was connected through Tygon® gas-tight tubing and the balloon valve was opened. The reaction mixture was stirred under $H_2$ at room temperature overnight. Then, the catalyst was filtered off and the solvent was removed by rotary evaporation giving **4** (1.50 g; 95 %) as a white solid. **$^1$H NMR ($D_2O$, 400 MHz):** 3.22 (4H, s, NC$H_2$CO), 2.63 (16H, bs, ring C$H_2$); **$^{13}$C{$^1$H} NMR ($D_2O$, 101 MHz):** 177.3 (*C*=O), 58.2 (N*C*$H_2$CO), 52.0 (*C*$H_2$NC$H_2$CO), 43.5 (*C*$H_2$C$H_2$NC$H_2$CO). **MS (ESI):** found (calcd) (+) 287.2 (287.2) $[M + H]^+$. **TLC:** ($SiO_2$/$^i$PrOH—25% aq. $NH_3$—$H_2O$=6:2:2): $R_f$(**3**) = 0.8, $R_f$(**4**) = 0.1. **HPLC (UV):** (Reprosil-C8 Gold/P59): $t$ = 2.5 min.

### 3.2.4 Synthesis of compound 5

*Trans*-cyclen-diacetamide (compound **4**) (0.717 g; 2.5 mmol) was dissolved in acetonitrile (240 ml) in 500-ml round-bottom flask and dried $K_2CO_3$ (2.1 g; 15 mmol; 6 equiv) was added as a base. *Tert*-butyl bromoacetate (1.1 g; 5.75 mmol; 2.3 equiv) dissolved in acetonitrile (40 ml) was added dropwise from dropping funnel during 1 h and the reaction mixture was stirred at RT for 2 days. The reaction mixture was filtered off, solvent was removed by rotary evaporation to dryness. The white solid residue was suspended in chloroform (cca. 50 ml) and undissolved KBr was filtered. The filtrate was evaporated *in vacuo* yielding **5** (1.24 g; 96 %) as a white solid. **$^1$H NMR ($CDCl_3$, 400 MHz):** 8.60 (2H, s, CON$H_2$), 5.44 (2H, s, CON$H_2$), 3.06 (4H, s, NC$H_2$C$O_2$), 2.97 (4H, s, NC$H_2$CONH$_2$), 2.59 (8H, s, C$H_2$NC$H_2$C$O_2$), 2.52 (8H, s, C$H_2$NC$H_2$CONH$_2$), 1.37 (18H, s, C$H_3$); **$^{13}$C{$^1$H} NMR ($CDCl_3$, 101 MHz):** 174.7 (*C*ON), 170.3 (*C*$O_2$), 81.5 (O*C*$(CH_3)_3$), 57.8 (N*C*$H_2$CONH$_2$), 57.4 (N*C*$H_2$C$O_2$), 55.1 (*C*$H_2$NCH2CONH2), 53.2 (*C*$H_2$NC$H_2$C$O_2$), 28.3 (*C*$H_3$). **MS (ESI):** found (calcd) (+) 553.4 (553.3) $[M + K]^+$, 537.4 (537.3) $[M + Na]^+$, 515.4 (515.4) $[M + H]^+$. **EA:** found (calcd for $C_{24}H_{46}N_6O_6$) C: 55.84 (56.01), H: 8.86 (9.01), N: 15.99 (16.33). **TLC:** ($SiO_2$/(25% aq. $NH_3$—EtOH = 1:5)—EtOAc = 8:2): $R_f$(**4**) = 0, $R_f$(**5**) = 0.8. **HPLC (UV):** (Reprosil-C18 Gold/P34): $t$ = 5.56 min.

Single crystals of the compound **5** were obtained by gas-phase diffusion of $Et_2O$ into a solution of **5** prepared by dissolving a spatula-tip amount of this compound in 0.4 ml of $CHCl_3$. After 1 day, crystals suitable for X-ray crystallographic analysis were formed.

### 3.2.5 Synthesis of *t*DODAM (compound 6)

Di-*t*-butyl ester (compound **5**) (0.722 g; 1.403 mmol) was dissolved in dichloromethane (20 ml) in 50-ml pear-shaped flask and trifluoroacetic acid (5 ml) was added. The solution was stirred at 35 °C overnight. Volatiles were removed by rotary evaporation yielding a white solid. This was dissolved in a minimal amount of water and trifluoroacetate anion was removed by ion-exchange chromatography on Dowex 50 WX4-100 (strongly acidic cation-exchange resin) in $H^+$-cycle. The title compound

was eluated by 10% pyridine in water. The eluate was collected until drop of eluate gave negative reaction with Dragendorff reagent on TLC plate. The solvents were removed by rotary evaporation and the slightly yellow solid residue was re-dissolved in water (50 ml) and evaporated a few times with water in order to remove pyridine (its complete removal was proven by the lack of signals in aromatic region in $^1$H NMR spectrum). The crude product was dissolved in a small amount of water (10 ml) and acetone was added until cloudiness and the mixture was left to crystallise in a fridge overnight. The white crystalline solid was filtered, washed with acetone and thoroughly dried on air. The overall yield of the reaction after the purification was 0.550 g, corresponding to 86 % (calcd for $\mathbf{6} \cdot 3\,H_2O$). **$^1$H NMR ($D_2O$, pD = 5.2, 400 MHz):** 3.85 (4H, s, $CH_2CONH_2$), 3.50 (8H, bs, $CH_2NCH_2CONH_2$), 3.48 (4H, s, $CH_2CO_2$), 3.24–2.85 (8H, m, $CH_2NCH_2CO_2$); **$^{13}$C{$^1$H} NMR ($D_2O$, pD = 5.2, 101 MHz):** 175.2 ($CO_2H$), 169.8 ($CONH_2$), 56.5 ($CH_2CONH_2$), 55.2 ($CH_2CO_2H$), 51.2 ($CH_2NCH_2CONH_2$), 48.3 ($CH_2NCH_2CO_2$). **MS (ESI):** found (calcd) (+) 425.5 (425.2) $[M + Na]^+$; (–) 401.3 (401.2) $[M - H]^-$. **EA:** found (calcd for $C_{16}H_{30}N_6O_6 \cdot 3\,H_2O$) C: 41.66 (42.10), H: 7.73 (7.95), N: 18.06 (18.41). **TLC:** ($SiO_2$/(25% aq. $NH_3$—EtOH = 1:5)—EtOAc = 8:2): $R_f$(**5**) = 0.8, $R_f$(**6**) = 0.05. **HPLC (UV):** (Reprosil-C18 Gold/P59): $t$ = 3.52 min.

Single crystals of *t*DODAM were obtained by slow crystallisation from small volume of aqueous solution of **6** (prepared by dissolving a spatula-tip amount of the ligand *t*DODAM in three drops of deionised water) in closed glass vial by adding a layer of ethanol on top of the aqueous solution. After a week, crystals suitable for X-ray crystallographic analysis were formed.

## 3.3 Kinetics of the system $Ce^{3+}$—*t*DODAM

### 3.3.1 UV-VIS spectra of $[Ce(H_2O)_9]^{3+}$, and the *out-of-cage* and *in-cage* complexes

In the spectrophotometric quartz cell, 0.1 M aq. $CeCl_3$ (10 µl; final total concentration in the cell $1 \times 10^{-3}$ M), 4M aq. KCl (125 µl; final concentration in the cell 0.5 M) and 1M aq. MES/KOH (pH=5.47, 200 µl; final total concentration in the cell 0.2 M) and water (655 µl) were mixed and UV-VIS spectrum was recorded in the range of wavelengths of 190–400 nm (spectrum of $[Ce(H_2O)_9]^{3+}$). After addition of the 0.1M aq. ligand solution (10 µl; final total concentration in the cell $1 \times 10^{-3}$ M), UV-VIS spectrum corresponding to formation of the *out-of-cage* complex was recorded immediately (spectrum of a mixture of $[Ce(H_2O)_9]^{3+}$ and the *out-of-cage* complex). After gradual addition of aq. KOH (1 M) until the pH 7 in the cell was reached (checked by pH-meter), a quantitative formation of the *in-cage* complex could be observed in the UV-VIS spectrum. In order to find out if the complexation occurs through the same *out-of-cage* complex under both ligand and metal ion excess, following experiment was conducted. Absorption

spectra of reaction mixtures containing 50-fold excess of either the ligand or the metal ion (the final total concentration in the cell $5 \times 10^{-2}$ M) at pH 5.47 and 6.90 immediately after the addition of the solution of the reactant used in smaller concentration (the final total concentration in the cell $1 \times 10^{-3}$ M) were recorded. For these measurements, the solution containing the buffer (MES = 2-(*N*-morpholino)ethanesulfonic acid or HEPES = 2-[4-(2-hydroxyethyl)piperazin-1-yl]ethanesulfonic acid; the final concentration in the cell 0.2 M), KCl (the final concentration in the cell 0.5 M), and the reactant used in the 50-fold excess was used as a blank; in other measurements, an empty cell was used.

### 3.3.2 Formation kinetics

The experiments were carried out in the pH range of 5.47–6.90 at the temperature 25 ± 0.1 °C. The kinetics was studied using the following f-block metal ion non-coordinating buffers ($c$ = 0.2 M): MES (pH 5.47–6.65) and HEPES (pH 6.90). Constant ionic strength was maintained by KCl (0.5 M). The complexation was observed under both the ligand and the metal ion excess. Stock solution of $Ce^{3+}$ ($c \approx 0.1$ M) was prepared by dissolving $CeCl_3 \cdot 7\,H_2O$ (0.3761 g) in water (10 ml) and the stock solutions of ligand ($c \approx 0.060$ and 0.25 M) were prepared by dissolving the ligand (0.096 or 0.151 g, respectively) in water (4 or 1.5 ml, respectively).[2] Buffer solutions were prepared by dissolving MES or HEPES (0.9762 g or 1.1915 g; 5 mmol) in water (3 ml), adjusting pH to the desired value by addition of the stock KOH solution (1.8 M). Then, such volume of water was added that the total volume of the buffer solution was 5 ml. Finally, pH of the prepared buffers was re-checked.

Appropriate buffer solution (0.2 ml; 1 M; final total concentration in cell 0.2 M), KCl (0.125 ml; 4 M; final total concentration in cell 0.5 M), the ligand and water (such volume that the total volume of the solution in the cell after the addition of the stock $CeCl_3$ solution was 1.0 ml) were mixed in 1-cm sample cell, pH was checked and the temperature of the solution was set to 25 °C using Peltier block. Enough time was allowed for the solution to reach the desired temperature (at least 5–10 min) and the stock $CeCl_3$ solution was added. The solution in the cell was briefly shaken and the absorbance at 320 nm was measured immediately (measurement dead time ≈ 10 s). The measurements were conducted generally for at least three half-times. After the measurement, pH was checked in order to ensure that pH during the reaction was constant. Also, absorption spectrum of the final mixture was measured in order to check that no other form of ligand—metal complex than $[CeL]^{IC}$ is present.

[2] All masses, molar quantities and concentrations of the ligand and its solutions were calculated using the molar mass of anhydrous ligand. Although, it was later found by elemental analysis that the ligand crystallises as a trihydrate, these values were not recalculated, since the measurements are mostly done under a large excess of ligand or metal ion. Thus, the relatively small error will not significantly affect the measurement.

### 3.3.3 Dissociation kinetics

Approximately 0.01 M solution of the cerium(III) complex of *t*DODAM was prepared as follows: into a 4-ml vial, the ligand as **6** · 3 $H_2O$ (0.0092 g; 0.02 mmol) was weighed, 0.05119 M aq. $CeCl_3$ (0.390 ml, 0.02 mmol, 1 equiv) was added and the pH was raised by addition of 0.5 M aq. NaOH to 6.5. The solution was stirred overnight in an oil bath at 50 °C and then its pH was readjusted to 6.5, and the solution was stirred overnight again. When the pH did not change anymore after stirring overnight, 0.5 M solution of NaOH was added until pH 10 was reached. The solution was then filtered through 0.2μm microfilter into a clean 4-ml vial, neutralised to pH = 7 by addition of 0.25 M aq. HCl and evaporated *in vacuo* to dryness. The obtained white solid was dissolved in deionised water (1.000 ml) to get stock solution.

The experiments were carried out in perchloric acid in the concentration range 0.05–3 M and at the temperature 25 ± 0.1 °C. The concentration of the cerium(III) complex in the cell was 2 mM and the ionic strength was maintained by combination of $HClO_4$ and $NaClO_4$ ($I$[(H, Na)$ClO_4$] = 3 M). The absorbance at 252 nm (wavelength of absorption maximum of $[Ce(H_2O)_9]^{3+}$) was observed until at least three half-times elapsed.

## 3.4 Potentiometric titrations

Potentiometric titrations were conducted according to the procedure previously described in literature. [28] Analytical concentration of a ligand stock solution was determined together with protonation constants using OPIUM software package. The in-cell titrations were carried out in a vessel thermostatted at 25.0 ± 0.1 °C, at ionic strength $I$ = 0.1 M ($(NMe_4)Cl$) and in the presence of extra HCl using a PHM 240 pH-meter, a 2-ml ABU 900 automatic piston burette and a GK 2401C combined electrode (all Radiometer, Denmark). The in-cell titrations were carried out in pH range 1.7–12.0 with at least 40 points per titration and at least three parallel titrations ($c_L$ = 0.004 M, $c_M$ = 0.004 M).

The stability constants of the $Ln^{III}$ complexes were obtained by *out-of-cell* method. The batches (starting volume 1 ml) were prepared under Ar stream in tubes with ground joints from ligand, metal ion and HCl/$(NMe_4)Cl$ stock solutions and water ($c_L$ = $c_M$ ≈ 0.004 M, 5% ligand excess). Then a known amount of $(NMe_4)OH$ standard solution was added under Ar. The tubes were firmly closed with stoppers and the solutions were equilibrated at room temperature for 21 days. Titrations were performed in the pH ranges 1.6–6.2 (the final pH values) with 23 data points per whole titration and two titrations per system. The constants (with standard deviations) were calculated with program OPIUM. The program minimises the criterion of the generalized least-squares method using the calibration function (Equation (1.37), p. 16). The cali-

bration parameters were determined from titration of standard aq. HCl with standard aq. ($NMe_4$)OH before and after each ligand or ligand–metal titration to give pairs of calibration and titration, which was used for calculations of the constants. The overall protonation constants $\beta_n$ are defined by Equation (3.1).

$$\beta_n = \frac{[H_nL]}{[H^+]^n[L]} \tag{3.1}$$

Overall protonation constants were transformed to consecutive protonation constants according to Equations (3.2) and (3.3):

$$\log K_1 = \log \beta_1 \tag{3.2}$$

$$\log K_n = \log \beta_n - \log \beta_{n-1} \tag{3.3}$$

The overall stability constants are defined by Equation (3.4):

$$\beta_{hlm} = \frac{[H_hL_lM_m]}{[H]^h[L]^l[M]^m} \tag{3.4}$$

Titrations were conducted with the free ligand and its complexes with the following metal ions: $Cu^{2+}$, $Zn^{2+}$, $Pb^{2+}$, $Ce^{3+}$, $Eu^{3+}$, $Lu^{3+}$.

## 3.5 NMR titration

The prepared ligand *t*DODAM was also studied in aqueous solution by NMR titration. For this experiment, 23 mg of the ligand were weighted into a NMR tube and dissolved in 0.5 ml of $H_2O$. The pH of this solution was measured and coaxial insert tube containing *t*BuOH in 10% $D_2O$ was used for locking and shimming and then the $^1H$ NMR spectrum was obtained. All NMR spectra were referenced to *t*BuOH ($\delta$ = 1.24 ppm). Then, the pH of the solution was changed by addition of 3 or 0.3% aq. HCl. The pH was changed between the measurements by about 0.2 to 0.4 units and the lowest pH at which the NMR spectrum was taken was 0.2. Then the pH was raised gradually to 13.01 by addition of 5 or 1% aq. CsOH. Again the difference in pH between two measurements was about 0.2 to 0.4 units. After each pH change the spectrometer was locked and shimmed. Obtained spectra were processed using MestReNova and the data (dependences of chemical shifts on pH) were fitted using program P from the OPIUM software package. [32]

## 3.6 Synthesis of lanthanide(III) complexes of the ligand *t*DODAM

In a 4-ml glass vial charged with ligand *t*DODAM · 3 $H_2O$ (40.0 mg; 0.081 mmol), solid salt $LnCl_3 \cdot 6\,H_2O$ (Ln = Nd, Sm, Tb, Dy, Ho, Er, Tm, and Lu) or $LnCl_3 \cdot 7\,H_2O$ (Ln = La, Ce, Pr) (0.07 mmol; 0.95 equiv) was weighted. Alternatively, standardised aq. $EuCl_3$ ($c$ = 0.05742 mol $dm^{-3}$), $YbCl_3$ ($c$ = 0.04817 mol $dm^{-3}$) or $GdCl_3$ ($c$ = 0.05796 mol $dm^{-3}$) were used. In the case of the solid salts, water (1 ml) was added to get solution. The pH of the solution was continually adjusted to 6.5 by dropwise addition of 1M aq. LiOH and the pH was followed by pH-meter. When no change of pH was observed, the solution was further stirred at 60 °C for 1 day. The pH was checked and, if needed, readjusted to 6.5 again. This procedure was repeated until no change in pH after overnight heating was observed. Then, the pH of the solution was raised to 10 by addition of aq. LiOH, the suspension was filtered through 0.2-μm syringe microfilter and the filtrate was evaporated to dryness. The resulting solid was re-dissolved in water (0.5 ml) and pH of the solution was re-adjusted by addition of 0.25M aq. HCl to ≈ 7.[3] Then the vial was placed into a closed vessel filled with acetone at the bottom. This way, diffusion of acetone vapour occurred and over several days, formation of crystalline complexes was observed. The solid was filtered (in some cases after X-ray measurements), washed with acetone and dried in air to get white solids except for La(III) (only oil was obtained and it was dried *in vacuo* after removing the supernatant), Pr(III) (green crystals), Nd(III) (violet crystals) and Ho(III) and Er(III) (pink crystals).

## 3.7 Luminescence spectrophotometry

The measurements were done using Thermo Spectronic AMINCO Bowman® Series 2 spectrophotometer in 1-ml quartz cells with four clear sides. Measured solutions were prepared by dissolving the europium(III) complex (about 1 mg) in $H_2O$ or $D_2O$ (1 ml). Emission spectra were measured after excitation ($\lambda$ = 395 nm) and excitation spectra were measured observing wavelength of emission maximum ($\lambda$ = 595 nm in case of $H_2O$ and $\lambda$ = 590 nm in case of $D_2O$).

In order to determine $q$, the spectrophotometer was used in flash mode, *i.e.* the sample was briefly irradiated by an intense pulse with wavelength of excitation maximum (395 nm). After the pulse, luminescence at the wavelength of 616 nm or 590 nm was observed for 2.5 ms in $H_2O$ solution and 6 ms in $D_2O$ solution, respectively. The measurement was repeated 1000 times in order to get less noisy data and the dependence of emission on time was averaged. Life-times $\tau$ were obtained by fitting the luminescence

[3] If the pH of the solution was alkaline (pH > 10) for several hours or days, significant hydrolysis of amide groups was observed.

decay curve by exponential function (Equation (3.5)).

$$I = I_0 \cdot e^{-\frac{t}{\tau}} \tag{3.5}$$

## 3.8 NMR spectra of lanthanide(III) complexes

All spectra were measured in $D_2O$ and referenced to *t*BuOH as internal standard. In the case of Nd(III), Sm(III), Pr(III) and La(III) complexes, the measurements had to be done at lower temperature (as low as −35 °C), therefore these complexes were dissolved in a mixture $D_2O$—$CD_3OD$=3:2 and measurements were carried out using Varian VNMRS 400 spectrometer which allows for low-temperature measurements. In the case of complexes with very large spectral widths (such as those with Dy(III), Tm(III), Tb(III), etc.) the spectra were recorded in several parts, each part had spectral width 260 ppm and the transmitter offset frequency was changed by 100 ppm. Every part was then phased, baseline corrected using a polynomial function and processed parts of spectra were then stacked using MestReNova software to obtain full spectrum.

## 3.9 2D NMR of europium(III) complex

2D spectra were acquired at 5 °C on Bruker Avance III 600 and further processed using sine square window function, phase corrected in such a way that all peaks were purely positive and baseline corrected using third-order polynomial function in both dimensions. 2D-EXSY spectra used to inspect the dynamics in solution were then stacked and integration of the diagonal peaks and the crosspeaks was performed manually. The same integration boundaries were used for all spectra. The processing was done using MestReNova software. The dependence of integral intensities on EXSY mixing time was fitted using Matlab routine by Jan Blahut.

# Chapter 4

# Results and Discussion

## 4.1 Synthesis of *t*DODAM

The title compound was synthesized by a simple 5-step procedure starting from commercially available cyclen (Compound **1**). The first step, preparation of *trans*-diprotected cyclen followed the previously published procedure. [33] This intermediate is alkylated by chloroacetamide in $S_N2$ reaction employing similar conditions as in literature for alkylation using bromoacetamide. [34] Due to the use of a less electrophilic alkylating reagent, the reaction had to be run for a longer time and at a higher temperature. Obtained yield was slightly better than that reported in literature. After removal of the Cbz protecting groups using dihydrogen and palladium on carbon as a catalyst, next alkylation step was carried out to attach acetate pendant arms. Dropwise addition of *t*-butyl bromoacetate at room temperature worked best and required no further purification steps to obtain the protected title compound in a nearly quantitative yield. Final step was deprotection of *t*-butyl ester groups and, after purification on strong cationic ion exchanger and crystallisation yielded pure title compound as trihydrate in the zwitterionic form. Overall yield of the 5-step synthesis was 50 % based on cyclen.

## 4.2 UV-VIS spectra of $[Ce(H_2O)_9]^{3+}$, *out-of-cage* and *in-cage* complexes

UV-VIS spectrum of aq. $CeCl_3$ contains two bands with absorption maxima at 240 and 252 nm corresponding to ligand-to-metal charge transfer absorption bands of $[Ce(H_2O)_9]^{3+}$. After addition of 1 equiv of the ligand, these two absorption bands at 240 and 252 nm decreased and a new band at 296 nm is formed due to the formation of the *out-of-cage* complex. The formation of the *out-of-cage* complex was not quantitative under these conditions due to relatively low thermodynamic stability of the

*out-of-cage* complex. After raising the pH to 7, quantitative formation of the *in-cage* complex was observed due to the absence of the absorption bands at wavelengths 240, 252 and 296 nm and the formation of a new absorption bands with absorption maxima at $\lambda$ = 320 nm and 271 nm. Since at wavelength $\lambda$ = 320 nm, only the *in-cage* complex absorbs, this wavelength was chosen for the future measurements. Obtained spectra are shown in Fig. 4.1.

In order to confirm that the complexation occurs through the same intermediate *out-of-cage* complex, UV-VIS spectra of *out-of-cage* complexes formed immediately after mixing of the reactants at the lowest and the highest used pH and M:L and L:M ratios were measured. Obtained absorption spectra are shown in Fig. 4.2. Since all the spectra contain the same absorption bands (neglecting the absorption band of the *in-cage* complex in the spectra measured at higher pH), it was proven that the complexation proceeds through the same reaction intermediate independently of the reaction conditions under which the complexation was studied.

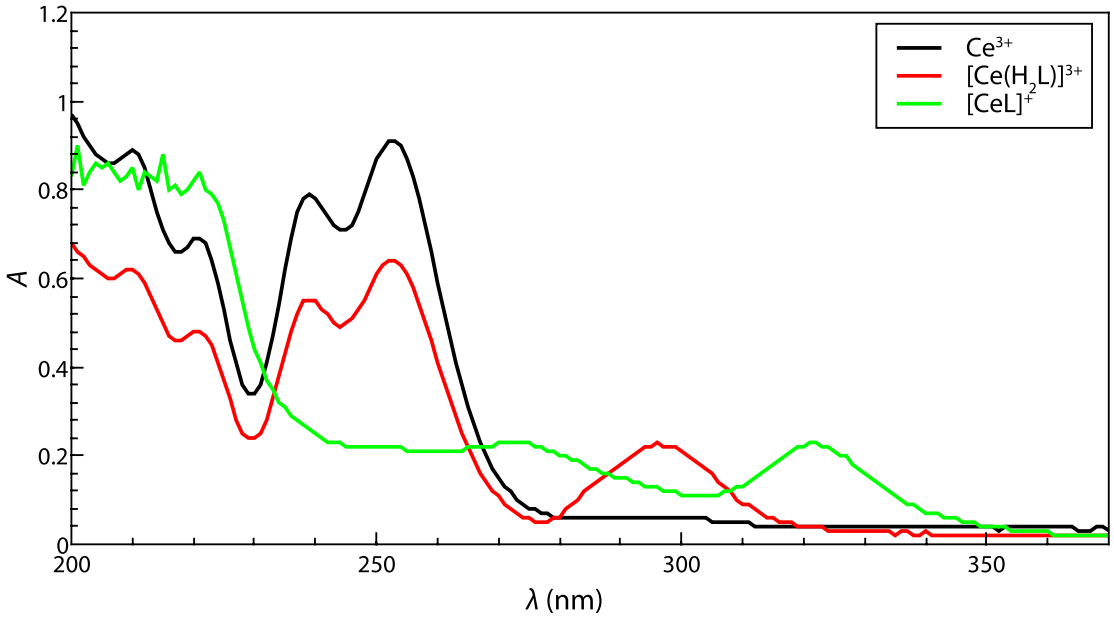


Figure 4.1: Absorption spectra of $CeCl_3$, *out-of-cage* (pH = 5.47 and *in-cage* (pH = 7.00 complexes. The concentration of both ligand and metal ion in the cell was $1 \times 10^{-3}$ M. *Out-of-cage* complex is not formed quantitatively under these conditions. Therefore, the absorption bands of $[Ce(H_2O)_9]^{3+}$ ion are present in the spectrum of the *out-of-cage* complex.

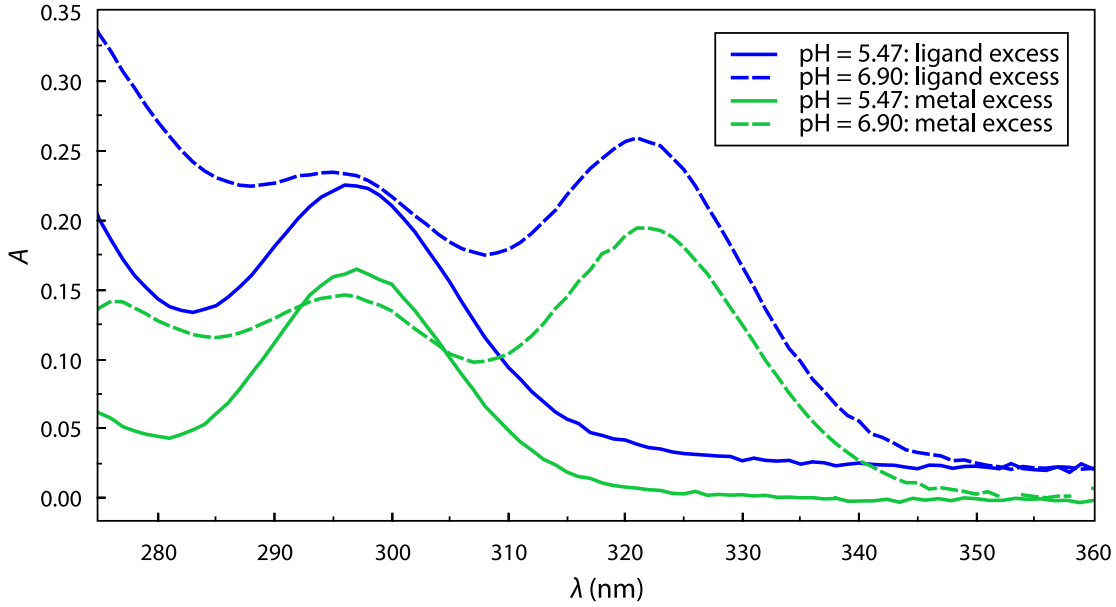


Figure 4.2: Absorption spectra of *out-of-cage* complexes obtained under both ligand and metal ion excesses at two different pH immediately after mixing the reagents (measurement dead time ≈ 10 s). At the higher pH, a significant amount of *in-cage* complex was formed during the dead time. The concentration of the ligand in the cell was $1 \times 10^{-3}$ M or $5 \times 10^{-2}$ M and the concentration of the metal ion was $5 \times 10^{-2}$ M or $1 \times 10^{-3}$ M, respectively.

## 4.3 Formation kinetics of $[Ce(tdodam)(H_2O)]^+$ complex

The time dependence of the absorbance at 320 nm was fitted with the general exponential function (Equation (4.1)) where $A$ is absorbance, $A_f$ is the final absorbance, $A_0$ is the initial absorbance, $t$ is time and ${}^{f}k_{obs}$ is the experimentally observed rate constant of the reaction.

$$A = A_f + (A_0 - A_f) \cdot e^{-{}^{f}k_{obs} \cdot t} \tag{4.1}$$

The data were fitted by means of a least-squares fitting procedure using the Micromath Scientist program. [35] In order to determine parameters ${}^{f}K$ or ${}^{f}K'$ and ${}^{f}k$ or ${}^{f}k'$, the plots of ${}^{f}k_{obs}$ and ${}^{f}k'_{obs}$ (for definitions of these parameters, see subsection 1.2.4, p. 12) against the metal ion-to-ligand concentrations ratio and against the ligand-to-metal ion concentrations ratio (saturation curves under both metal ion and ligand excess) were constructed for each pH value (Fig. 4.3). The dependences were fitted by means of least-squares procedure according to Equation (1.23) or (1.24), respectively (p. 14). Thus, the parameters ${}^{f}K$, ${}^{f}K'$, ${}^{f}k$ and ${}^{f}k'$ were obtained for each pH value. These constants were

plotted against pH (Fig. 4.4) in order to show that the values of ${}^{\mathrm{f}}K$ and ${}^{\mathrm{f}}K'$ are virtually independent on pH while the values of ${}^{\mathrm{f}}k$ and ${}^{\mathrm{f}}k'$ show a linear trend. Under the metal ion excess, the stability constant of the *out-of-cage* complex is $\log {}^{\mathrm{f}}K' = 2$ and the hydroxide-assisted rate constant of the transfer of the metal ion into the macrocyclic cavity is $\log {}^{\mathrm{f}}k'_1 = 5.8$ $\mathrm{dm^3 mol^{-1} s^{-1}}$. Under the ligand excess, stability constant of the *out-of-cage* complex is $\log {}^{\mathrm{f}}K = 1.8$ and hydroxide-assisted rate constant of the transfer of the metal ion into the macrocyclic cavity is ${}^{\mathrm{f}}k_1 = 5.8$ $\mathrm{dm^3 mol^{-1} s^{-1}}$. Under both ligand and metal ion excess, the hydroxide-non-assisted rate constant of transfer of the metal ion into the macrocylic cavity was determined to be negligible and excluded during the final refinement using least-squares fit.

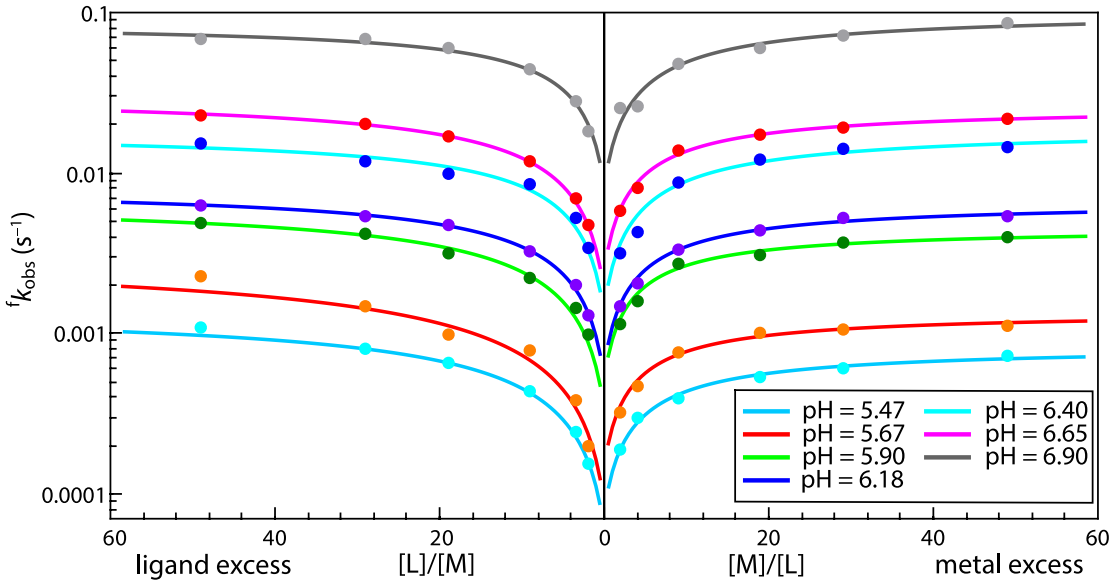


Figure 4.3: Saturation curves for kinetics under both metal and ligand excess. The curves represent the best fits according to the Equations (1.23) (ligand excess) and (1.24) (metal ion excess) (p. 14). $c_{\mathrm{M}} = 1 \times 10^{-3}$ M and $c_{\mathrm{L}} = 1 \times 10^{-3}$–$5 \times 10^{-2}$ M for the measurements under the ligand excess and $c_{\mathrm{L}} = 1 \times 10^{-3}$ M and $c_{\mathrm{M}} = 1 \times 10^{-3}$–$5 \times 10^{-2}$ M for the measurements under the metal ion excess.

Since the transfer of the metal ion into the macrocyclic cavity is base-catalysed [36], it can be assumed that Equation (4.2) is valid.

$$ {}^{\mathrm{f}}k = {}^{\mathrm{f}}k_0 + {}^{\mathrm{f}}k_1 \cdot c_{\mathrm{OH^-}} \tag{4.2} $$

The plots of ${}^{\mathrm{f}}k$ and ${}^{\mathrm{f}}k'$ against the concentration of hydroxide ions (Fig. 4.5) show that the rate constants of the transfer of the metal ion into the macrocyclic cavity is base-catalysed under both metal ion and ligand excess conditions. By means of the least-

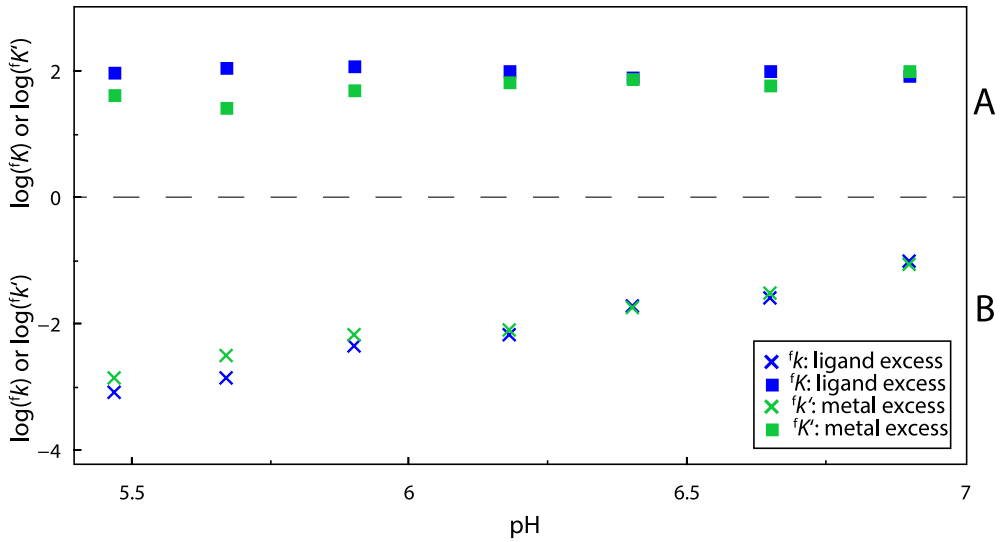


Figure 4.4: Dependence of ${}^{\mathrm{f}}K$ and ${}^{\mathrm{f}}K'$ (A) and ${}^{\mathrm{f}}k$ and ${}^{\mathrm{f}}k'$ (B) on pH for both metal and ligand excess.

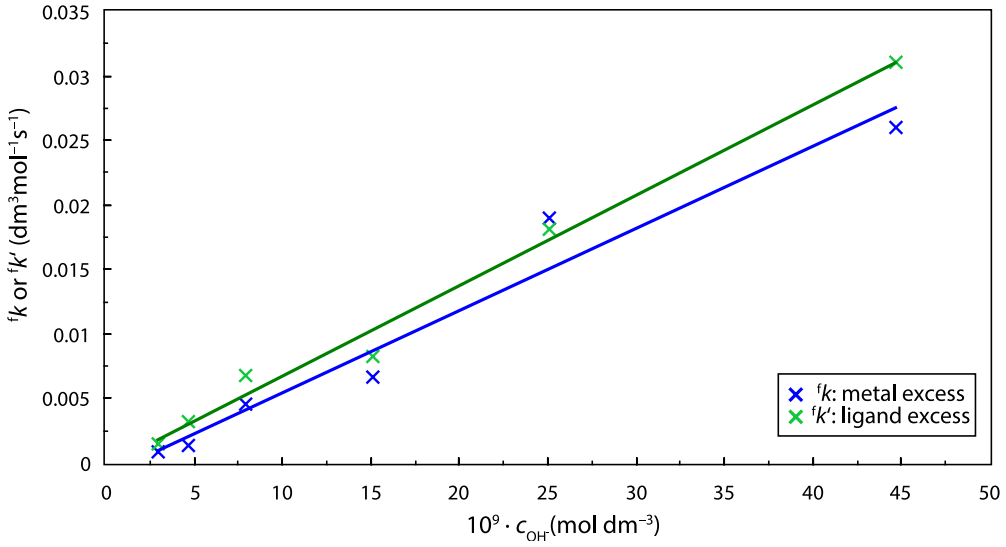


Figure 4.5: Dependence of ${}^{\mathrm{f}}k$ on $c_{\mathrm{OH}^-}$ for both metal and ligand excess. The lines represent the best fits according to the Equation (4.2).

squares linear regression, it was possible to determine the first-order rate constant for the base-catalysed process of the transfer of the metal ion into the macrocyclic cavity. The zero-order rate constant which describes the process of the *in-cage* complex formation without the basic catalysis is negligible under both ligand and metal ion excesses and was omitted in the final refinement using the least-square fits. According to the obtained kinetic data, mechanism of complex formation can be suggested as shown in Scheme 4.1. The observed formation rate constant of cerium(III) complex of the ligand *t*DODAM is compared with those for Ce(III)-DOTA and Ce(III)-DOTAM systems in the plot (Fig. 4.6).

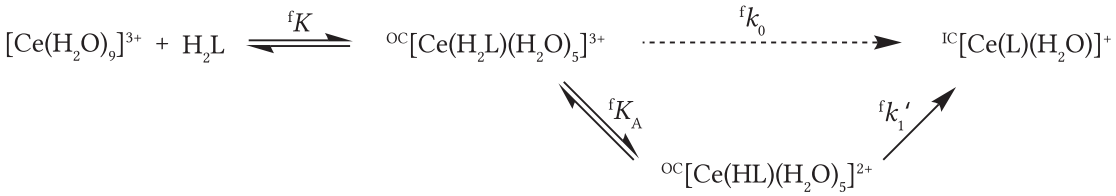


Scheme 4.1: Mechanism suggested for cerium(III) complex formation. Values of constants ${}^{\mathrm{f}}K_{\mathrm{A}}$ and ${}^{\mathrm{f}}k_1'$ cannot be obtained separately. Only value of their product ${}^{\mathrm{f}}k_1 = {}^{\mathrm{f}}k_1' \cdot {}^{\mathrm{f}}K_{\mathrm{A}}$ could be obtained.

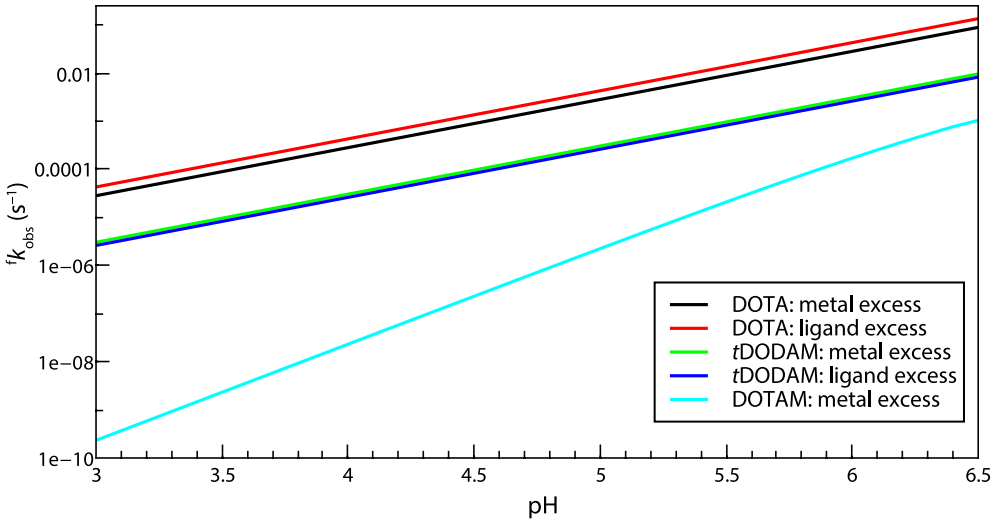


Figure 4.6: Comparison of the observed rate constants of the complexation of the cerium(III) ion by *t*DODAM or DOTA under both metal ion and ligand excess and DOTAM under metal ion excesses. In all cases, the limiting reactant was present in concentration $1 \times 10^{-3}$ M and the other reactant was present in tenfold excess. Data for the DOTA and DOTAM systems were taken from literature. [14, 36]

In order to compare the kinetics of complexation of these two ligands numerically, half-times of the complexation $t_{1/2}$ at pH 6 were calculated according to Equation (4.3). The complexation half-time of *t*DODAM using tenfold metal excess is 230 s, whereas the complexation half-time of DOTA under the same conditions is 25 s. [36] Complexation halftime of DOTAM under these conditions is 4060 s. [14] Thus, it can be said that destabilisation of the *out-of-cage* complex does not lead to the faster complex formation and that the rate of the proton transfer and the corresponding rate constant need to be considered.

$$t_{1/2} = \frac{\ln(2)}{{}^{\mathrm{f}}k_{\mathrm{obs}}} \tag{4.3}$$

## 4.4 Dissociation kinetics of the $[Ce(tdodam(H_2O))]^+$ complex

The dependence of the observed rate constant ${}^{\mathrm{d}}k_{\mathrm{obs}}$ on the concentration of $HClO_4$ is shown in Fig. 4.7. This dependence is almost linear, but there is a significant neg-

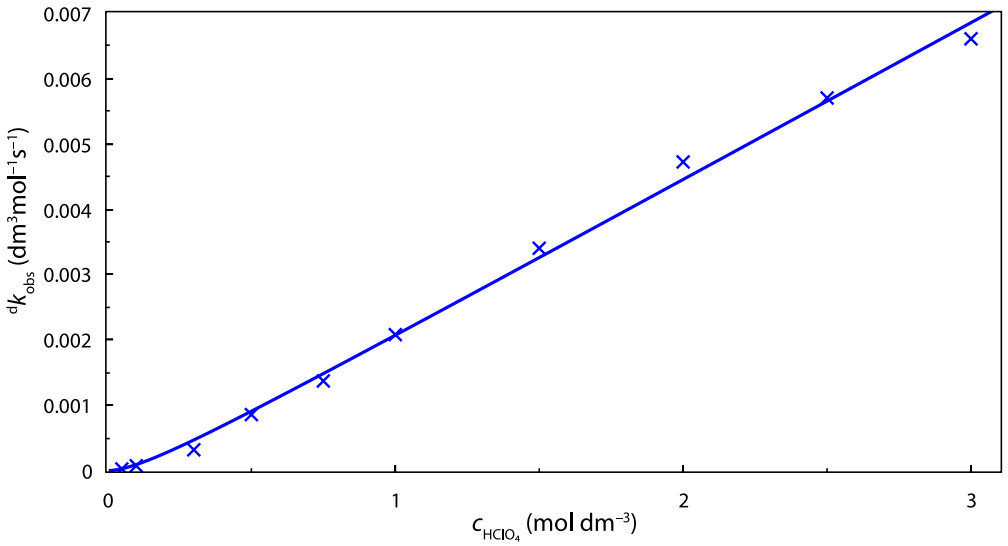


Figure 4.7: Dependence of observed rate of dissociation ${}^{\mathrm{d}}k_{\mathrm{obs}}$ on the concentration of $HClO_4$. The curve represents the best fit according to the Equation (1.36).

ative intercept on *y*-axis if fitting is done by Equation (1.27) (p. 14). Therefore, the dependence cannot be fitted by this Equation and it is necessary to consider the second protonation of the complex. Then, the dependence of ${}^{\mathrm{d}}k_{\mathrm{obs}}$ on $[HClO_4]$ has to be fitted by more complicated Equation (1.36) (p. 15) that takes into account also the first protonation equilibrium. By means of the least-squares fitting procedure, it was found

that, ${}^{d}k_{10} = 0$, ${}^{d}k_{11} = 2.41 \times 10^{-3} \pm 8 \times 10^{-5}$ dm$^3$mol$^{-1}$s$^{-1}$ and ${}^{d}K_A = 0.16 \pm 0.07$.[1] Thus, it was concluded that two subsequent protonations are necessary and the species formed upon the first protonation does not spontaneously dissociate. Therefore, the dissociation of the cerium(III) complex can be divided into steps (1.28)–(1.30) and the reaction (1.29) does not occur (all Equations are shown in subsection 1.2.5, p. 15). According to the obtained kinetic data, mechanism of complex dissociation can be suggested as shown in Scheme 4.2. Comparison of dissociation rates of *t*DODAM, DOTA and DOTA-(MeAM)$_4$ cerium(III) complexes is shown in Fig. 4.8. For the DOTA and DOTA-(MeAM)$_4$ complexes, the kinetic data were taken from literature. [17, 21]

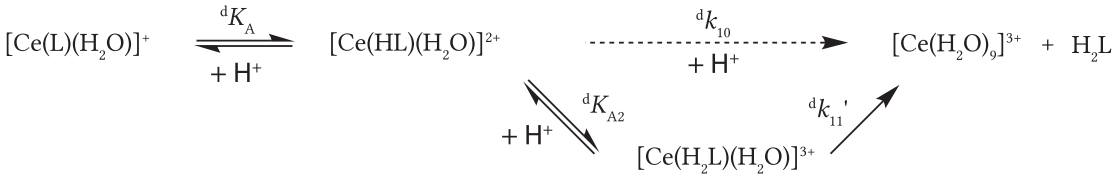


Scheme 4.2: Suggested mechanism of cerium(III) complex dissociation. Values of constants ${}^{d}K_{A2}$ and ${}^{d}k'_{11}$ cannot be obtained separately. Only value of their product ${}^{d}k_{11} = {}^{d}k'_{11} \cdot {}^{d}K_{A2}$ could be obtained.

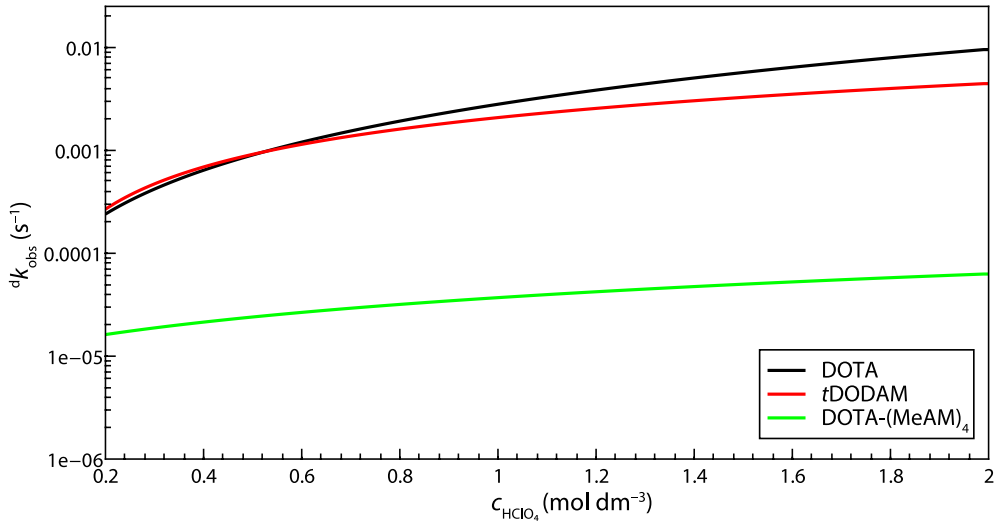


Figure 4.8: Comparison of the dependences of the observed dissociation rates of cerium(III)-DOTA, -*t*DODAM and -DOTA-(MeAM)$_4$ complexes on acid concentration. Curves were calculated from data reported in literature for DOTA [17] and DOTA-(MeAM)$_4$ [21] and data given in the Thesis for *t*DODAM.

[1] In the first fitting, it was found that standard deviation of ${}^{d}k_{10}$ was much larger than its value and, therefore, ${}^{d}k_{10}$ was omitted during the final refinement by the least-squares fit.

## 4.5 Potentiometric titrations

Results of the potentiometric titrations are summarised in Tables 4.1 and 4.2. Comparison of the stability constants of different ligands is shown in Table 4.4. For all available stability constants, it holds true that the complex of DOTA is more stable than the complex of *t*DODAM and the complex of *t*DODAM is in turn more stable than the corresponding complex of DOTAM. The protonation constant of [M(L)] complex, $\log {}^{\mathrm{H}}K_{\mathrm{M(L)}}$, is calculated according to Equation (4.6). The equilibrium constants describing reactions (4.4) and (4.5), $\log K_{\{\mathrm{M[L(OH)]}\}}$ and $\log K_{\{\mathrm{M[L(OH)_2]}\}}$, respectively, are calculated according to Equation (4.7) and (4.8), respectively.

$$[\mathrm{M(L)}] + \mathrm{H_2O} \longrightarrow \{\mathrm{M[L(OH)]}\} + \mathrm{H^+} \tag{4.4}$$

$$\{\mathrm{M[L(OH)]}\} + \mathrm{H_2O} \longrightarrow \{\mathrm{M[L(OH)_2]}\} + \mathrm{H^+} \tag{4.5}$$

$$\log {}^{\mathrm{H}}K_{\mathrm{M(L)}} = \log \beta_{111} - \log \beta_{011} \tag{4.6}$$

$$\log K_{\{\mathrm{M[L(OH)]}\}} = \log \beta_{011} - \log \beta_{-111} \tag{4.7}$$

$$\log K_{\{\mathrm{M[L(OH)_2]}\}} = \log \beta_{-111} - \log \beta_{-211} \tag{4.8}$$

These reactions occurring in alkaline solutions can be considered as an exchange of coordinated pendant for hydroxide anion or deprotonation of the coordinated water molecule. These two processes cannot be distinguished by potentiometry. These proton-associated equilibrium constants are summarised in Table 4.3. It is important to note that the dissociation constant of the first coordinated water is higher than that of the second in the case of copper(II) complex, which suggests very low abundance of the monohydroxo-complex. Distribution diagrams of the ligand, its cerium(III), copper(II), zinc(II) and lead(II) complexes are shown in Fig. 4.9.

Table 4.1: The experimentally determined overall protonation constants $\log \beta_h$ of the ligand (25 °C, $I$ = 0.1 M ($NMe_4$)Cl) and consecutive protonation constants of the ligand and consecutive protonation constants of DOTA and DOTAM for comparison.

| | $\log \beta_h$ | | $\log K_h$ | |
|---|---|---|---|---|
| $h$ | $H_2$*t*DODAM | $H_4$DOTA [19] | $H_2$*t*DODAM | DOTAM [21] |
| 1 | 11.42(1) | 12.9 | 11.42 | 9.08 |
| 2 | 20.10(1) | 9.72 | 8.68 | 6.44 |
| 3 | 22.27(2) | 4.62 | 2.17 | |
| 4 | 24.44(1) | 4.15 | 2.17 | |
| 5 | | 2.29 | | |
| 6 | | 1.34 | | |

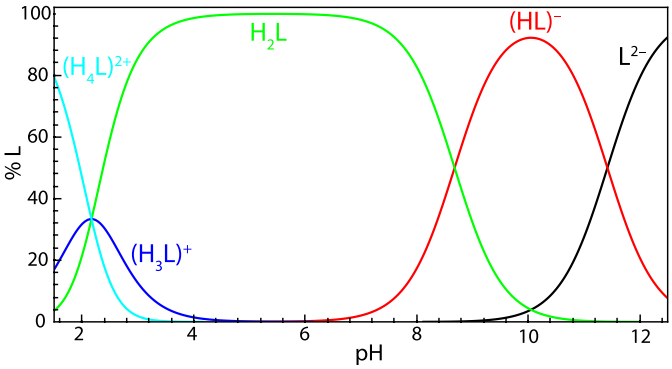


(a) Ligand—$H^+$ ($c_L$ = 0.004 м).

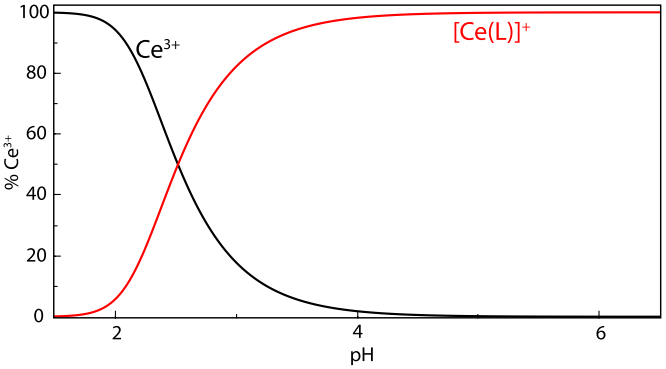


(b) Ligand—$Ce^{3+}$ ($c_L = c_{Ce^{3+}}$ = 0.004 м).

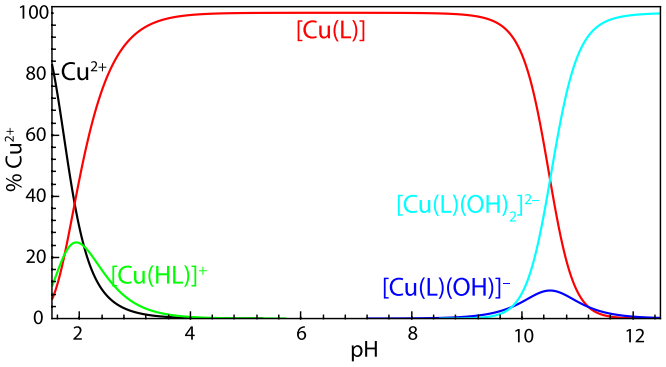


(c) Ligand—$Cu^{2+}$ ($c_L = c_{Cu^{2+}}$ = 0.004 м).

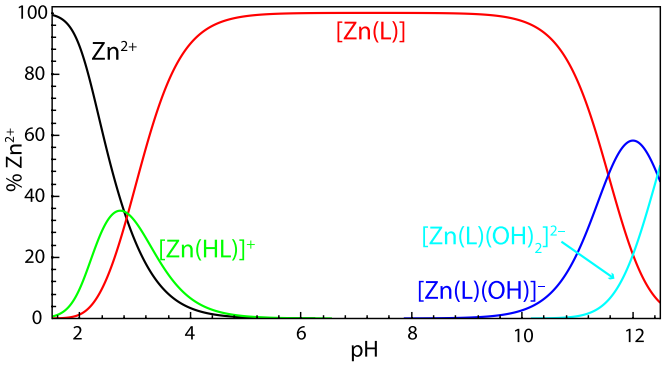


(d) Ligand—$Zn^{2+}$ ($c_L = c_{Zn^{2+}}$ = 0.004 м).

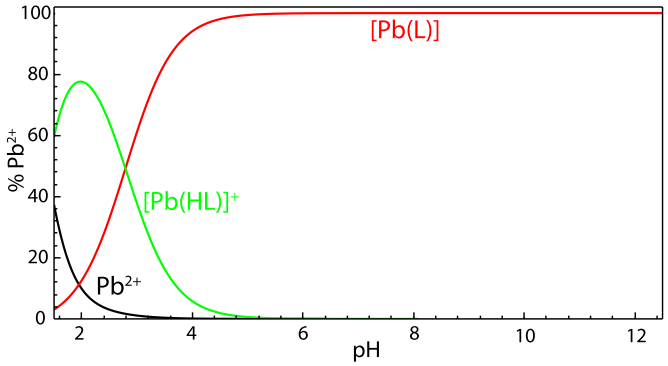


(e) Ligand—$Pb^{2+}$ ($c_L = c_{Pb^{2+}}$ = 0.004 м).

Figure 4.9: Distribution diagrams of *t*DODAM and its complexes.

Table 4.2: The experimentally determined overall stability constants $\log \beta_{hlm}$ of the complexes (25 °C, $I$ = 0.1M $(NMe_4)Cl$). The numbers in brackets signify the error of the last significant digit.

| Species | $hlm$ | $Cu^{2+}$ | $Zn^{2+}$ | $Pb^{2+}$ | $Ce^{3+}$ | $Eu^{3+}$ | $Lu^{3+}$ |
|---|---|---|---|---|---|---|---|
| [M(L)] | 011 | 19.89(1) | 17.39(1) | 20.28(1) | 17.98(2) | 18.93(1) | 18.50(1) |
| [M(HL)] | 111 | 21.62(4) | 20.26(1) | 23.07(2) | | | |
| [M(L)(OH)] | −111 | 8.69(7) | 5.83(2) | | | | |
| $[M(L)(OH)_2]$ | −211 | −1.12(1) | −6.62(2) | | | | |

Table 4.3: Protonation constants of the metal complexes of *t*DODAM and dissociation constants of the hydroxocomplexes.

| Constant | $Cu^{2+}$ | $Zn^{2+}$ | $Pb^{2+}$ |
|---|---|---|---|
| $\log K_{M(L)}$ | 1.73 | 2.87 | 2.79 |
| $pK_{\{M[L(OH)]\}}$ | 11.2 | 11.56 | |
| $pK_{\{M[L(OH)_2]\}}$ | 9.81 | 12.45 | |

Table 4.4: Comparison of the metal complex stability constants $\log K_{ML}$ of *t*DODAM, DOTA and DOTAM.

| metal ion | $H_4$DOTA [19] | $H_2$*t*DODAM | DOTAM [21] |
|---|---|---|---|
| $Cu^{2+}$ | 22.72 | 19.89 | 14.50 |
| $Zn^{2+}$ | 18.17 | 17.39 | 13.77 |
| $Pb^{2+}$ | – | 20.28 | >19 |
| $Ce^{3+}$ | 23.4 | 17.98 | 11.93 |
| $Eu^{3+}$ | 23.5 | 18.93 | 13.80 |
| $Lu^{3+}$ | 25.4 | 18.50 | 13.53 |

## 4.6 NMR titration

The dependence of the chemical shifts on pH of the solution is shown in Fig. 4.10. For stacked spectra obtained during the titration, see Fig. A.1 (p. 68). The calculated protonation constants and their comparison to the values obtained using potentiometric titration are given in Table 4.5. These values are in a good agreement.

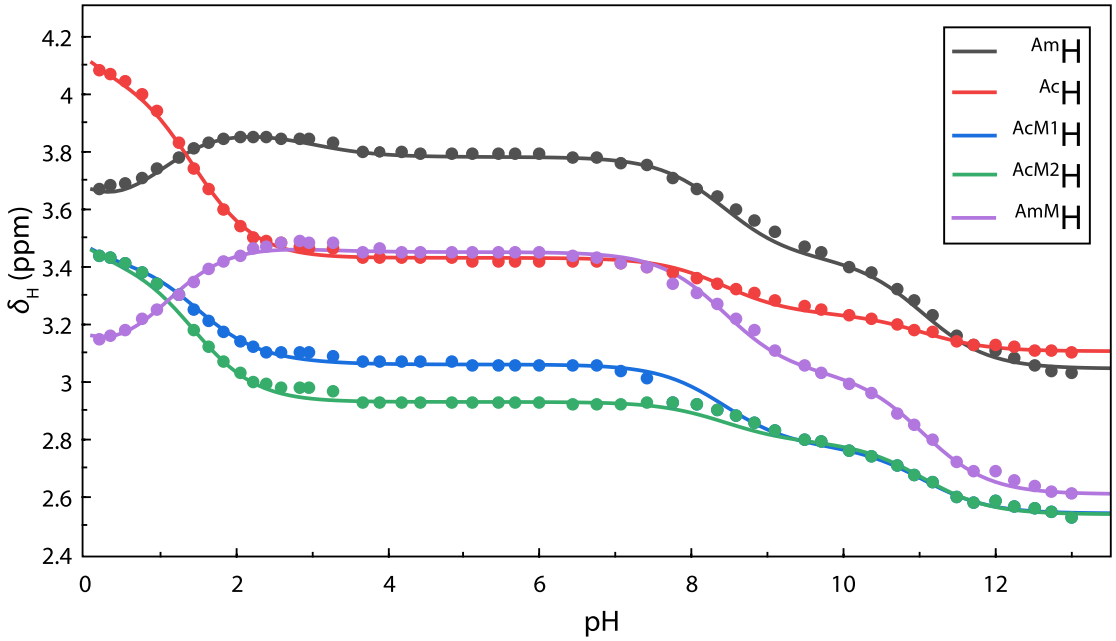


Figure 4.10: The dependence of the chemical shifts of protons in *t*DODAM on pH of the solution. All chemical shifts were referenced to methyl group of *t*BuOH. Points represents measured values and lines represents the best fits calculated using the program P from the OPIUM software package. The assignment of hydrogen atoms is explained in Fig. 4.11.

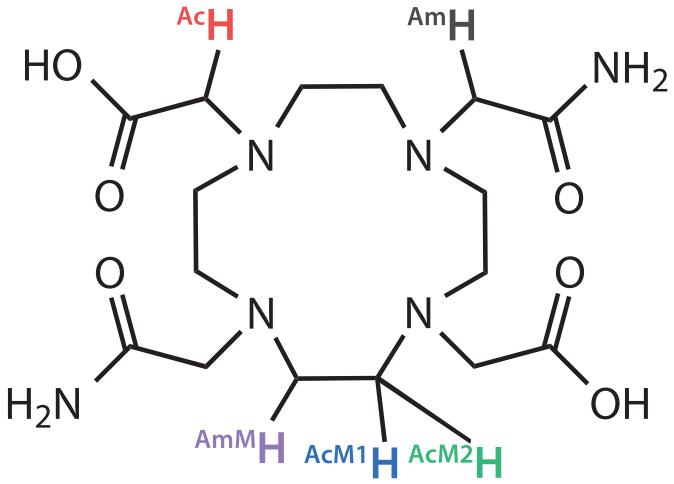


Figure 4.11: Formula of the title ligand with hydrogen atoms labeled to explain the legend of the plot (Fig. 4.10).

Table 4.5: Comparison of stepwise protonation constants determined using potentiometric and NMR titrations.

| No. of protonation | $\log K_{\mathrm{NMR}}$ | $\log K_{\mathrm{pot}}$ | protonation site |
|---|---|---|---|
| 1 | 11.05 | 11.42 | macrocyclic amine |
| 2 | 8.43 | 8.68 | macrocyclic amine |
| 3 | 2.99 | 2.17 | carboxylate |
| 4 | 1.28 | 2.17 | carboxylate |

## 4.7 Luminescence spectrophotometry of the [Eu(*t*dodam)($H_2O$)]$^+$ complex

Emission spectra measured with excitation wavelength of 395 nm in $H_2O$ and $D_2O$ are shown in Fig. 4.12. Excitation spectra measured while observing the emission wavelength of 590 nm are shown in Fig. 4.13. The exponential luminescence decay curves measured using excitation wavelength $\lambda_{ex}$ = 395 nm and emission wavelength $\lambda_{em}$ = 616 nm are shown in Fig. 4.14 for both solutions. These curves were fitted by simple exponential function (Equation (4.9)) where $I$ is intensity of luminescence in time $t$, $I_0$ is intensity of luminescence in time $t = 0$ and $\tau$ is luminescent life-time. Data fitting was done using Micromath Scientist program. [35]

$$I = I_0 \cdot e^{-\frac{t}{\tau}} \tag{4.9}$$

Parameters of the decay curves and their standard deviations and regression coefficients $R^2$ are shown in Table 4.6. Luminescence life-times were used to calculate $q$ according to Equation (1.11) ($n_{OH} = 0$, $n_{NH} = 0$, $n_{O=CNH} = 4$) (p. 11). [13]

$$q_{590} = 1.11[(0.660\ \text{ms})^{-1} - (2.69\ \text{ms})^{-1} - 0.31 + 0.075 \cdot 4)] \tag{4.10}$$

$$q_{590} = 1.26 \tag{4.11}$$

$$q_{616} = 1.11[(0.70\ \text{ms})^{-1} - (2.76\ \text{ms})^{-1} - 0.31 + 0.075 \cdot 4)] \tag{4.12}$$

$$q_{616} = 1.17 \tag{4.13}$$

Therefore, the number of coordinated water molecules is close to 1, slightly higher calculated value of $q$ can be explained by contribution of outer coordination sphere which is not accounted for in Equation (1.11) (p. 11).

Table 4.6: Fitted parameters of luminescence decay curves.

| Parameter | $H_2O$ (590 nm) | $H_2O$ (616 nm) | $D_2O$ (590 nm) | $D_2O$ (616 nm) |
|---|---|---|---|---|
| $\tau$ (ms) | 0.660 | 0.70 | 2.69 | 2.76 |
| $\sigma(\tau)$ (ms) | $8 \cdot 10^{-3}$ | $1.1 \cdot 10^{-2}$ | $3 \cdot 10^{-2}$ | $3 \cdot 10^{-2}$ |
| $I_0$ (a.u.) | 0.707 | 0.633 | 0.452 | 0.380 |
| $\sigma(I_0)$ (a.u.) | 0.007 | 0.007 | 0.004 | 0.003 |
| $R^2$ | 0.99 | 0.99 | 0.98 | 0.98 |

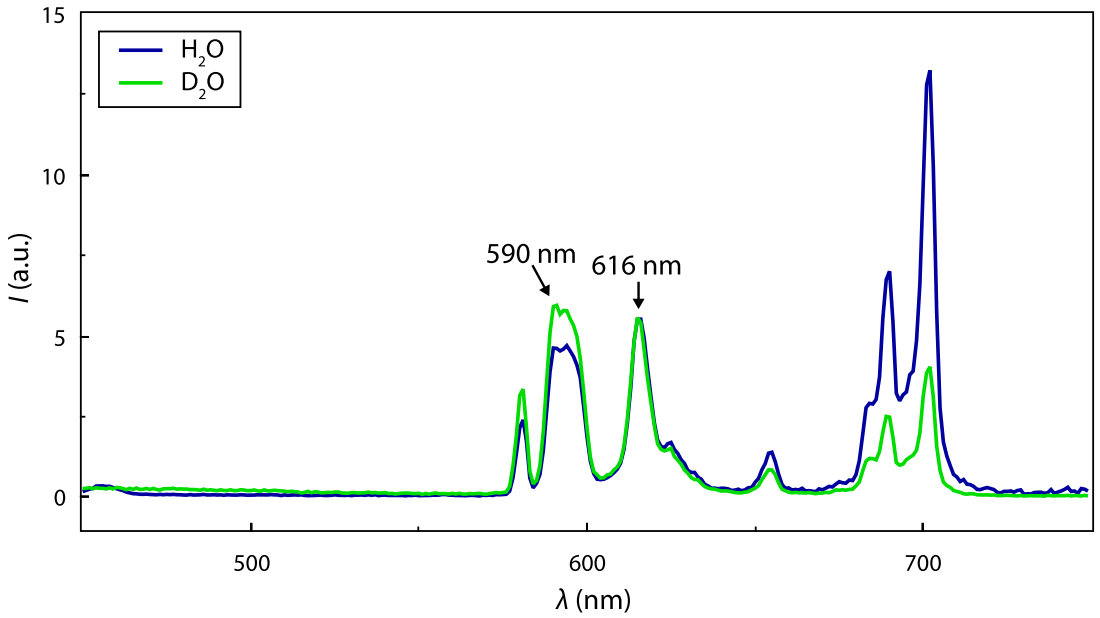


Figure 4.12: Emission spectra of the europium(III) complex of *t*DODAM ($\lambda_{ex}$ = 395 nm)

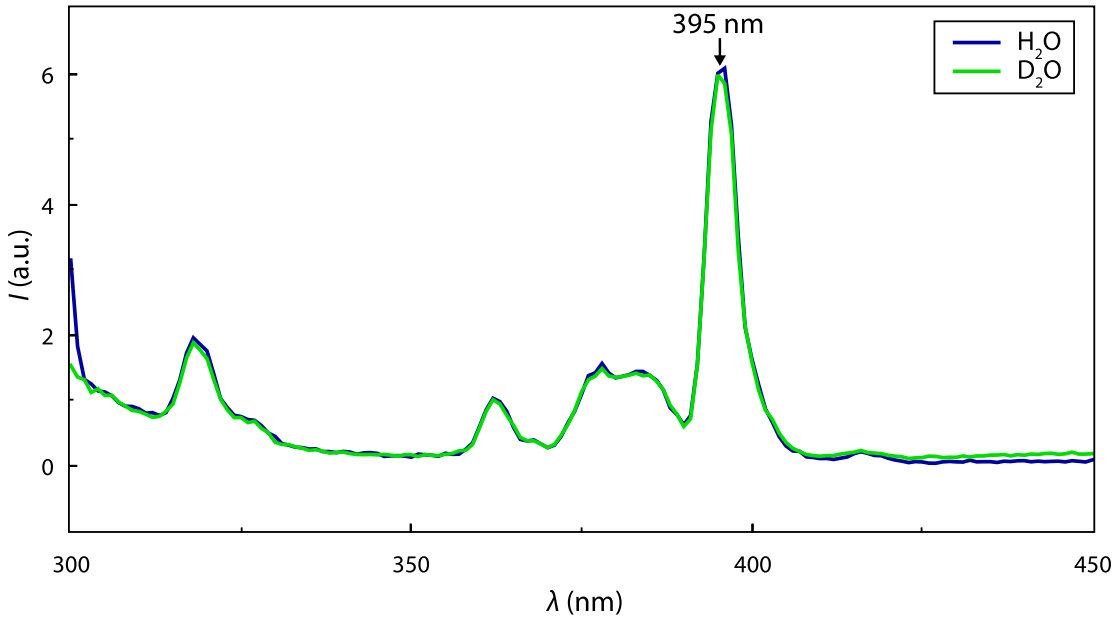


Figure 4.13: Excitation spectra of the europium(III) complex of *t*DODAM ($\lambda_{em}$ = 590 nm)

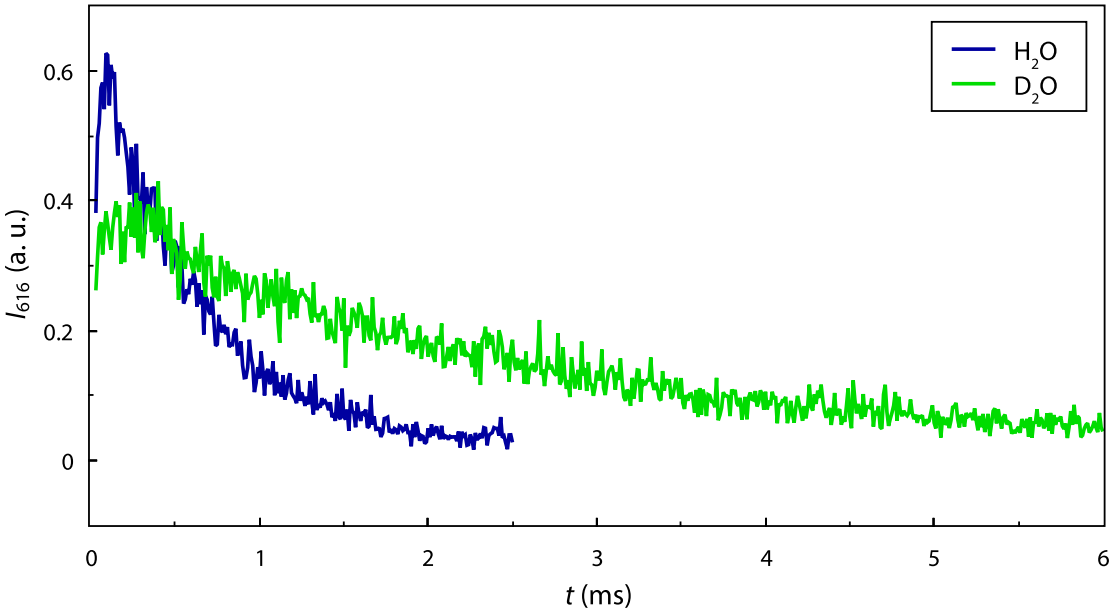


Figure 4.14: Luminescence decay curves of $[Eu(t\text{dodam})(H_2O)]^+$ in $H_2O$ and $D_2O$ solutions.

## 4.8 NMR spectra of lanthanide(III) complexes

The $^1H$ NMR spectra of lanthanide(III) complexes of *t*DODAM contain 12 resonances belonging to 12 non-equivalent proton nuclei in the complexes assuming that the complex is $C_2$-symmetrical with the symmetry axis perpendicular to the $N_4$ plane and principal magnetic axis coincident with molecular $C_2$ symmetry axis. Depending on the metal ion, two most upfield or downfield shifted signals belong to the so-called *"axial"* protons that are located close to the principal magnetic axis and are, therefore, the most affected by the paramagnetic metal ion. NMR spectra of some lanthanide(III) complexes contain two sets of peaks belonging to two isomers (SA and TSA) present in the solution. The ratio of the isomers in equilibrium is dependent on the size of the metal ion and the coordination properties of the ligand. Table 4.7 lists the $^1H$ chemical shifts of lanthanide(III) complexes of *t*DODAM. The ratio of the isomers in the solution was determined through integration of the peaks assigned to the axial protons and is shown in Table 4.8. In the case of the spectra recorded in several parts, integrals of the axial peaks were measured in the part of the spectrum obtained with the transmitter offset frequency nearest the resonances of the axial protons. Plot of abundance of both isomers in the aqueous solutions of the Ln(III) complexes is shown in Fig. 4.15.

Table 4.7: $^{1}$H NMR characterisation of the prepared complexes. Chemical shifts of the axial protons are in bold. The first row for each element belongs to the major isomer and the second row belongs to the minor isomer. In most cases, only some of the peaks belonging to the minor isomer were found due to overlap with peaks of the major isomer and baseline distortions. Unless otherwise stated, each peak represents two protons and is a broad singlet.

| | |
|---|---|
| La | 4.00, 3.80, 3.53 (4H), 3.35, 3.06 (6H), 2.50 (8H). |
| Ce | 12.42, 10.82, 7.10, 6.77, 4.47, 3.35, 1.74 (4H), 0.60, 0.54, −**7.43**, −**8.13**. |
| Pr | 56.06, 52.14, 32.51, 29.21, 17.37 (4H), −5.59, −12.49, −22.10, −31.03, −**32.00**, −**35.62**.<br>34.53, 23.97, 21.14, 9.23, 7.40, −1.96, −13.72, −19.63, −**52.28**, −**62.99**. |
| Nd | 24.31 (4H), 22.52, 14.98 (4H), 14.38, 10.57, 6.41, 5.64, −0.87, −4.34, −8.55, −**11.23**(**4H**).<br>28.18, 24.31 (4H), 7.24, 6.41, −0.87, −4.34, −8.55, −13.46 (4H), −**31.16**, −**34.64**. |
| Sm | 6.49, 5.98, 4.10, 3.86, 2.90, 1.46, 1.11, 0.83, 0.70, 0.43, −**2.86**(**4H**).<br>7.01, 6.31, 4.26, 3.58, 3.08, 1.79 (4H), 1.67, 0.99, 0.43, −**3.53**(**4H**). |
| Eu | **32.53, 30.59**, 0.22, −0.77, −5.29, −7.66, −9.62, −12.09, −15.67, −16.27 (4H), −19.75.<br>11.12, **9.14, 9.06**, 0.36, 0.22, −0.30, −6.92, −8.37, −9.62, −10.38, −12.09, −16.60. |
| Tb | 261.85, 256.34, 219.41, 131.95, 17.25, −10.99, −36.85, −47.63, −58.63, −122.89, −136.57, −**348.47**, −**382.34**.<br>75.99, 28.06, −15.77, −43.58, −58.63, −77.75, −106.59, −**165.29**, −**182.28**. |
| Dy | 393.49, 306.38, 272.43, 237.18, −4.85, −43.58, −77.75, −87.83, −141.89, −194.39, −**397.69**, −**477.91**. |
| Ho | 167.10, 148.44, 146.34, 92.40, −8.78, −19.62, −34.39, −71.18, −84.62, −**206.89**, −**231.38**. |
| Er | **136.80, 128.78**, 28.91, 15.14, 5.74, −0.59, −8.32, −30.87, −63.23, −76.13, −80.31, −83.90.<br>**48.67, 45.39**. |
| Tm | **306.85, 301.90**, 65.13, 48.92, 38.11, 30.22, −63.30, −70.62, −111.91, −148.89, −190.51, −198.87.<br>**232.20, 226.45**. |
| Yb | **125.91, 119.27**, 32.91, 25.38, 12.54, 12.21, −10.25, −18.92, −48.92, −70.83, −72.82, −77.08.<br>**55.01 (4H)**. |
| Lu | 3.80 (d, $J$ = 16.9 Hz), 3.62 (d, $J$ = 16.9 Hz), 3.57 (d, $J$ = 16.8 Hz), 3.48 (t, $J$ = 14.4 Hz, 4H),<br>3.33 (d, $J$ = 16.8 Hz), 2.88 (dd, $J$ = 14.1, 3.5 Hz), 2.83 (dd, $J$ = 14.8, 3.3 Hz), 2.76 (t, $J$ = 13.6 Hz),<br>2.72 (td, $J$ = 14.5, 3.3 Hz), 2.58 (d, $J$ = 14.2 Hz), 2.52 (d, $J$ = 13.5 Hz). |

Table 4.8: Abundance of SA and TSA isomers in the solution of the lanthanide(III) complexes determined through integration of the peaks assigned to the axial protons. Integration error for broad peaks may be as high as ±5 %.

| Ion | $x_{SA}$ (%) | $x_{TSA}$ (%) |
|---|---|---|
| Ce(III) | 0 | 100 |
| Pr(III) | 10 | 90 |
| Nd(III) | 29 | 71 |
| Sm(III) | 25 | 75 |
| Eu(III) | 79 | 21 |
| Tb(III) | 91 | 9 |
| Dy(III) | 100 | 0 |
| Ho(III) | 100 | 0 |
| Er(III) | 96 | 4 |
| Tm(III) | 98 | 2 |
| Yb(III) | 97 | 3 |

Ratio of the two isomers in solution was determined for all paramagnetic lanthanide(III) complexes and, with an exception of samarium(III) complex, shows a similar trend with complexes of DOTAM. [37] The reason for the Sm(III) exception might be the different conditions of the measurement (different solvent was used and the measurement was carried out at low temperature). It should be noted that different lanthanide(III) complexes show different dependencies of the isomer ratio on temperature [38] and used solvent. [39] For VT $^{1}$H NMR spectra of the Sm(III) complex, see Fig. C.1 (p. 76).

The complicated nature of the $^{1}$H NMR spectra of paramagnetic complexes does not allow for an easy assignment of most of the peaks and only the axial peaks were assigned by comparison with published LIS data for DOTA complexes. [40] Also unfortunately, 2D spectra could not be obtained for most of the complexes due to very large spectral widths and fast relaxation. Thus, 2D spectra ($^{1}$H – $^{1}$H COSY, $^{1}$H – $^{1}$H EXSY, $^{1}$H – $^{13}$C HMQC (or $^{1}$H – $^{13}$C HSQC in the case of Lu(III) complex)) were successfully obtained only for cerium(III), europium(III) and lutetium(III) complexes. Therefore, better NMR characterisation is possible only for these compounds. In $^{1}$H – $^{1}$H COSY spectra, only interactions between hydrogen atoms within the particular spin systems are visible. In other words, one can assign which protons are macrocyclic ones (each of them has three crosspeaks with other macrocyclic hydrogen atoms of the same ethylene group) and which protons belong to the pendant arms (each of them has only one crosspeak with the other proton on the same pendant methylene group). In $^{1}$H – $^{1}$H EXSY spectra, each proton has theoretically three crosspeaks due to the chemical exchange between the two isomeric forms since there are three modes of the interconversion between the

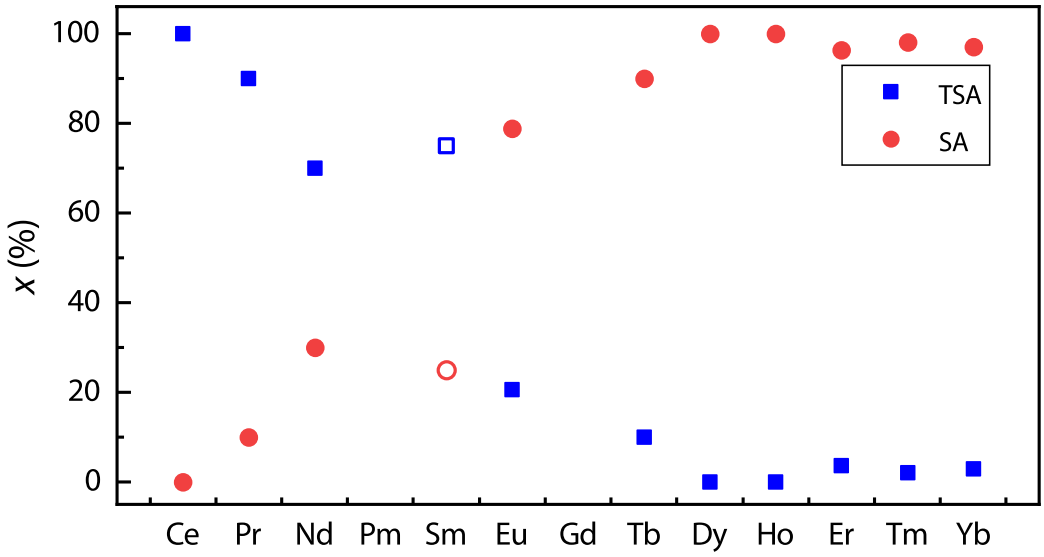


Figure 4.15: Abundance of SA and TSA isomers in the solutions across the lanthanide(III) series. Points representing the Sm(III) complex are empty because they do not follow the trend probably due to different conditions of the measurement.

isomers (arm rotation, ring inversion and both movements). Two of these movements produce crosspeaks between signals of the major and the minor isomers (arm rotation and ring inversion) and both movements subsequently produce crosspeaks between two signals of the same isomer (enantiomerisation). An example of $^{1}$H – $^{1}$H EXSY spectrum of the Eu(III) complex with classification of the peaks according to the origin of their formation is in Fig. 4.16d.

## 4.9 Analysis of NMR spectra of the [Eu(*t*dodam)($H_2O$)]$^{+}$ complex

Assignment of NMR signals of paramagnetic complexes is not simple and rely heavily on use of 2D spectra. Nonetheless, some information is available in $^{1}$H spectrum alone as well. Two most downfield shifted peaks belong to so-called axial protons of the macrocycle which are close to principal magnetic axis of the complex. Next information is that the solution of the complex contains 2 isomers, the minor one has abundance about 20 %. Integration of the peaks in the spectrum allowed for classifying the peaks into two groups according to the isomer they belong to. This also helped to resolve overlapped peaks. For easier orientation, all necessary NMR spectra of the europium(III) complex are shown in Fig. 4.16, $^{1}$H and $^{13}$C{$^{1}$H} NMR spectra are already assigned.

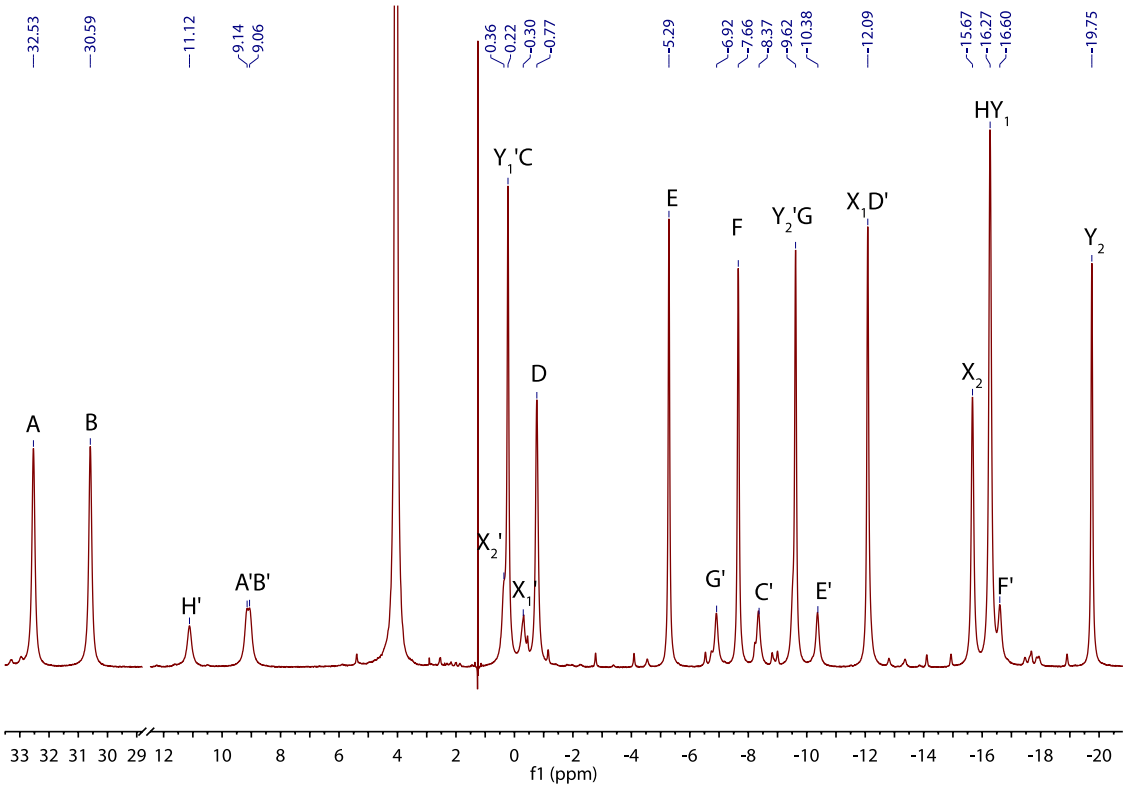


(a) $^{1}$H NMR spectrum of the [Eu(*t*DODAM)($H_2O$)]$^{+}$ complex

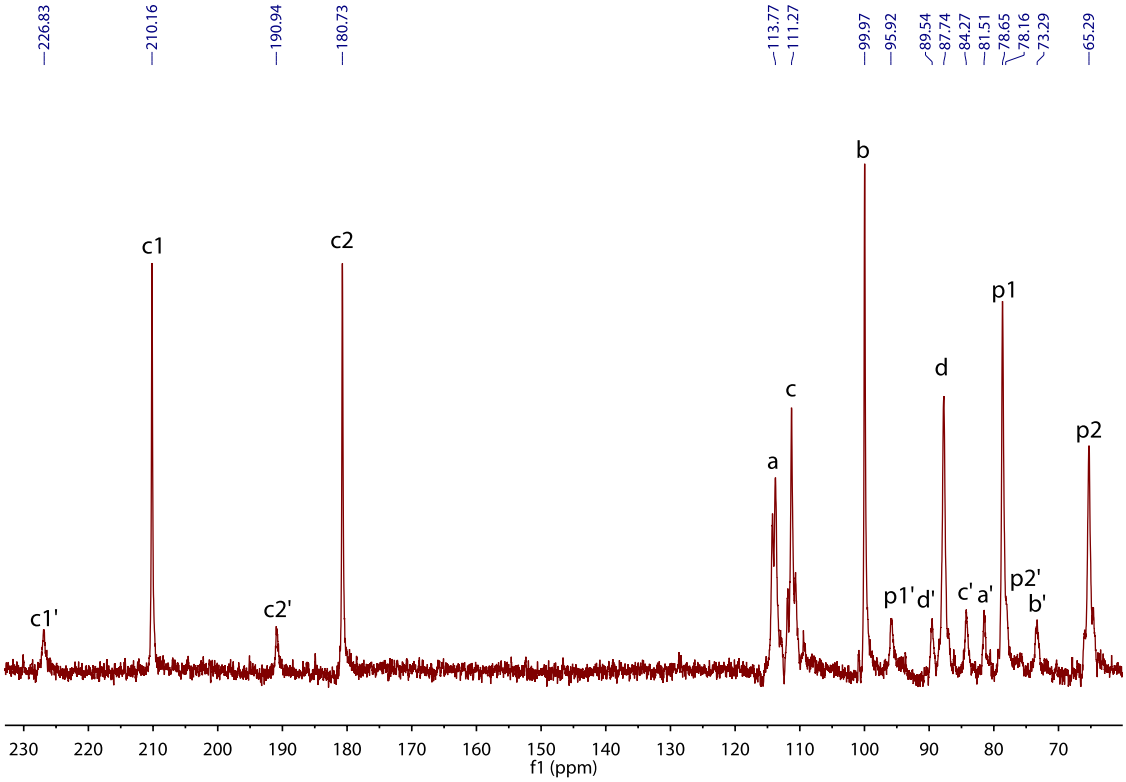


(b) $^{13}$C{$^{1}$H} NMR spectrum of the [Eu(*t*DODAM)($H_2O$)]$^{+}$ complex

Figure 4.16: NMR spectra of the europium(III) complex.

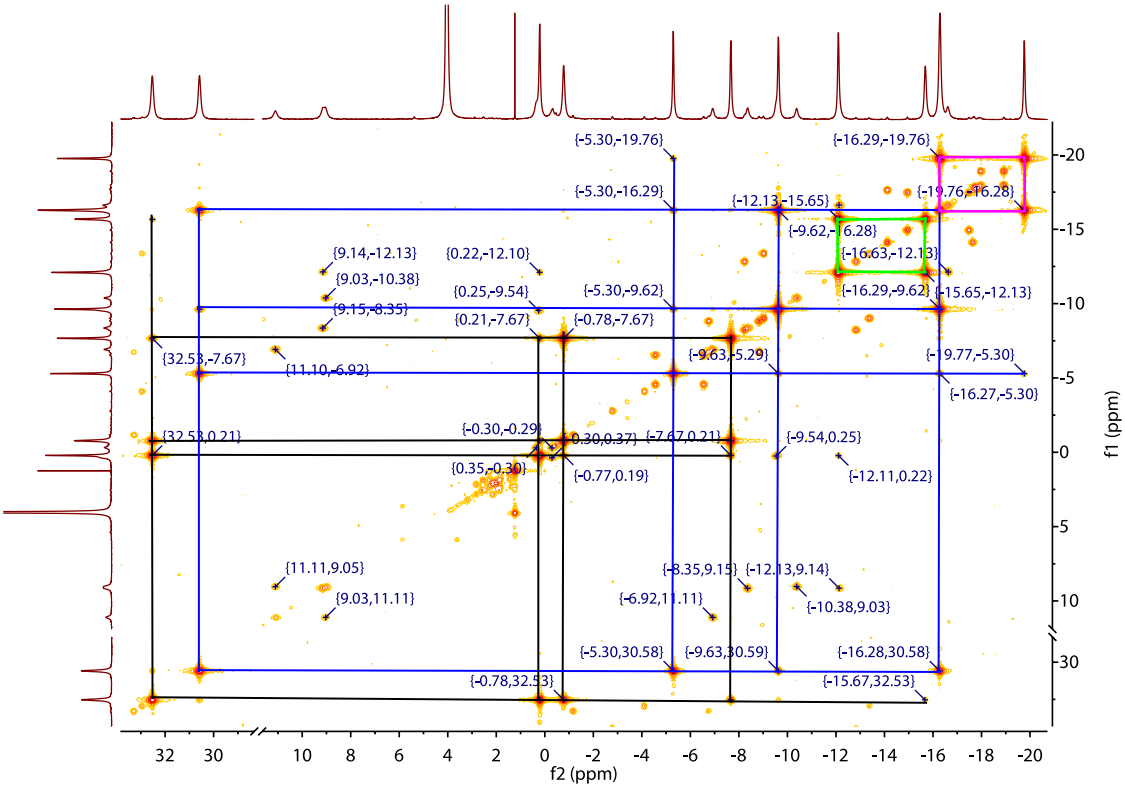


(c) $^{1}$H – $^{1}$H COSY spectrum of the [Eu(*t*DODAM)($H_2O$)]$^{+}$ complex. Lines represent correlations inside the spin systems of the SA isomer. Unlabeled peaks are due to impurity of DOTA-monoamide complex which formed during complexation.

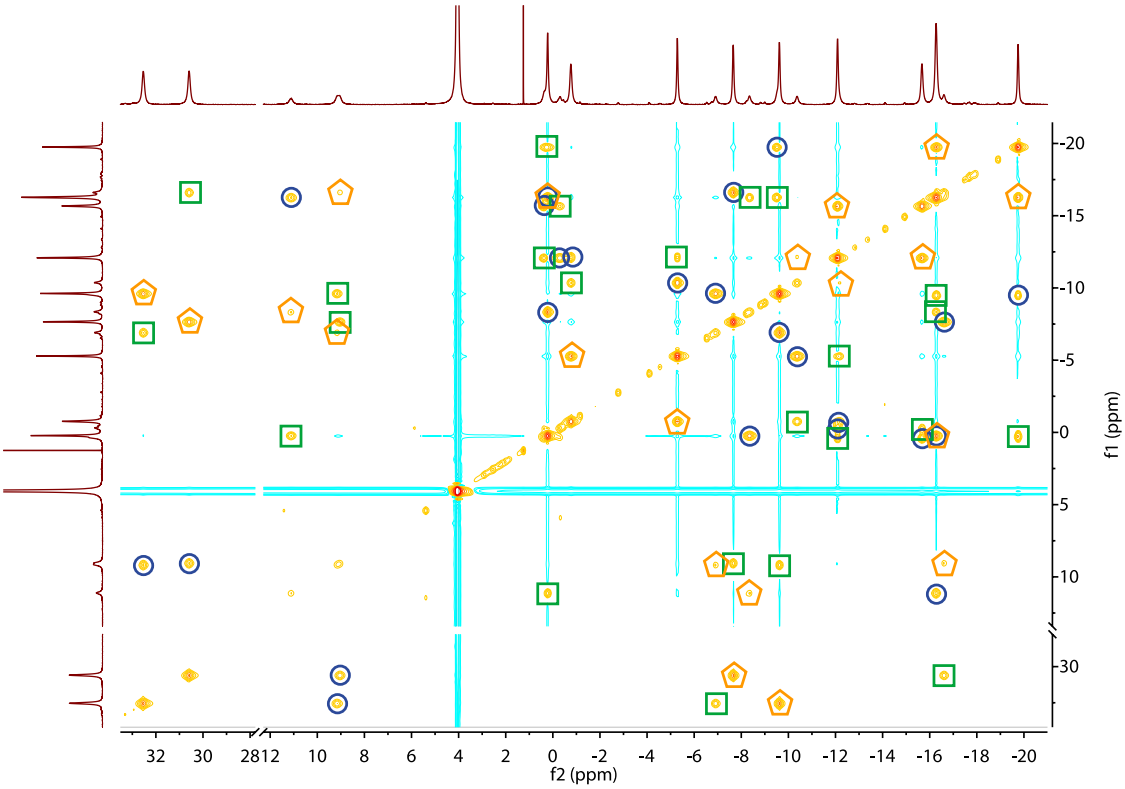


(d) $^{1}$H – $^{1}$H EXSY spectrum of the [Eu(*t*DODAM)($H_2O$)]$^{+}$ complex measured at 600 MHz and 5 °C, $\tau_M$ = 25 ms. Blue circles represent crosspeaks due to the arm rotation, green squares represent crosspeaks due to the ring inversion and the orange pentagons represent crosspeaks due to both movements in succession.

Figure 4.16: NMR spectra of the europium(III) complex.

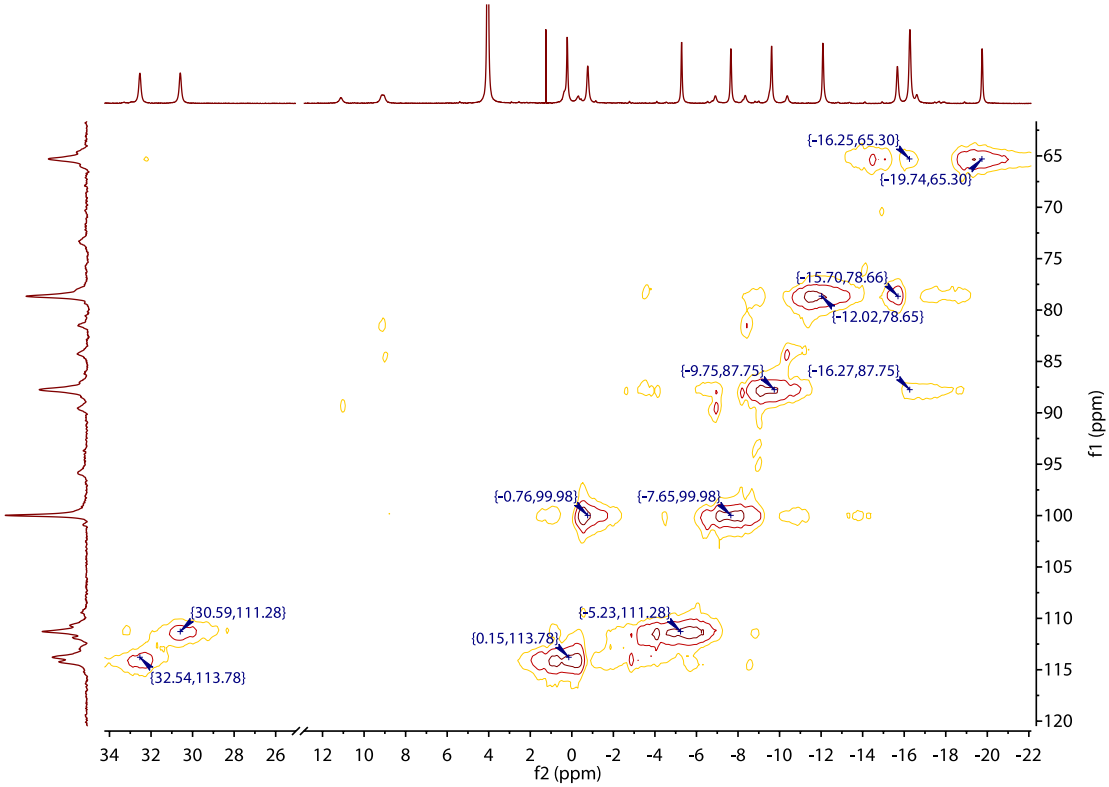


(e) $^{1}H - {}^{13}C$ HMQC spectrum of the $[Eu(t\text{DODAM})(H_2O)]^+$ complex.

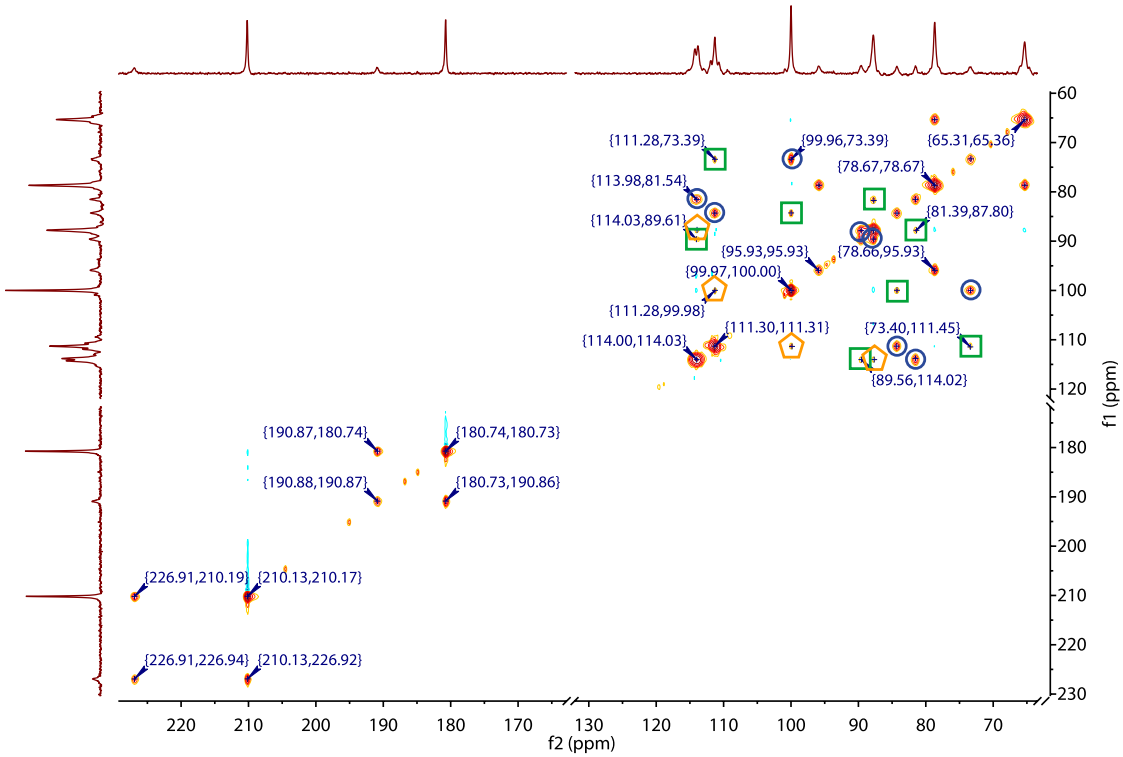


(f) $^{13}C - {}^{13}C$ EXSY spectrum of the $[Eu(t\text{DODAM})(H_2O)]^+$ complex measured at 600 MHz and 5 °C, $\tau_M$ = 5 ms. Blue circles represent crosspeaks due to the arm rotation, green squares represent crosspeaks due to the ring inversion and the orange pentagons represent crosspeaks due to both movements in succession.

Figure 4.16: NMR spectra of the europium(III) complex.

### 4.9.1 Square-antiprismatic isomer of [Eu(*t*dodam)($H_2O$)]$^+$ complex

The assignment was done using NMR spectra obtained at 5 °C and using 600 MHz spectrometer. For better orientation, the signals assigned to the ring protons are marked by letters A–H starting from the most downfield peak. Assignment starts with assumption that two most paramagneticaly shifted signals (A, B) belong to the ring axial protons of the major (SA) isomer. For now, let's assign these two protons randomly. According to the $^1$H – $^1$H COSY spectrum (Fig. 4.16c), the peaks can be divided into two groups: those having 3 crosspeaks and are assigned to the ring protons (black and blue lines in the spectrum) and those having 1 crosspeak and are assigned to the pendant protons (green and magenta lines in the spectrum). Using the $^1$H – $^1$H COSY spectrum, two foursomes (A, C, D, F and B, E, G, H) and two pairs ($X_1$, $X_2$ and $Y_1$, $Y_2$) of peaks were found. These four groups form four isolated spin systems. The assignment at this point is shown in Fig. 4.17a.

In order to classify the peaks according to their orientation on the cycle (whether they are axial or equatorial), $^1$H – $^1$H EXSY spectrum Fig. 4.16d was studied. In EXSY spectrum, each peak has three crosspeaks, only one of them belongs to the same isomer and it arises due to ring inversion and arm rotation in succession. In terms of molecular structure, this means that two protons that are symmetrical with respect to the time-averaged plane of symmetry defined by two opposite pendant arms and have different position on the ring have a crosspeak. Proton A has a crosspeak with proton G and proton B has a crosspeak with proton F. Therefore, position of these protons on the macrocycle is fixed. It is also known that protons C, H and D, E are related but this information is not enough for assignment of these protons. Assignment at this stage is shown in Fig. 4.17b.

Using $^1$H – $^{13}$C HMQC Fig. 4.16e, we can find which two protons are bound to the same carbon atom. This also determines the connectivity to carbon atoms. $^{13}$C{$^1$H} NMR spectrum is shown in Fig. 4.16b. Carbon atoms of the macrocycle were labeled a–d starting at the carbon connected to proton A going anti-clockwise. Also carbon atoms of pendant methylene groups ($p_1$ and $p_2$) are assigned to pendant protons ($X_1$, $X_2$ and $Y_1$, $Y_2$, respectively). Assignment at this stage is shown in Fig. 4.17c.

After more thorough inspection of the COSY spectrum, few weak crosspeaks between macrocyclic protons and pendant methylenes were found. Protons A and C have crosspeaks with protons $X_1$ and $X_2$, respectively. Proton E has crosspeak with proton $Y_2$. Thus, methylene groups were assigned. However, it is not possible to assign carbonyl groups and it is not possible to determine the position of the amide or acetate pendant arms on the cycle. Therefore, two assignments are possible, shown in Figs. 4.17d and 4.17e.

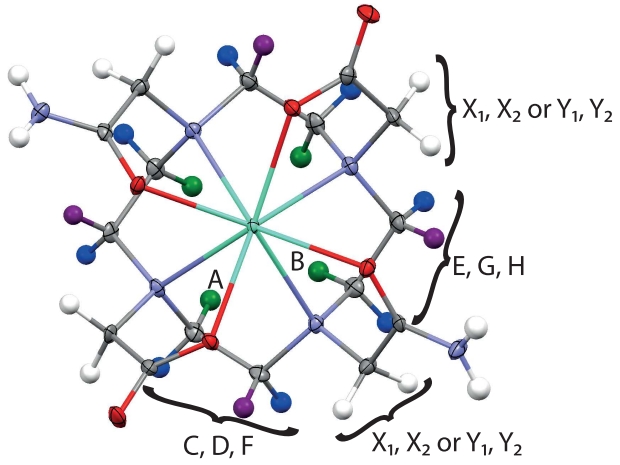


(a) Assignment using only $^{1}H-{}^{1}H$ COSY spectrum.

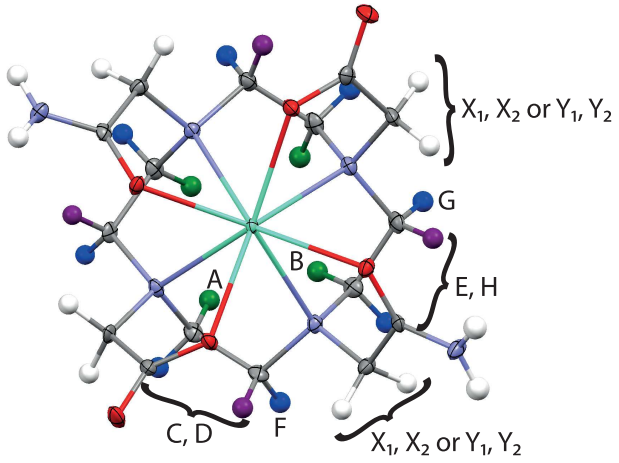


(b) Assignment using $^{1}H-{}^{1}H$ COSY and $^{1}H-{}^{1}H$ EXSY spectra.

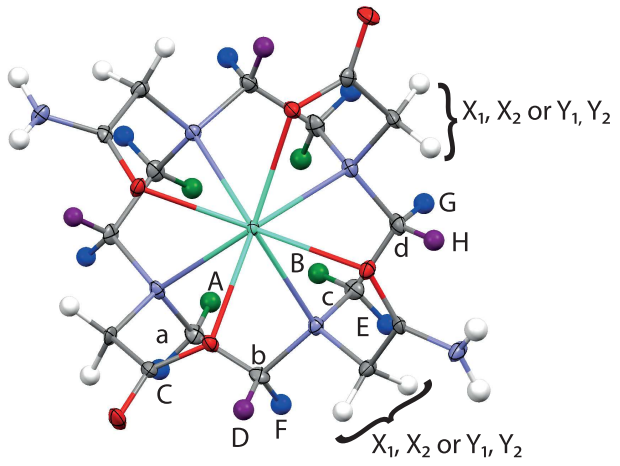


(c) Assignment using $^{1}H-{}^{1}H$ COSY, $^{1}H-{}^{1}H$ EXSY and $^{1}H-{}^{13}C$ HMQC spectra.

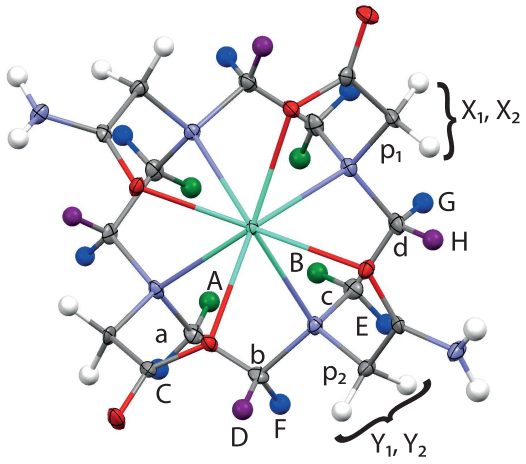


(d) Final assignment of the SA isomer (variant A).

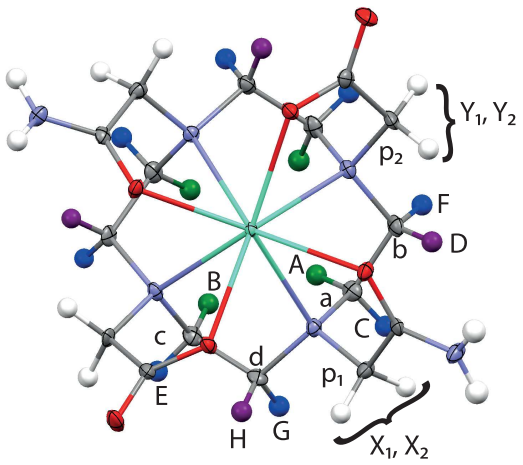


(e) Final assignment of the SA isomer (variant B).

Figure 4.17: Process of assignment of $^{1}H$ and $^{13}C$ NMR spectra of the europium(III) complex.

### 4.9.2 Twisted-square antiprismatic isomer of the [Eu(*t*dodam)($H_2O$)]$^+$ complex

Assignment of the peaks of the TSA isomer was copied from the assignment of the SA isomer using $^1$H – $^1$H and $^{13}$C – $^{13}$C EXSY spectra Fig. 4.16d and Fig. 4.16f. Also, some crosspeaks of the TSA isomer were found in the $^1$H – $^1$H COSY spectrum, however, most of the peaks have only one or two visible crosspeaks, largely due to the lower intensity and overlaps. HMQC did not contain any information about TSA isomer. Peaks of the TSA isomer were labeled with primes and correspond to the peaks of the SA isomer after arm rotation. Of note is the fact that the most downfield peak of the TSA isomer is not the axial proton (A' or B') which would be most paramagneticaly shifted in the case of $C_2$ symmetry with the principal magnetic axis coincident with the molecular symmetry axis. The pendant methylene protons are also interesting since they have a lot higher chemical shifts than the corresponding peaks of the SA isomer. Thus, it can be said that the TSA isomer does not have principal magnetic axis coincident with the $C_2$ molecular symmetry axis.

## 4.10 Solution dynamics of the [Eu(*t*dodam)($H_2O$)]$^+$ complex

In the aqueous solution of the Eu(III) complex, an equilibrium of 79 % of SA isomer and 21 % of TSA isomer is established (determined by integration of the axial proton signals in the $^1$H NMR spectrum). Interconversion between the two isomers was followed by measuring $^1$H – $^1$H EXSY spectra with mixing time ranging from 0.1 ms to 25 ms. Crosspeaks of SA axial protons were integrated and dependence of the integral on the mixing time $\tau_M$ was fitted numerically in MATLAB using script written by Jan Blahut to solve Bloch-McConnell Equation (4.14) where $\mathbf{R}$ is diagonal matrix of $R_1$ relaxation rates of the exchanging protons, $\mathbf{M}(t)$ is a vector of diagonal peak of the axial proton and its three crosspeaks corresponding to arm rotation, ring inversion and both movements in succession, $\mathbf{M}_{eq}$ is its equilibrium value and $\mathbf{k}$ is exchange matrix which describes all exchange processes and is shown in Equation (4.15) (subscripts AR and RI means arm rotation and ring inversion, respectively). [16]

$$\frac{\mathrm{d}\mathbf{M}(t)}{\mathrm{d}t} = -\mathbf{R}(\mathbf{M}(t) - \mathbf{M}_{eq}) + \mathbf{k}\mathbf{M}(t) \tag{4.14}$$

$$\mathbf{k} = \begin{pmatrix} -k_{\text{SA-AR}} - k_{\text{SA-RI}} & 0 & k_{\text{TSA-AR}} & k_{\text{TSA-RI}} \\ 0 & -k_{\text{SA-AR}} - k_{\text{SA-RI}} & \text{TSA-RI} & k_{\text{TSA-AR}} \\ k_{\text{SA-AR}} & k_{\text{SA-RI}} & -k_{\text{TSA-AR}} - k_{\text{TSA-RI}} & 0 \\ k_{\text{SA-RI}} & k_{\text{SA-AR}} & 0 & -k_{\text{TSA-AR}} - k_{\text{TSA-RI}} \end{pmatrix} \tag{4.15}$$

Solution of Equation (4.14) yields relaxation rates $R_1$ of the exchanging protons and exchange rate constants describing arm rotation and ring inversion processes from SA to TSA and from TSA to SA isomers. Dependences of integrals of the crosspeaks and the diagonal peaks on mixing time $\tau_M$ are shown in Fig. 4.18 together with the numerical fits. The fitting was done on group of peaks belonging to both axial protons of the SA isomer separately and both axial protons of the TSA isomer together due to the extensive overlap of their diagonal peaks. The results of the fit together with literature data obtained for the DOTA complex are shown in Table 4.9.

Table 4.9: Exchange rates of the $[Eu(t\text{dodam})(H_2O)]^+$ complex and relaxation rates of the corresponding protons compared with the previously published data for the $[Eu(dota)(H_2O)]^-$ complex.

| | Complex | |
|---|---|---|
| Parameter | $[Eu(t\text{dodam})(H_2O)]^+$ | $[Eu(dota)(H_2O)]^-$ [16] |
| $k_{SA-AR}$ ($s^{-1}$) | 31(2) | 5.58 |
| $k_{SA-RI}$ ($s^{-1}$) | 12(2) | 10.60 |
| $k_{TSA-AR}$ ($s^{-1}$) | 122(4) | 25.80 |
| $k_{TSA-RI}$ ($s^{-1}$) | 26(2) | 52.30 |
| | | |
| $R_{1,SA-Ax}$ ($s^{-1}$) | 78(3) | 69.1 |
| $R_{1,SA-Eq}$ ($s^{-1}$) | 0(15) | 22.53 |
| $R_{1,TSA-Ax}$ ($s^{-1}$) | 92(5) | 47.6 |
| $R_{1,TSA-Eq}$ ($s^{-1}$) | 25(48) | 18.3 |

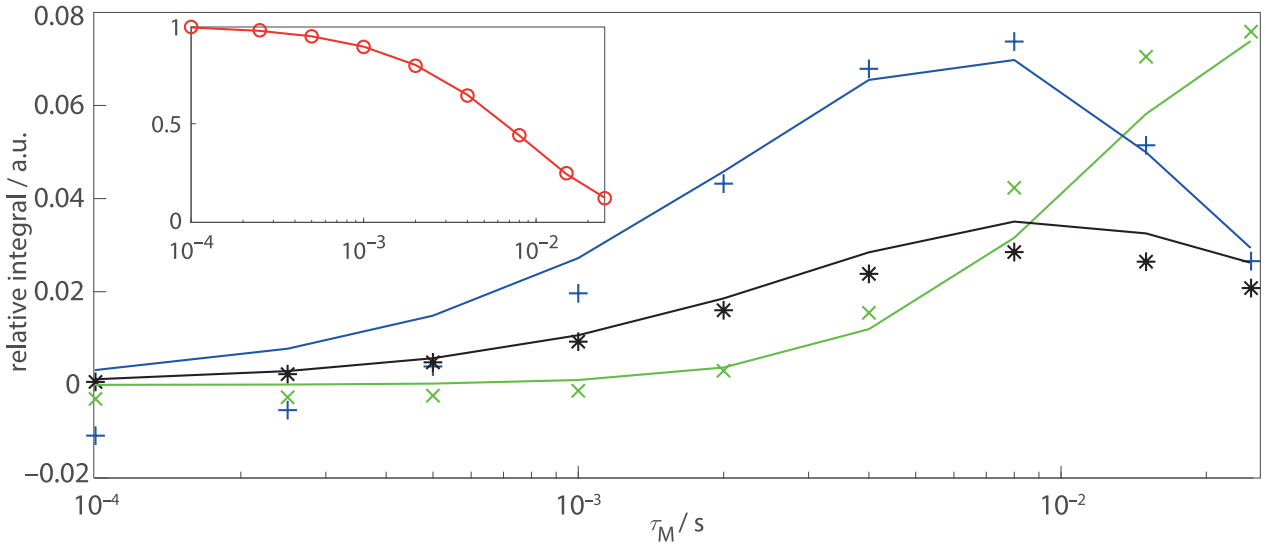


(a) Fit of crosspeaks belonging to axial proton A of SA isomer

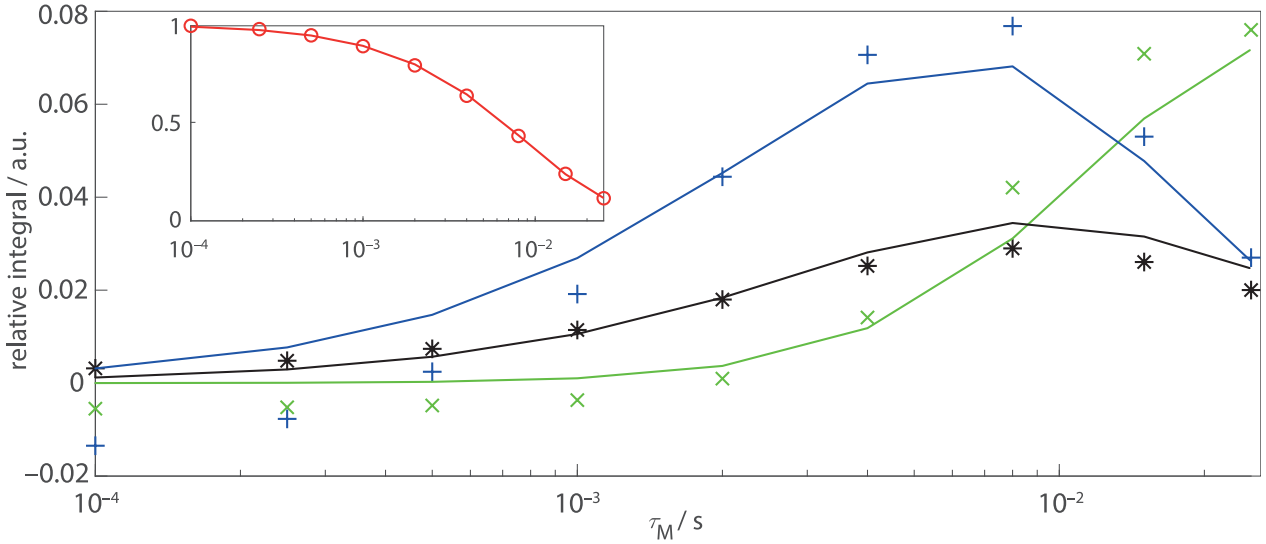


(b) Fit of crosspeaks belonging to axial proton B of SA isomer

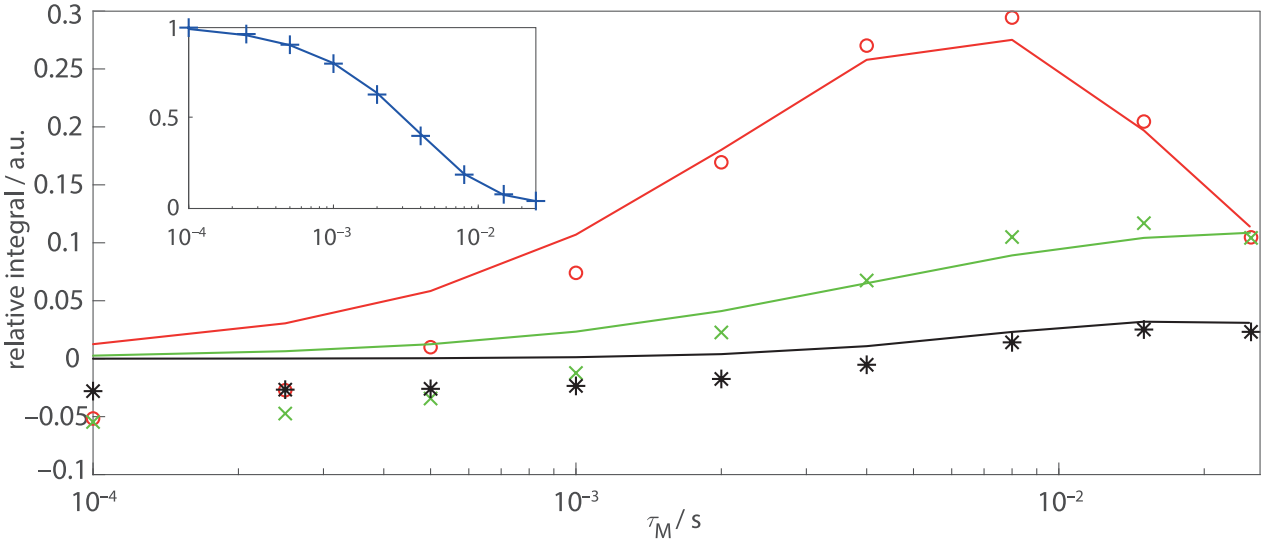


(c) Fit of crosspeaks belonging to axial protons A' and B' of TSA isomer

Figure 4.18: Numerical fits of integral intensities of crosspeaks in respect to the EXSY mixing time $\tau_M$. Legend: red circles: axial protons of SA isomer, blue crosses: axial protons of TSA isomer, green crosses: equatorial protons of SA isomer and black stars: equatorial protons of TSA isomer. For $^1H - ^1H$ EXSY spectra of the axial protons A and B, see Fig. D.1, p. 77.

## 4.11 Relaxometry of [Gd(*t*dodam)($H_2O$)]$^+$ complex

The $^1$H NMRD profiles at pH 7 were obtained at temperatures 10, 25 and 37 °C and are shown in Fig. 4.19. At the time of writing this Thesis, full analysis of relaxometric data has not been available, therefore, only comparison of previously published relaxivities of DOTA and DOTAM was made and is shown in Table 4.10. The values quoted were obtained or published for magnetic field intensity corresponding to the proton Larmor frequency 20 MHz at temperature 25 °C.

Table 4.10: Comparison of proton relaxivities of Gd(III) complexes of DOTA, *t*DODAM and DOTAM at proton Larmor frequency 20 MHz and temperature 25 °C.

| Complex | $r_1$ (mM$^{-1}$s$^{-1}$) | ref. |
|---|---|---|
| [Gd(dota)($H_2O$)]$^-$ | 4.74 | [20] |
| [Gd(*t*dodam)($H_2O$)]$^+$ | 4.05 | This Thesis |
| [Gd(dotam)($H_2O$)]$^{3+}$ | 2.5 | [22] |

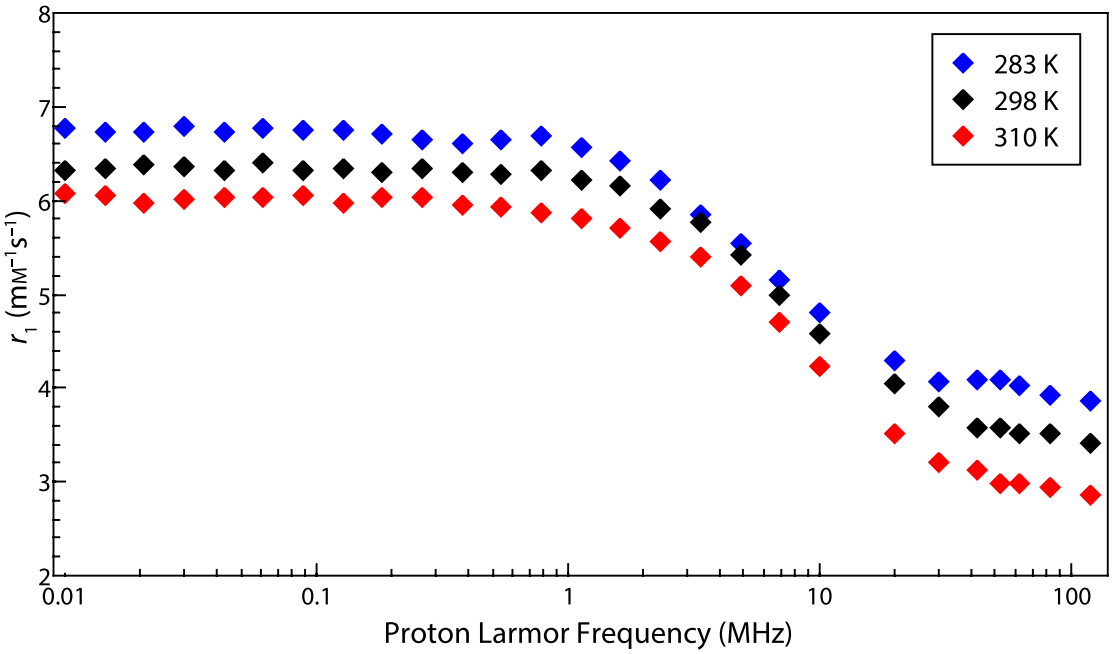


Figure 4.19: The $^1$H NMRD profiles of [Gd(*t*dodam)($H_2O$)]$^+$ complex measured at 10, 25 and 37 °C.

## 4.12 XRD structures

Single crystals of $t$Bu$_2$$t$dodam · 2 $CHCl_3$ were grown by diffusion of $Et_2O$ into a chloroform solution of $t$Bu$_2$$t$dodam during 1 day. Single crystals of $H_2$($t$dodam) · 3 $H_2O$ were grown by overlaying aq. $H_2$($t$dodam) by ethanol and letting the crystals grow over several weeks. Single crystals of the complexes were isolated from the bulk material during preparation of the complexes for solution study (by diffusion of acetone vapour into aq. solution of the complex with chloride as counterion). Perchlorate salts of complexes were grown by diffusion of isopropanol into solution of the complex in 0.8 M aq. $LiClO_4$ over 2 weeks. Table E.1 (p. 78) contains experimental crystallographic parameters for the structures reported in this Thesis. Four different structural types were obtained for the complexes. Isostructural crystals were obtained for complexes of Ce(III), Ho(III) and Tm(III), and Gd(III) and Yb(III). Eu(III) and Tb(III) were not isostructural with any other complex. Ce(III) complex crystallised as TSA isomer, all other complexes crystallised as SA isomers. Figures of obtained structures are shown in Fig. 4.20 (solvent molecules and counterions are omitted for clarity). Differences between the structures of the two isomers are summarised in Table 4.11 ($d$ is distance, $\measuredangle O_{ac}$-Ln-$O_{ac}$ is angle between coordinated oxygen atom of acetate pendant arm, lanthanide(III) ion and coordinated oxygen atom of second acetate pendant arm and $\phi$ is torsion angle of $N_4$ and $O_4$ planes). The distance of the coordinated water molecule from the lanthanide(III) ion decreases as the ionic radius of the metal ion decreases and the distance of the metal to $N_4$ plane decreases. TSA isomer is preferred for larger lanthanide(III) ions due to larger macrocyclic cavity as documented by larger distance of $N_4$ and $O_4$ planes in the cerium(III) complex.

Table 4.11: Differences in geometrical parameters of TSA and SA isomers shown on the example of Ce(III) and Eu(III) complexes.

| Parameter | [Ce($t$dodam)($H_2O$)]$^+$ | [Eu($t$dodam)($H_2O$)]$^+$ |
|---|---|---|
| $d$(Ln—$OH_2$) (Å) | 2.527 | 2.448 |
| $d$(Ln—$N_4$) (Å) | 1.759 | 1.64 |
| $d$(Ln—$O_4$) (Å) | 0.768 | 0.714 |
| $d$($N_4$—$O_4$) (Å) | 2.527 | 2.354 |
| $\measuredangle O_{ac}$-Ln-$O_{ac}$ (°) | 144.4 | 145.9 |
| $\measuredangle O_{am}$-Ln-$O_{am}$ (°) | 142.8 | 144.1 |
| average $\phi$ (°) | 23.1 | 38.1 |

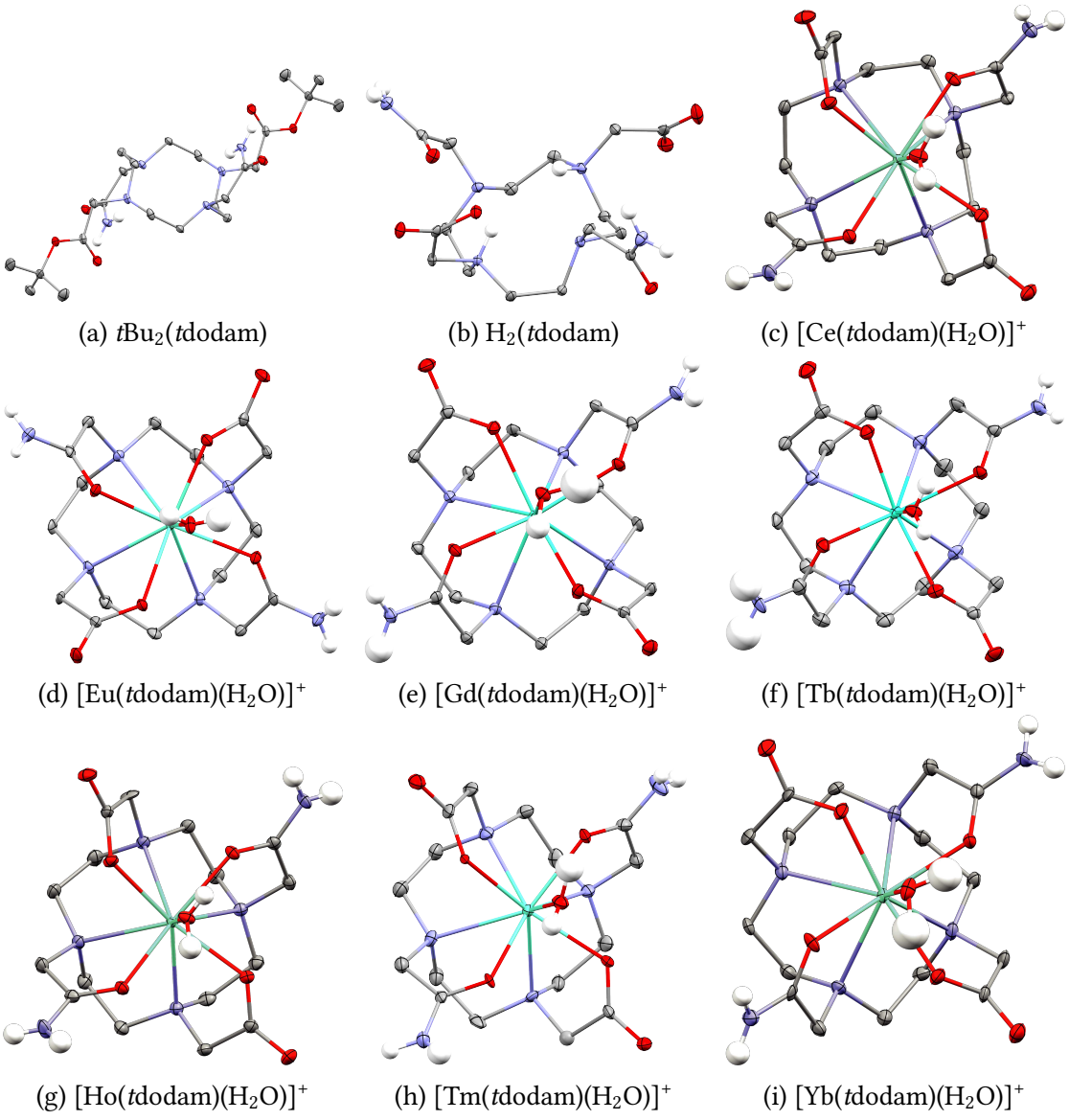

(a) $t$Bu$_2$($t$dodam) (b) H$_2$($t$dodam) (c) [Ce($t$dodam)(H$_2$O)]$^+$

(d) [Eu($t$dodam)(H$_2$O)]$^+$ (e) [Gd($t$dodam)(H$_2$O)]$^+$ (f) [Tb($t$dodam)(H$_2$O)]$^+$

(g) [Ho($t$dodam)(H$_2$O)]$^+$ (h) [Tm($t$dodam)(H$_2$O)]$^+$ (i) [Yb($t$dodam)(H$_2$O)]$^+$

Figure 4.20: XRD structures of obtained single crystals. Colour code: **carbon**, **nitrogen**, **oxygen**, **lanthanide** and hydrogen atoms bound to heteroatoms are light grey. Hydrogen atoms bound to carbon atoms, solvate water molecules and anions are omitted for the sake of clarity.

# Chapter 5

# Conclusion

New macrocyclic ligand, the simplest diamide derivative of DOTA, was synthesised and its properties were thoroughly studied. By means of UV-VIS spectrophotometry, it was found that the formation of its cerium(III) complex is faster than formation of $[Ce(dotam)(H_2O)]^{3+}$ and slower than formation of $[Ce(dota)(H_2O)]^-$. The opposite trend is observed in dissociation kinetics of these complexes. The reason for this trend in rate of formation of the complexes is the decreasing stability of the *out-of-cage* complexes, DOTA>*t*DODAM>DOTAM, and slower proton transfer in the case of *t*DODAM complex than in the case od DOTA complex. In the case of DOTAM complex, no proton transfer was observed as, instead, fully deprotonated ligand reacts directly with metal ion without *out-of-cage* intermediate. The opposite trend for decomplexation reaction is explained mechanistically. In order for the complex to dissociate, it has to undergo protonation. It is natural to expect that positively charged $[Ce(tdodam)]^+$ and $[Ce(dotam)]^{3+}$ complexes protonises less efficiently than negatively charged $[Ce(dota)]^-$ complex due to Coulombic repulsion.

Potentiometric titrations showed that substitution of acetate pendant arms of the ligand DOTA for acetamide pendant arms destabilises all examined complexes (Cu(II), Zn(II), Ce(III), Eu(III), Lu(III)) but no comparison was possible for Pb(II) complex since only lower estimate was published for DOTAM and no data are available for DOTA.

Luminescence spectrophotometry showed that the europium(III) complex of the ligand *t*DODAM has one directly coordinated water molecule. NMR study of the complexes provided the isomeric ratio in solution for whole lanthanide series and it is most alike to the complexes of DOTAM. The EXSY study showed that the europium(III) complex of the ligand *t*DODAM is more fluxional than the respective complex of the ligand DOTA, mainly due to higher fluxionality of amide pendant arms. Using several 2D NMR techniques, $^1H$ and $^{13}C\{^1H\}$ NMR spectra of europium(III) complex were assigned.

Relaxometric measurements of gadolinium(III) complex were done. Relaxivity of this complex is between the published values for gadolinium(III) complexes of DOTA and DOTAM. Full evaluation of these measurements has not been done as of the time of writing this Thesis; thus, no conclusion can be made about the coordinated water molecule exchange rate.

# Acknowledgment

First of all, I have to express my sincere gratitude to my supervisor Petr Hermann for a lot of great ideas and countless consultations. Next, I have to thank all those people who helped me with preparation of this Thesis, namely Vojta Kubíček for help with evaluation of the kinetic measurements, Ivana Císařová for X-ray measurements and Honza Kotek for data refinement, Zdeněk Tošner for measurement of almost a gigabyte of spectral data of weird paramagnetics and Honza Blahut for help with the evaluation of 2D EXSY experiments, Zuzka Böhmová for execution of potentiometric titrations and Ondra Zemek for obtaining mass spectra. Last, my thanks go to Italy to Mauro Botta and Fabio Carniato for help with obtaining $^{1}$H NMRD profiles and their evaluation.

Next, I would like to thank to all the people who made the time spent in the lab time well and pleasantly spent. Even though there are too many people to explicitly name each and everyone, I am glad that I had the opportunity to spend time with you and I am thankful for all the great moments in (and also outside) the lab.

Last, but certainly not least, I would like to thank to my family for raising me and supporting me thorough my whole life and study at the Charles University in every possible way. Thank you, mum, thank you, dad.

# Bibliography


1. Caillé, J.-M., Lemanceau, B. & Bonnemain, B. Gadolinium as a contrast agent for NMR. *Am. J. Neuroradiol.* **4,** 1041–1042 (1983).
2. Weinmann, H. J., Brasch, R. C., Press, W. R. & Wesbey, G. E. Characteristics of gadolinium-DTPA complex: A potential NMR contrast agent. *Am. J. Roentgenol.* **142,** 619–624 (1984).
3. Tweedle, M. F. Physicochemical properties of Gadoteridol and other magnetic resonance contrast agents. *Invest. Radiol.* **27,** 2–6 (1992).
4. Pan, D. *et al.* Revisiting an old friend: Mn-based MRI contrast agents. *Wiley Interdiscip. Rev. Nanomed. Nanobiotechnol.* **2,** 162–173 (2011).
5. Vallabani, N. V. S. & Singh, S. Recent advances and future prospects of iron oxide nanoparticles in biomedicine and diagnostics. *3 Biotech* **8,** 1–23 (2018).
6. Meckel, M, Bergmann, R, Miederer, M & Roesch, F. Bone targeting compounds for radiotherapy and imaging : *Me(III)-DOTA conjugates of bisphosphonic acid, pamidronic acid and zoledronic acid. *EJNMMI Radiopharm. Chem.* **1,** 1–14 (2016).
7. Breeman, W. A., De Jong, M., Visser, T. J., Erion, J. L. & Krenning, E. P. Optimising conditions for radiolabelling of DOTA-peptides with $^{90}$Y, $^{111}$In and $^{177}$Lu at high specific activities. *Eur. J. Nucl. Med. Mol. Imaging* **30,** 917–920 (2003).
8. Liu, Z. *et al.* Measurement of reaction kinetics of [$^{177}$Lu]Lu-DOTA-TATE using a microfluidic system. *Dalton Trans.* **46,** 14669–14676 (2017).
9. *Radioisotopes in medicine, World Nuclear Association, http://www.world-nuclear.org/information-library/non-power-nuclear-applications/radioisotopes-research/radioisotopes-in-medicine.aspx, accessed on 16/05/19* 2018.
10. Corsi, D. M., Platas-iglesias, C., Bekkum, H. V. & Peters, J. A. Determination of paramagnetic lanthanide ( III ) concentrations from bulk magnetic susceptibility shifts in NMR spectra. *Magn. Reson. Chem.* **39,** 723–726 (2001).
11. Sorace, L. & Gatteschi, D. *Electronic Structure and Magnetic Properties of Lanthanide* p. 7 (2015).

12. Jeener, J., Meier, B. H., Bachmann, P. & Ernst, R. R. Investigation of exchange processes by two-dimensional NMR spectroscopy. *J. Chem. Phys.* **71,** 4546–4553 (1979).

13. Supkowski, R. M. & Horrocks, W. D. W. On the determination of the number of water molecules, q, coordinated to europium(III) ions in solution from luminescence decay lifetimes. *Inorg. Chim. Acta* **340,** 44–48 (2002).

14. Baranyai, Z., Bányai, I., Brücher, E., Király, R. & Terreno, E. Kinetics of the formation of $[Ln(DOTAM)]^{3+}$ complexes. *Eur. J. Inorg. Chem.* 3639–3645 (2007).

15. Stenson, P. A., Thompson, A. L. & Parker, D. Structural characterisation of a diprotonated ligand lanthanide complex — a key intermediate in lanthanide ion association and complex dissociation pathways. *Dalton Trans.* **99,** 3291–3293 (2006).

16. Blahut, J., Hermann, P., Tošner, Z. & Platas-Iglesias, C. A combined NMR and DFT study of conformational dynamics in lanthanide complexes of macrocyclic DOTA-like ligands. *Phys. Chem. Chem. Phys.* **19,** 26662–26671 (2017).

17. Brücher, E, Laurenczy, G & Makra, Z. Studies on the kinetics of formation and dissociation of the cerium(III)-DOTA complex. *Inorg. Chim. Acta* **139,** 141–142 (1987).

18. Burai, L., Fábián, I., Szilágyi, E. & Brücher, E. Equilibrium and kinetic studies on the formation of the lanthanide(III) complexes, $[Ce(dota)]^-$ and $[Yb(dota)]^-$. *Dalton Trans.* 243–248 (1998).

19. Pniok, M. *et al.* Thermodynamic and kinetic study of scandium(III) complexes of DTPA and DOTA: A step toward scandium radiopharmaceuticals. *Chem. Eur. J.* **20,** 7944–7955 (2014).

20. Powell, D. H. *et al.* Structural and dynamic parameters obtained from 17O NMR, EPR, and NMRD studies of monomeric and dimeric $Gd^{3+}$ complexes of interest in magnetic resonance imaging: An integrated and theoretically self-consistent approach. *J. Am. Chem. Soc.* **118,** 9333–9346 (1996).

21. Pasha, A., Tircsó, G., Benyó, E. T., Brücher, E. & Sherry, A. D. Synthesis and characterization of DOTA-$(amide)_4$ derivatives: Equilibrium and kinetic behavior of their lanthanide(III) complexes. *Eur. J. Inorg. Chem.* **27,** 4340–4349 (2007).

22. Aime, S. *et al.* NMR , Relaxometric , and Structural Studies of the Hydration and Exchange Dynamics of Cationic Lanthanide Complexes of Macrocyclic Tetraamide Ligands. *J. Am. Chem. Soc.* **121,** 5762–5771 (1999).

23. Zhang, S. *et al.* {DOTA-bis(amide)}lanthanide complexes: NMR evidence for differences in water-molecule exchange rates for coordination isomers. *Chem. Eur. J.* **7,** 288–296 (2001).

24. Burnett, M. E. *et al.* Electrochemical investigation of the $Eu^{3+/2+}$ redox couple in complexes with variable numbers of glycinamide and acetate pendant arms. *Eur. J. Inorg. Chem.* **2017,** 5001–5005 (2017).

25. Burnett, M. E., Adebesin, B., Ratnakar, S. J. & Green, K. N. Crystallographic characterization and non-innocent redox activity of the glycine modified DOTA scaffold and its impact on $Eu^{III}$ electrochemistry. *Eur. J. Inorg. Chem.* **2018,** 1556–1562 (2018).

26. Pujales-Paradela, R. *et al.* Gadolinium(III)-based dual $^{1}H/^{19}F$ magnetic resonance imaging probes. *Chem. Eur. J.* **25,** 4782–4792 (2019).

27. Procházková, S., Hraníček, J., Kubíček, V. & Hermann, P. Formation kinetics of europium(III) complexes of DOTA and its bis(phosphonate) bearing analogs. *Polyhedron* **111,** 143–149 (2016).

28. Procházková, S. *et al.* DOTA analogues with a phosphinate-iminodiacetate pendant arm: modification of the complex formation rate with a strongly chelating pendant. *Dalton Trans* **46,** 10484–10497 (2017).

29. Sheldrick, G. M. *SHELXT-2014: Program for crystal structure solution from diffraction data.* Göttingen, 2014.

30. Sheldrick, G. M. *SHELXL-2014: Program for crystal structure refinement from diffraction data.* Göttingen, 2014.

31. Hübschle, C. B., Sheldrick, G. M. & Dittrich, B. ShelXle: a Qt graphical user interface for SHELXL. *J. Appl. Cryst.* **2011,** 1281–1284 (2011).

32. Kývala, M. Solution equilibria analysis with the OPIUM computer program. https://web.natur.cuni.cz/~kyvala/opium.html.

33. De León-Rodríguez, L. M., Kovacs, Z., Esqueda-Oliva, A. C. & Miranda-Olvera, A. D. Highly regioselective *N-trans* symmetrical diprotection of cyclen. *Tetrahedron Lett.* **47,** 6937–6940 (2006).

34. Vipond, J. *et al.* A bridge to coordination isomer selection in lanthanide(III) DOTA-tetraamide complexes. *Inorg. Chem.* **46,** 2584–2595 (2007).

35. MicroMath Inc, Salt Lake City, U. & USA. *Micromath Scientist (Version 2.0)* 1995.

36. Tóth, É., Lázár, I. & Tóth, I. Kinetics of formation and dissociation of lanthanide(III)-DOTA complexes. *Inorg. Chem* **33,** 4070–4076 (1994).

37. Vipond, J. *et al.* A bridge to coordination isomer selection in lanthanide(III) DOTA-tetraamide complexes. *Inorg. Chem.* **46,** 2584–2595 (2007).

38. Aime, S. *et al.* Conformational and coordination equilibria on DOTA complexes of lanthanide metal ions in aqueous solution studied by $^{1}H$-NMR spectroscopy. *Inorg. Chem.* **36,** 2059–2068 (1997).

39. Kyle J. Miller *et al.* The population of SAP and TSAP isomers in cyclen-based lanthanide(III) chelates is substantially affected by solvent. *Inorg. Chem. Commun.* **49,** 8662–8664 (2010).

40. Marques, M. P. *et al.* NMR conformational study of the lanthanide(III) complexes of DOTA in aqueous solution. *J. Alloys Compd.* **225,** 303–307 (1995).

# Appendices

## A $^{1}$H NMR titration of *t*DODAM

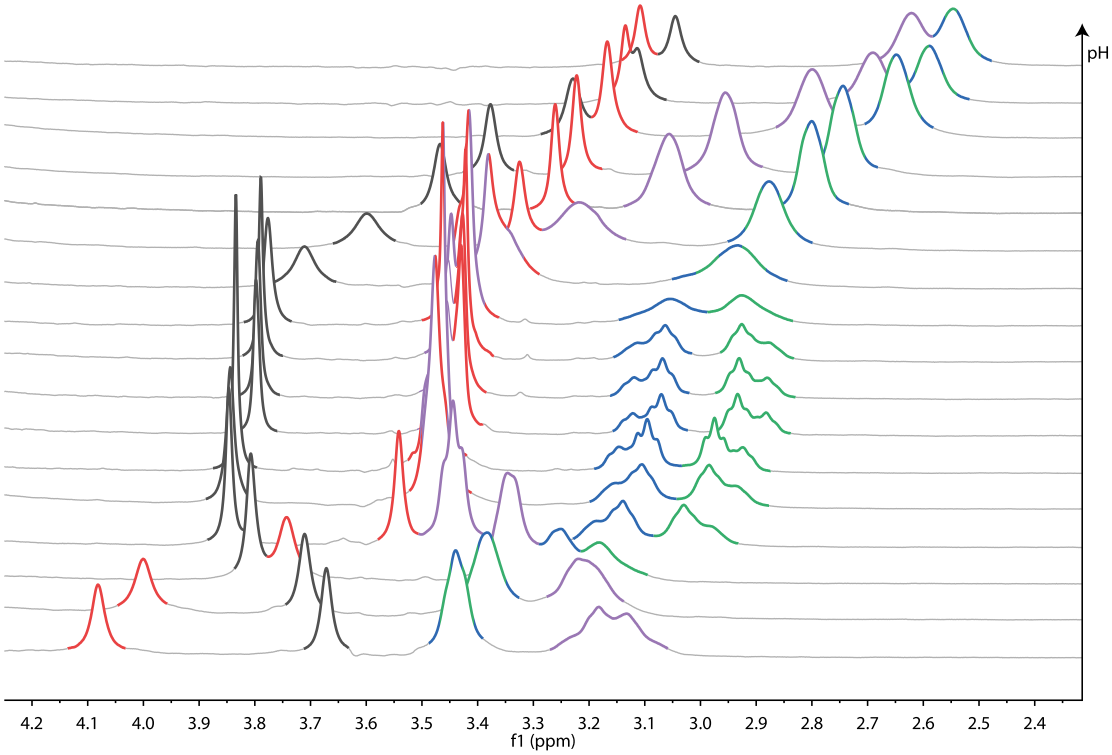


Figure A.1: $^{1}$H NMR spectra obtained during the NMR titration of *t*DODAM. Peaks are coloured according to their assignment to individual protons as shown in Fig. A.2. All NMR spectra were referenced to *t*BuOH signal (not shown) $\delta_{H}$ = 1.24 ppm. For a plot of chemical shifts of individual peaks against pH, see Fig. 4.10 (p. 43).

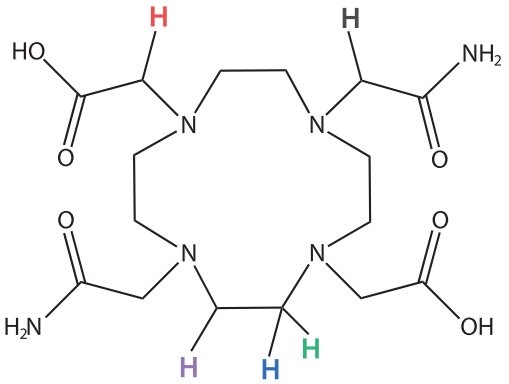


Figure A.2: Formula of the title ligand with hydrogen atoms labeled to explain the peak labeling in the plot (Fig. A.1).

In the pH range 2–7, somewhat strange appearance of the $^1$H NMR spectrum can be observed. Two chemically equivalent ring protons give rise to two multiplets that are symmetrical in respect to their average chemical shift. This pH range is identical to pH range where zwitterionic form is prevalent (see distribution diagram, Fig. 4.9a, p. 41). This is most likely due to formation of slowly-exchanging conformation isomers which may be stabilised by hydrogen bonds. This was supported by variable-temperature experiment. In this experiment, $^1$H NMR spectra of $D_2O$ solution of *t*DODAM (pD = 4) were measured at temperatures ranging from 25 to 90 °C. Coalescence of the two multiplets was observed at approximately 59 °C. The $^1$H NMR spectra obtained at various temperatures are given in Fig. A.3.

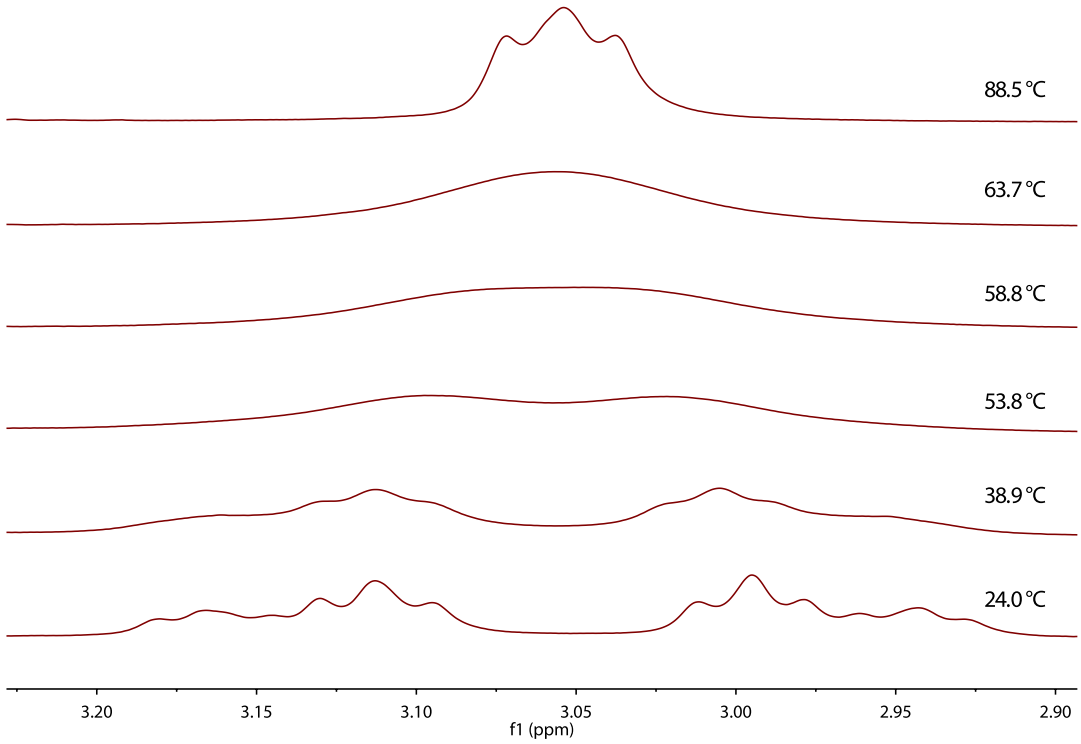


Figure A.3: $^1$H NMR spectra obtained during the variable-temperature experiment. All NMR spectra were referenced to HDO signal (not shown).[1] Temperature was measured using second NMR tube with pure ethyleneglycol and was calculated using the tempcal macro in VNMRJ program.

[1] The dependence of the chemical shift of the residual HDO resonance on temperature is described in Gottlieb, H. E., Kotlyar, V. & Nudelman, A. NMR Chemical Shifts of Common Laboratory Solvents as Trace Impurities. *J. Org. Chem.* **62**, 7512–7515 (1997).

# B $^{1}$H NMR spectra of lanthanide(III) complexes

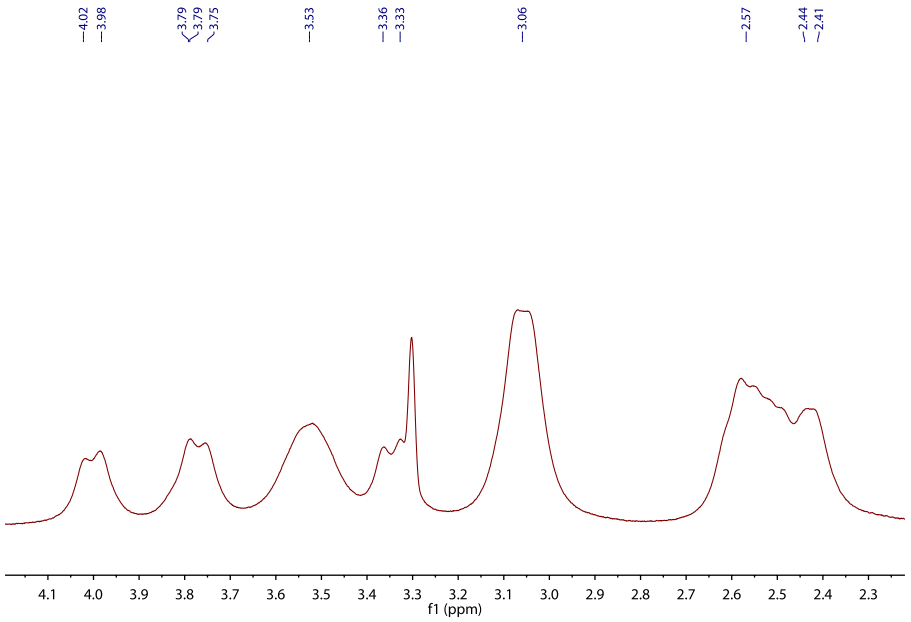


Figure B.1: $^{1}$H NMR spectrum of La(III) complex (400 MHz, −35 °C, 40 % $CD_3OD/D_2O$ v/v)

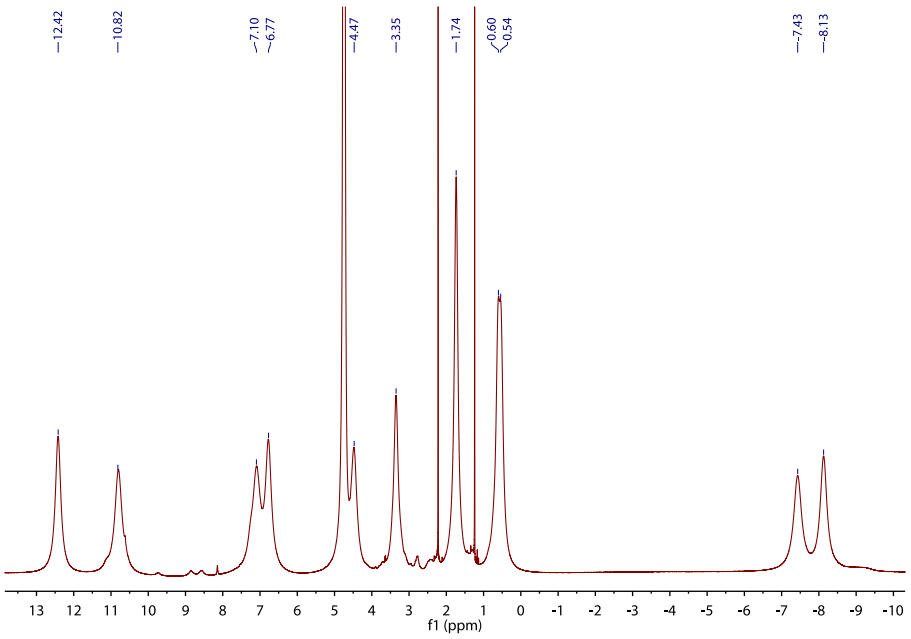


Figure B.2: $^{1}$H NMR spectrum of Ce(III) complex (600 MHz, 25 °C, $D_2O$)

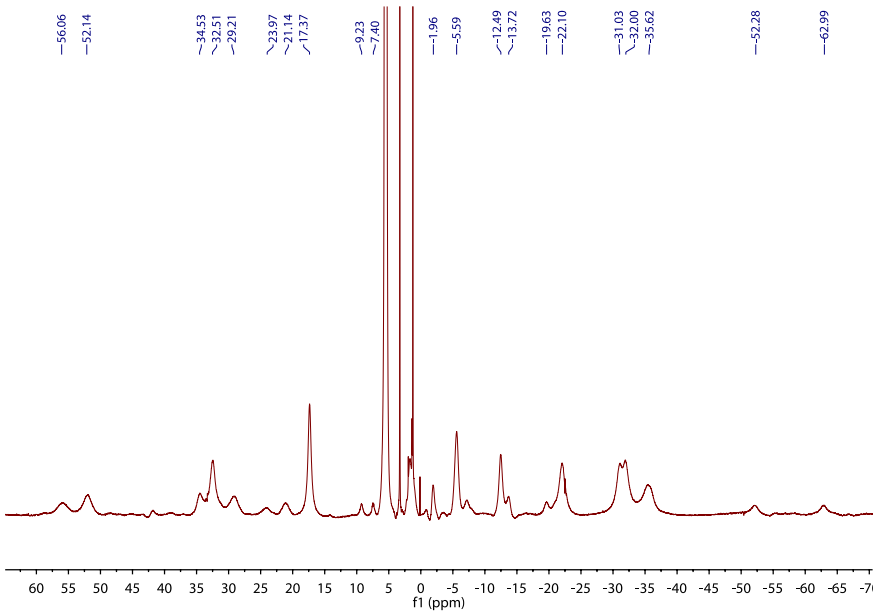


Figure B.3: $^{1}$H NMR spectrum of Pr(III) complex (400 MHz, −35 °C, 40 % $CD_3OD/D_2O$ v/v)

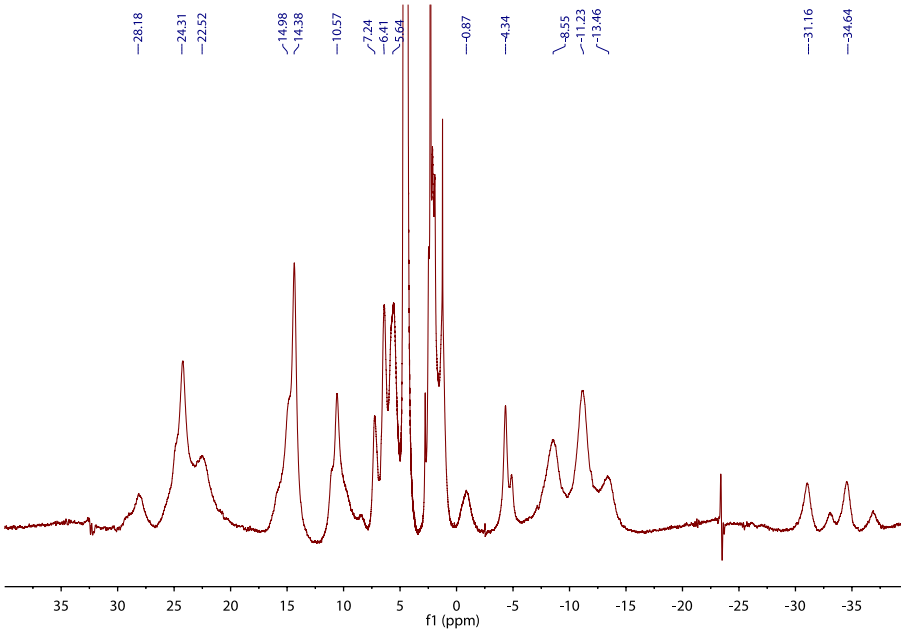


Figure B.4: $^{1}$H NMR spectrum of Nd(III) complex (400 MHz, −35 °C, 40 % $CD_3OD/D_2O$ v/v)

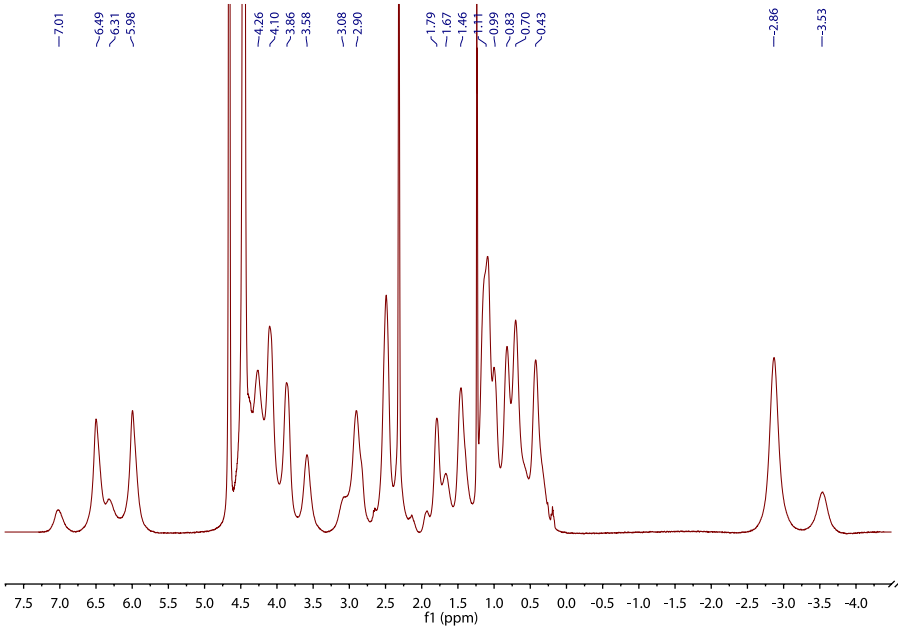


Figure B.5: $^{1}$H NMR spectrum of Sm(III) complex (400 MHz, −35 °C, 40 % $CD_3OD/D_2O$ v/v)

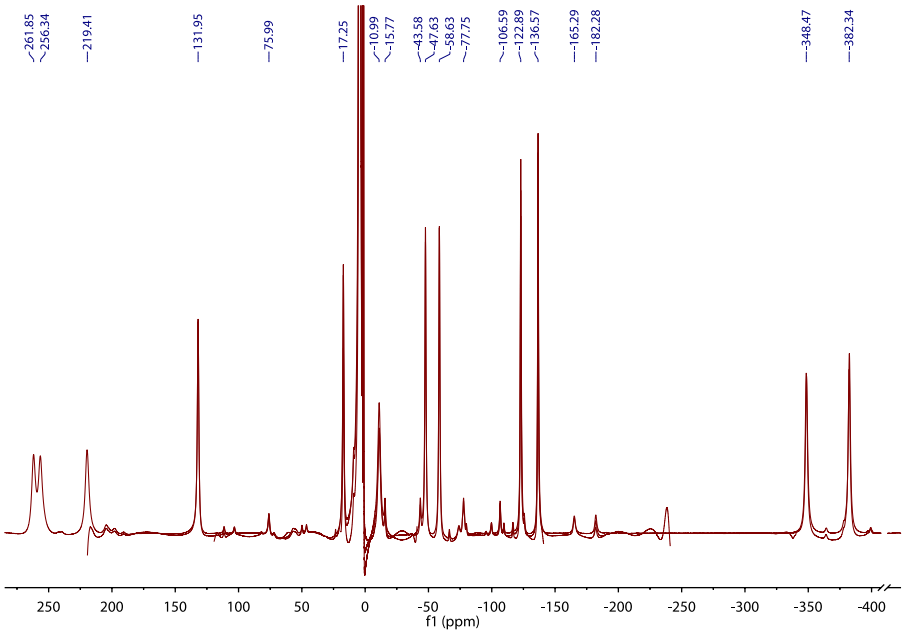


Figure B.6: $^{1}$H NMR spectrum of Tb(III) complex (600 MHz, 25 °C, $D_2O$)

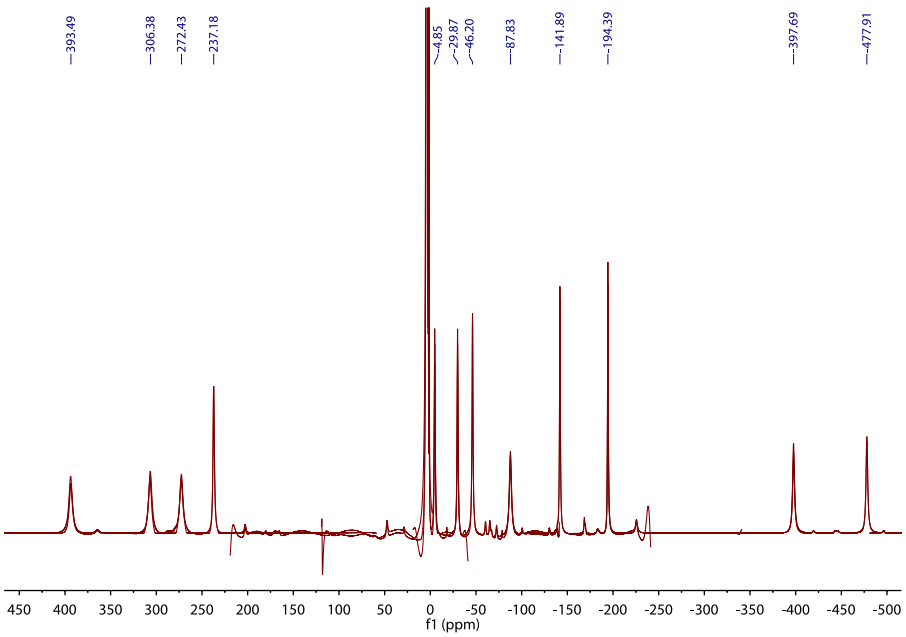


Figure B.7: $^{1}$H NMR spectrum of Dy(III) complex (600 MHz, 25 °C, $D_2O$)

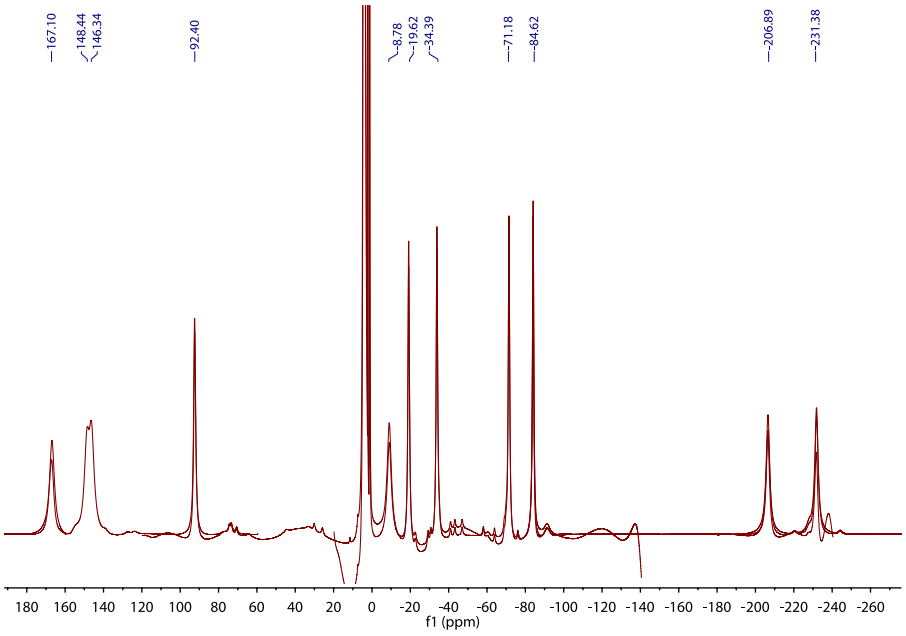


Figure B.8: $^{1}$H NMR spectrum of Ho(III) complex (600 MHz, 25 °C, $D_2O$)

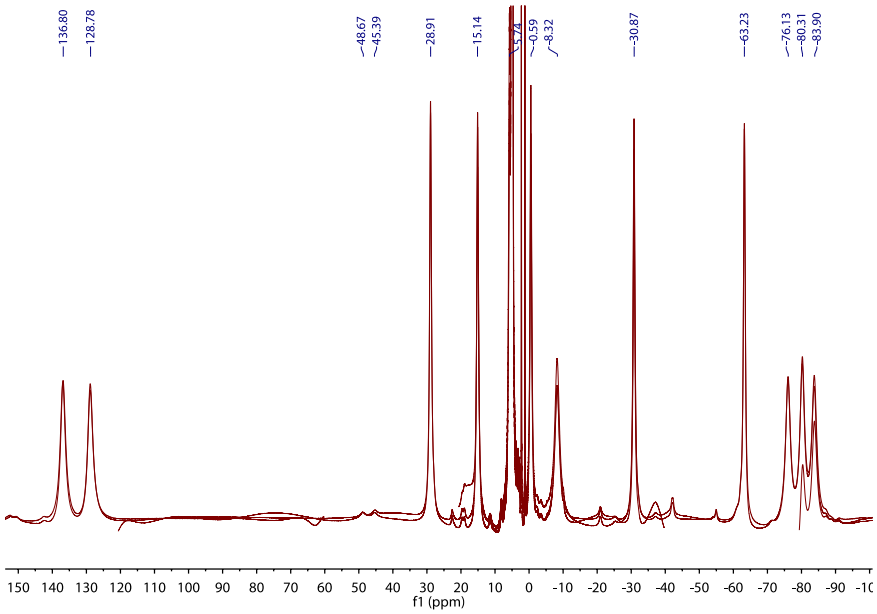


Figure B.9: $^{1}$H NMR spectrum of Er(III) complex (600 MHz, 25 °C, $D_2O$)

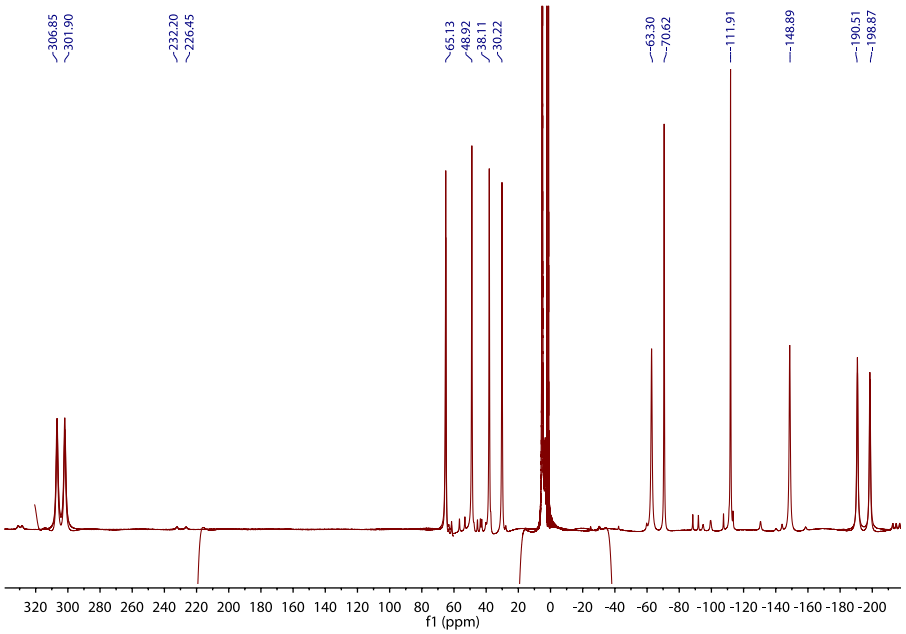


Figure B.10: $^{1}$H NMR spectrum of Tm(III) complex (600 MHz, 25 °C, $D_2O$)

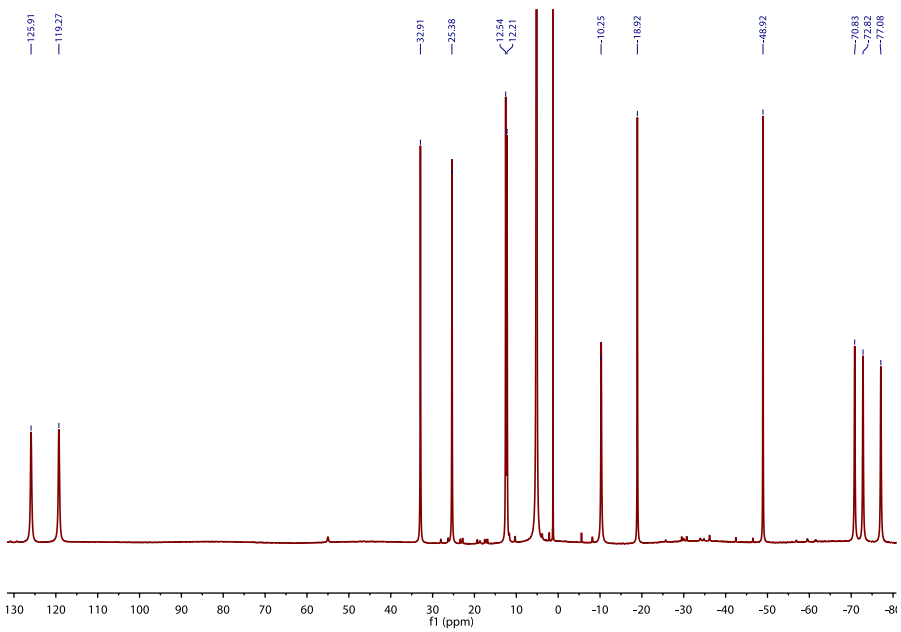


Figure B.11: $^{1}$H NMR spectrum of Yb(III) complex (600 MHz, 5 °C, $D_2O$)

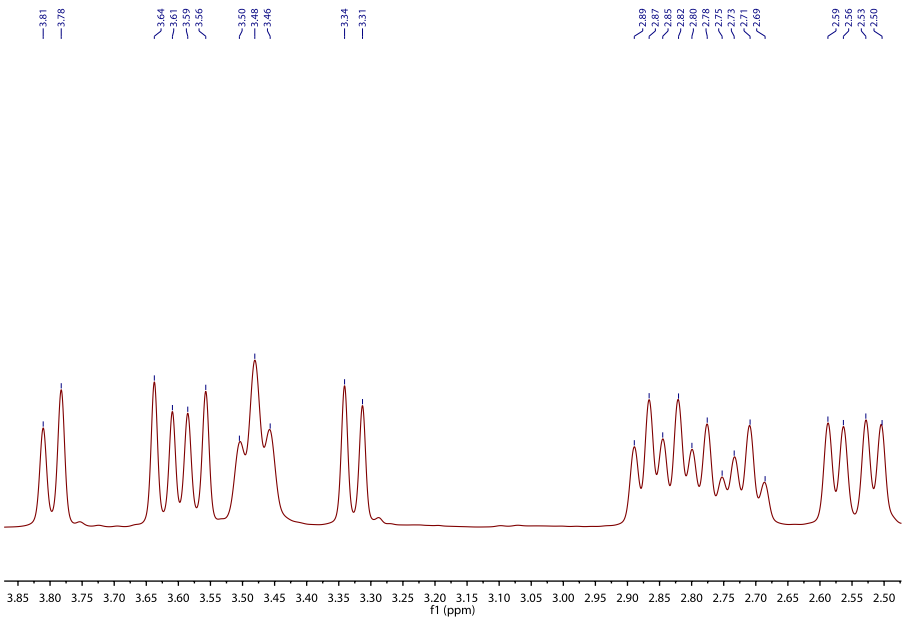


Figure B.12: $^{1}$H NMR spectrum of Lu(III) complex (600 MHz, 5 °C, $D_2O$)

# C Variable-temperature NMR spectra of Sm(III) complex

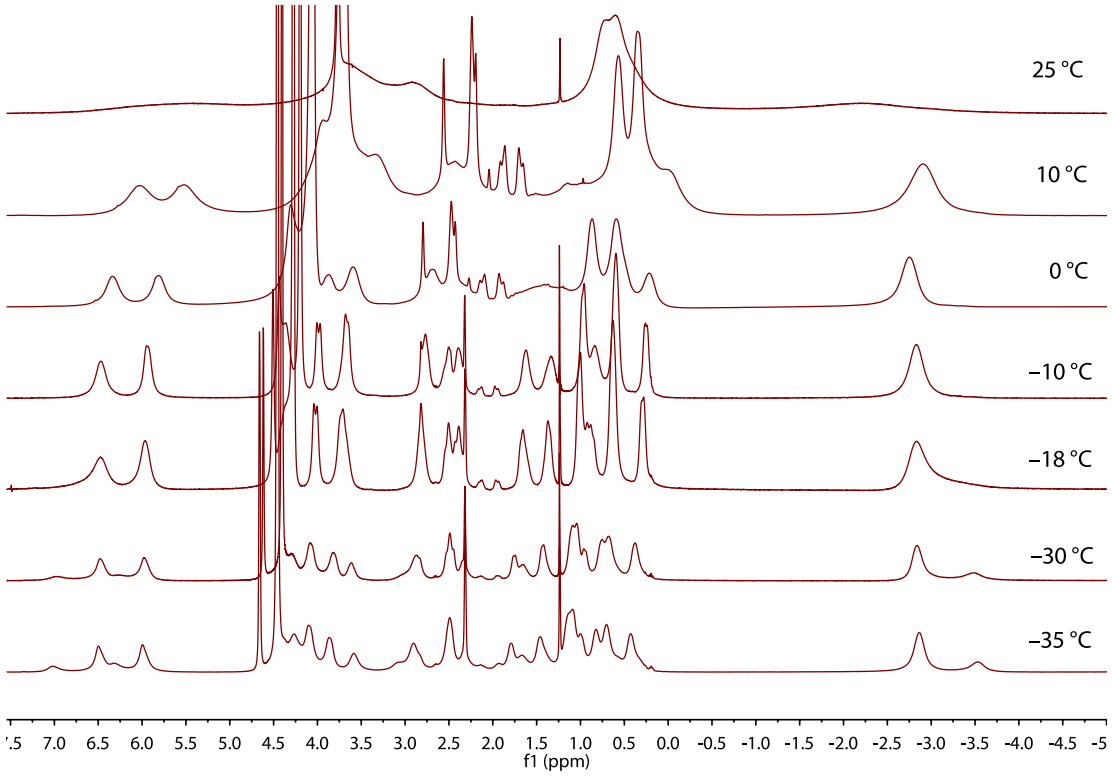


Figure C.1: $^{1}$H NMR spectrum of Sm(III) complex (400 MHz, 40 % $CD_3OD/D_2O$ v/v)) measured at temperatures ranging from −35 °C to 25 °C. At −35 °C, the two isomers present in solution have well-resolved peaks, which coalesce at temperature around −20 °C. At around 25 °C, another coalescence is observed. At this temperature, enantiomerisation occurs on NMR time-scale and at higher temperatures, only average spectrum consisting of four peaks would be observed (two different pendant $CH_2$ groups and two different ring $CH_2$ groups). From the spectra it is evident that it is possible to obtain the isomer ratio in solution only at a temperature lower than−30 °C. Similar behaviour was observed for La(III), Nd(III) and Pr(III) complexes.

# D $^1$H – $^1$H EXSY spectra of [Eu(*t*dodam)($H_2O$)]$^+$ complex

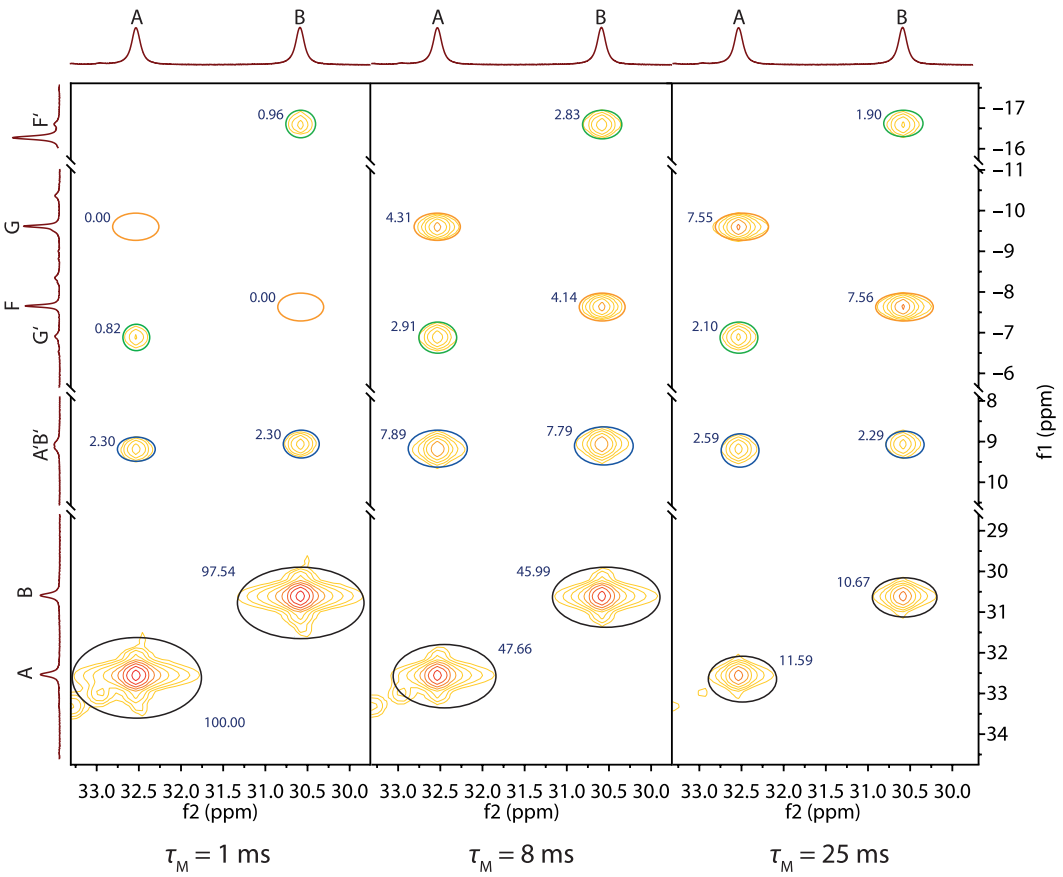


Figure D.1: Examples of $^1$H – $^1$H EXSY spectra of [Eu(*t*dodam)($H_2O$)]$^+$ complex measured using three different mixing times $\tau_M$. Only the parts of the spectra containing the crosspeaks and the diagonal peaks of the axial protons A and B are shown. Ellipses around the peaks show the integration intervals and the numbers next to the peaks show the integral intensities of the particular peaks relative to integral intensity of the diagonal peak of proton A ($I$ = 100) in the spectrum measured with mixing time $\tau_M$ = 1 ms. It is evident that the integral intensities of the crosspeaks decrease with increasing mixing time due to relaxation and cross-relaxation and that the integral intensities of the diagonal peaks increase at first due to the magnetisation transfer from the axial proton and then decrease due to relaxation and cross-relaxation processes. Plots of the evolution of the integral intensities of crosspeaks and diagonal peaks are shown in Fig. 4.18, p. 58. The colour of the ellipse shows the origin of the peak, blue = ring inversion, green = arm rotation, orange = both movements in succession, black = diagonal peak.

# E Experimental X-ray data

Table E.1: X-ray data of obtained structures

| Compound | *t*Bu$_2$*t*dodam · 2 $CHCl_3$ | $H_2$*t*dodam · 3 $H_2O$ | [Ce(*t*dodam)($H_2O$)] ($ClO_4$) · 5 $H_2O$ | [Eu(*t*dodam)($H_2O$)] Cl · 6 $H_2O$ | [Gd(*t*dodam)($H_2O$)] ($ClO_4$) · 4 $H_2O$ |
|---|---|---|---|---|---|
| Formula | $C_{26}H_{48}Cl_6N_6O_6$ | $C_{16}H_{36}N_6O_9$ | $C_{16}H_{40}CeClN_6O_{16}$ | $C_{16}H_{42}ClEuN_6O_{13}$ | $C_{16}H_{38}ClGdN_6O_{15}$ |
| $M_r$ | 753.4 | 456.51 | 748.11 | 713.96 | 747.22 |
| Habit | prism | prism | prism | plate | plate |
| Colour | colourless | colourless | colourless | colourless | colourless |
| Crystal system | triclinic | monoclinic | monoclinic | monoclinic | tricliclinic |
| Space group | *P*-1 | *P*21/*c* | *P*21/*n* | *P*21/*n* | *P*-1 |
| *a* (Å) | 9.2837(4) | 15.1139(5) | 8.9580(5) | 9.2776(8) | 9.1758(7) |
| *b* (Å) | 10.4796(5) | 9.4731(4) | 29.360(2) | 27.174(3) | 9.2174(8) |
| *c* (Å) | 10.5022(5) | 15.3059(5) | 10.6218(7) | 10.972(1) | 15.990(1) |
| $\alpha$ (°) | 104.085(2) | 90 | 90 | 90 | 91.378(2) |
| $\beta$ (°) | 109.278(1) | 103.783(1) | 94.369(2) | 95.252(3) | 91.704(2) |
| $\gamma$ (°) | 92.630(2) | 90 | 90 | 90 | 90.146(2) |
| $U$ (Å$^3$) | 926.53(7) | 2128.3(1) | 2785.5(3) | 2754.4(5) | 1351.4(2) |
| $Z$ | 1 | 4 | 4 | 4 | 2 |
| $F_{000}$ | 396 | 984 | 1524 | 1456 | 754 |
| $D_{calc}$ (g cm$^{-3}$) | 1.35 | 1.425 | 1.784 | 1.722 | 1.836 |
| $\mu$ (mm$^{-1}$) | 0.508 | 0.116 | 1.813 | 2.444 | 2.633 |
| Unique refl. | 4246 | 4903 | 6410 | 6315 | 6177 |
| Obsd. refl. ($I > 2\sigma(I)$) | 3910 | 4247 | 6155 | 5585 | 6092 |
| Parameters | 233 | 328 | 437 | 398 | 403 |
| GOF | 1.038 | 1.039 | 1.188 | 1.072 | 1.353 |
| $R(I > 2\sigma(I))$ | 0.0362 | 0.0339 | 0.0207 | 0.0226 | 0.0286 |
| $R'$(all) | 0.0392 | 0.0413 | 0.0218 | 0.0292 | 0.0293 |
| $wR(I > 2\sigma(I))$ | 0.0948 | 0.084 | 0.0532 | 0.0465 | 0.0747 |
| $wR'$(all) | 0.0976 | 0.0884 | 0.0537 | 0.048 | 0.0752 |

| Compound | [Tb(*t*dodam)($H_2O$)] $Cl \cdot 4\,H_2O$ | [Ho(*t*dodam)($H_2O$)] $Cl \cdot 6.85\,H_2O$ | [Tm(*t*dodam)($H_2O$)] $Cl \cdot 5\,H_2O$ | [Yb(*t*dodam)($H_2O$)] $(ClO_4) \cdot 4\,H_2O$ |
|---|---|---|---|---|
| Formula | $C_{16}H_{38}ClN_6O_{11}Tb$ | $C_{16}H_{43.7}ClHoN_6O_{13.85}$ | $C_{16}H_{40}ClN_6O_{12}Tm$ | $C_{16}H_{38}ClN_6O_{15}Yb$ |
| $M_r$ | 684.89 | 742.25 | 712.92 | 763.01 |
| Habit | prism | plate | plate | prism |
| Colour | colourless | pink | colourless | colourless |
| Crystal system | orthorhombic | monoclinic | monoclinic | triclinic |
| Space group | $Pcca$ | $P2_1/n$ | $P2_1/n$ | $P$-1 |
| $a$ (Å) | 19.3684(7) | 9.0968(5) | 9.0444(6) | 9.1112(7) |
| $b$ (Å) | 15.4429(7) | 28.2870(14) | 28.361(2) | 9.1648(7) |
| $c$ (Å) | 17.4448(7) | 10.9561(5) | 10.9336(8) | 15.9432(12) |
| $\alpha$ (°) | 90 | 90 | 90 | 91.386(2) |
| $\beta$ (°) | 90 | 94.1970(10) | 94.072(2) | 92.107(2) |
| $\gamma$ (°) | 90 | 90 | 90 | 90.184(2) |
| $U$ (Å$^3$) | 5217.8(4) | 2811.7(2) | 2797.5(3) | 1329.99(18) |
| $Z$ | 8 | 4 | 4 | 2 |
| $F_{000}$ | 2768 | 1506 | 1440 | 766 |
| $D_{calc}$ (g cm$^{-3}$) | 1.744 | 1.753 | 1.693 | 1.905 |
| $\mu$ (mm$^{-1}$) | 2.876 | 2.981 | 3.331 | 3.698 |
| Unique refl. | 6018 | 6472 | 5497 | 5241 |
| Obsd. refl. ($I > 2\sigma(I)$) | 5647 | 6285 | 5099 | 5230 |
| Parameters | 356 | 421 | 379 | 391 |
| GOF | 1.299 | 1.19 | 1.356 | 1.175 |
| $R(I > 2\sigma(I))$ | 0.0345 | 0.0248 | 0.0723 | 0.0323 |
| $R'$(all) | 0.0373 | 0.0256 | 0.0762 | 0.0324 |
| $wR(I > 2\sigma(I))$ | 0.0763 | 0.0623 | 0.1692 | 0.0893 |
| $wR'$(all) | 0.0771 | 0.0626 | 0.1707 | 0.0893 |